A Segmented-Ring Ion Trap Storage Source/Reflectron/Time-Of-Flight Mass Spectrometer

by

Qinchung Ji

A DISSERTATION

Submitted to
Michigan State University
in partial fulfillment of the requirements
for the degree of

DOCTOR OF PHILOSOPHY

Department of Chemistry

1996

Abstract

A segmented ring ion trap storage source (SRS) /reflectron/time-of-flight mass spectrometer

by

Qinchung Ji

The mass spectral detection of chromatographic eluents has suffered from trade-offs of the spectral generation rate, mass resolution, mass range, sensitivity and sample utilization efficiency. A segmented-ring ion trap storage source with electron impact ionization has been developed for use with time-of-flight mass analysis to overcome these trade-offs and provide high spectral generation rate and excellent sensitivity without loss of mass spectral (discriminating) information. During the ionization period, an RF voltage is applied between the ring and end cap electrodes. Most of the ions generated in the ion source accumulate there throughout the ionization period. A pulsed extraction of the ions stored in the ion source is accomplished by switching the trap electrodes from the RF storage voltage to the DC voltages required to provide a linear DC extraction field essential for the TOF analysis. The application of the pulsed extraction field is synchronized with the phase of RF voltage applied during the ion storage period.

A mathematical model of a reflectron which is able to temporally focus isomass ions at the detector surface was established. A numerical solution and a general procedure for constructing a broad range energy focusing reflectron was developed.

A segmented ring ion trap storage source/reflectron/ time-of-flight mass spectrometer was fabricated. A gas chromatograph was interfaced to the time-of-flight mass spectrometer. Without component optimization, better than unit mass resolution is achieved through m/z 500 without the need for collisional ion cooling which is mandated for quadrupole ion trap mass analysis. With an extraction rate of 1 kHz and a recording rate of 4 spectra/s, a linear working curve is obtained between 36 pg and 18 ng of chlorobenzene delivered chromatographically. The detection limit for chlorobenzene is 36 picogram with signal to noise ratio of approximately 50:1. The system has demonstrated the potential to achieve the sought-for goals of very high sample utilization efficiency at high spectral generation rates.

Acknowledgment

It was a challenge and opportunity for me to start a project to develop a mass spectrometer for my Ph. D. dissertation research. With the guidance of Professor Enke and Professor Holland, the assistance of the people in and outside of Professor Enke's research group, I am glad that I got through it.

I would like to thank my advisor, Professor Enke. It is he who brought the opportunity for me to work with this project. His trust, encouragement, and guidance have made significant improvement in my abilities of learning, creative thinking, Independent and collaborative researching, scientific presentation.

I would like to thank Professor Holland, who is the co-investigator and consultant on this project and second reader of my Ph. D. dissertation. The meetings with Professor Enke and Professor Holland during this project were always stimulating and productive.

I would like to thank Professor McGuffin and Professor Braselton. I learned a lot from their classes and discussion with them.

I would like to thank Michael Davenport. His help on the design and construction of the dynamic voltage and timing system was critical to the success of this project. I benefited a lot from working with him on electronic construction. I would like to thank Dr. George Yefchak and Hewlett Packard Inc. for providing me a data acquisition board with a computer software.

I would like to thank Fei Liu and Gregor Overney, good friends of my family, for their friendship. Gregor, with his advanced computer knowledge, has given me a lot of help also.

Dave McLane and Mary Seeterlin gave me a lot of help in the early stages of this project. I have enjoyed working with Eric Hemenway, Paul Vlasak, Calin Znamirovski, Paul Miyares, Douglas Beussman, Tina Erickson, Terri Constantopoulous and Michele Davenport.

I would like to thank the people in the machine shops and electronic shops at both Michigan State University and the University of New Mexico.

I would like to thank my former advisors, Professor D. F. Hunt at the University of Virginia; Professor Dengqui An and Professor Longsheng Sheng at China Pharmaceutical University, Professor Deshu Guan and Professor Xinming Li at Dalian Institute of Chemical Physics, Chinese Academy of Science. They help me lay the basis for starting my graduate study at Michigan State University and for working in this project.

I would like to thank my wife, Hua Tang and our son, Minchuan. When I was excited about my progress, she shared that joy with me. When I was upset or frustrated, She gave me encouragement and discussed ways to solve the problem. I would like to thank my parents. they came from China to help me so I have more time stay in the lab in the evenings and during the weekends for the final year of my graduate research.

Table of Contents

List of Figures

Fi

Fig

Fig

Fig

Fig

Figu

Figu

Figur

Figure

Fig

Fig

Fig

Fig

Fig

Fig

Figure

Figure
peak a

Figure

Figure

List of Tables

CHAPTER 1. INTRODUCTION

1.1 Background

In the 1980s, a group of scientists at Michigan State University realized that the advantage of combining gas chromatography with mass spectrometry was limited by the capabilities of the mass spectrometer[1]. Developments in chromatographic techniques had created a need for dramatic improvements in the spectral generation rate, sample utilization efficiency and mass range for mass spectrometric detectors.

For gas chromatography/mass spectrometry analysis, components of a mixture separated by a chromatograph enter the ion source of a mass spectrometer continuously. Typically, samples are ionized by electron impact ionization. Ions generated in the ion source are mass analyzed in either of two ways. In the first type of mass spectrometric analysis, all of ions in the ion source are transferred continuously to the mass analyzer and ions are analyzed exclusively and sequentially based on their m/z value. The m/z value of the ion is recognized by scanning a transmission window, which allows only ions of certain range of m/z values to pass through to the detector. Electronic properties (such as magnetic strength, DC offset and RF amplitude) that are applied to the mass spectrometer are varied to allow scanning of the mass window across the mass range of interest. The commonly used mass spectrometers of this type are the magnetic sector mass spectrometer and the quadrupole filter mass spectrometer. In the second type of mass spectrometric analysis, ions are mass analyzed in separate batches; all the ions with different m/z values in each individual batch are analyzed simultaneous or within a short period. The commonly used mass spectrometers of this type employ Fourier Transform mass spectrometry (FTMS), Time-of-Flight mass spectrometry (TOFMS) and Ion Trap Mass Spectrometry (ITMS). The batch mass analysis of ion packets with different m/z values is called *time array detection* (for TOFMS), *frequency array detection* (for FTMS), and *sequential destabilization scanning* (for ITMS).

1.1.1 Sample utilization efficiency

Sample utilization efficiency is defined as the ratio of the number of ions detected to the number of sample molecules introduced into the ion source. It depends on the sample ionization efficiency, the ion transfer efficiency, and the sample utilization duty cycle. This duty cycle can be defined as the fraction of the time of each analysis cycle during which detectable ions are being generated and measured.

For the scanning type of mass spectrometric analysis, the sample utilization efficiency suffers from a low duty cycle. For example, for a scan range of 500 mass units and a unit resolution mass window, individual m/z ions can at most only be detected over one five hundredth of the scan period; During the remaining 99.8% of the scan, this particular m/z value ion is lost. The scanning duty cycle is 0.2%.

spectrometer. In the second type of mass spectrometric analysis, ions are mass analyzed in separate batches; all the ions with different m/z values in each individual batch are analyzed simultaneous or within a short period. The commonly used mass spectrometers of this type employ Fourier Transform mass spectrometry (FTMS), Time-of-Flight mass spectrometry (TOFMS) and Ion Trap Mass Spectrometry (ITMS). The batch mass analysis of ion packets with different m/z values is called *time array detection* (for TOFMS), *frequency array detection* (for FTMS), and *sequential destabilization scanning* (for ITMS).

1.1.1 Sample utilization efficiency

Sample utilization efficiency is defined as the ratio of the number of ions detected to the number of sample molecules introduced into the ion source. It depends on the sample ionization efficiency, the ion transfer efficiency, and the sample utilization duty cycle. This duty cycle can be defined as the fraction of the time of each analysis cycle during which detectable ions are being generated and measured.

For the scanning type of mass spectrometric analysis, the sample utilization efficiency suffers from a low duty cycle. For example, for a scan range of 500 mass units and a unit resolution mass window, individual m/z ions can at most only be detected over one five hundredth of the scan period; During the remaining 99.8% of the scan, this particular m/z value ion is lost. The scanning duty cycle is 0.2%.

In TOF and FTMS mass spectrometric analysis, the duty cycle depends on the fraction of the batch mass analysis cycle during which detectable ions are generated and maintained in the ion source. The mass analysis time for TOF-MS is about 100 μs. While ions can be generated throughout this period, thermal motion of the ions created will carry most of them out of the source before they are analyzed. Unless some ion storage mechanism is invoked, only the ions created in the few microseconds prior to extraction will be analyzed. The sampling duty cycle is 1-2%.

For ion trap mass spectrometry, the ions are generated and stored in the ion source during the ionization portion of the analysis cycle. The duty cycle is thus dependent upon the ratio of the ionization/storage period to the total mass analysis cycle. This is always less than unity due to the ion cooling and mass analysis portions of cycle. In addition, at higher sample concentrations, ion production is automatically curtailed to avoid saturation of the ion trap capacity (limited to ~10^6 ions).

1.1.2 Spectrum generation rate

The spectral generation rate for all types of mass spectrometers is limited by some fundamental properties[1]. In scanning mass spectrometers, higher spectral generation rates are achieved by sacrifices in mass range, resolution or sensitivity. Narrowing the mass range, such as in the selected ion monitoring (SIM) technique, shortens the spectral data acquisition cycle, but limits the amount of the spectral information obtained during each cycle. Scanning filter m

to

lin

pa

hig

ma

ra

the

wa

how

rate

1.1.

For

the

sect

mass

over

slowe

cycle

samp

but it

mass spectrometers and ion trap mass spectrometers all involve some finite time to scan over the desired mass range. The spectrum generation rate is therefore limited to the mass range divided by the maximum scan rate. The mass analysis period for TOF mass spectrometers is set by the flight time of the ion with the highest m/z value to be detected. This is generally less than 200 μs, allowing a maximum spectral generation rate in excess of 5000 Hz for the entire mass range. Due to the physical nature of this technique, a transient waveform strikes the detector in an increasing m/z sequence after every source extraction. This waveform or transient, contains information for a complete mass spectrum, however, it is usually not converted and stored as an individual spectrum at this rate.

1.1.3 Mass spectral resolving power

For scanning mass spectrometry, the resolution can be improved by decreasing the window size of mass analysis. This slows the scanning rate. For magnetic sector mass spectrometry and quadrupole filter mass spectrometry, a narrower mass window will result in a smaller fraction of the ions reaching the detector over the whole mass range. For ITMS, the resolution is also improved by using a slower scanning rate. Scanning the ITMS more slowly results in a lower duty cycle, therefore a lower sample utilization efficiency.

For TOF and FTMS mass spectrometry, the resolution is not related to the sample utilization efficiency. FTMS can provide extremely high mass resolution but it requires an ultra high vacuum that is not readily compatible with sample in

ob

re

fig

inc

1.1

chr

A ti

eac

data

impl

ana

elec

utiliz

fast s

grou

goals

subse

rate a

contin

maxim

introduction through a gas chromatograph. The very high mass resolution is obtained by summing a large quantity of frequency domain transients[2]. This reduces the spectrum generation rate significantly. The resolution of a time-of-flight mass analyzer is related to the design of the ion optics and the electronics incorporated in the instrument.

1.1.4 Direction of the improvement of mass spectrometry detection for gas chromatography

A time-of-flight mass spectrometer can produce several thousands of transients each second, this gives a fundamental measurement base for fast GC/MS detection. The sample utilization efficiency of TOFMS could be improved by implementing some kind of ion storage between ion extractions for TOF analysis. The mass resolution could be improved by innovative ion optical and electronic control design. The improvement of the mass resolution and sample utilization efficiency of the time-of-flight mass spectrometer, while keeping its fast spectrum generation rate, has been a research direction in Professor Enke's group and the MSU/NIH Mass Spectrometer Facility for many years. These goals are essential to achieve the full capability of mass spectrometric detection subsequent to chromatographic separation. The goals of fast spectral generation rate and high sample utilization also require fast detector electronics and continuous recording of the individual extraction transients generated at their maximum rate.

1.2 Time-of-flight mass spectrometer

1.2.1 Introduction

The principles of mass analysis in TOF mass spectrometry can briefly be described as follows. Ions are either generated in the ion source, mainly by electron impact ionization, or introduced into the source region from an external ionization source such as electrospray, or API (atmospheric pressure ionization). The ions in the ion source are then extracted by the application of a short high voltage pulse across the ion source volume. Ions with different m/z values gain equal amounts of kinetic energy. These ions are directed through a field free region where they will be separated on the basis of their differing velocities. Ions with lower m/z values have higher velocities and will reach the detector earlier. Ions with higher m/z values have lower velocities and will reach the detector later. The arrival times of the isomass ion packets reaching the detector and the detector response to the consecutive isomass packets are recorded as a time domain transient. Each time domain transient can be converted into a mass spectrum.

Time-of-flight mass spectrometry was first introduced by Cameron and Eggers[3] in 1948. In 1955, Wiley and McLaren developed this technique and demonstrated its practical usefulness[4]. Time-of-flight mass spectrometry was also the first mass spectrometry technique to be interfaced with gas chromatography[5]. However, TOFMS was soon eclipsed by magnetic sector mass spectrometry and then scanning quadrupole mass spectrometry for oth

the

ren

unl

bec

ele

ext

bes

rec

1.2.

For

ligh

extr

and

requ

fligh

seco

repe

acqu

is us

Stor

gene

chromatographic detection due to the higher resolution and easier interface of the scanning instruments. Recently, time-of-flight mass spectrometry has gained renewed attention due to its simplicity, fast spectral generation rate and unlimited mass range[6]. The mass resolution has been improved significantly because of the theoretical and practical developments in ion optics and electronic control systems (such as the ion reflectron[7,8,9,15], high voltage extraction pulse, and dynamic field ion focusing[10,18]). The spectral output has been improved significantly because of the developments of the transient recorder and computer control systems[11,12,13].

1.2.2 Spectral generation rate and time array detection

For time-of-flight mass spectrometry, the spectral repetition rate is limited by the flight time of the heaviest (slowest) ion to reach the detector after being extracted. For a 1 meter flight tube reflectron/time-of-flight mass spectrometer and an ion kinetic energy of 1800 eV, an ion with an m/z value of 800 daltons requires a flight time of less than 100 μs. For this upper mass limit, the time-of-flight mass spectrometer is able to generate more than 10,000 transients each second. If an analog oscilloscope is used, transients are displayed on the screen repeatedly. Since the detection of the complete transient is essentially the acquisition of an entire array of time domain data, the term *time-array detection* is used for this detection scheme. However, it is not practical to encode and store each transient as an individual mass spectrum at the maximum transient generation rate. Fortunately, even for very fast chromatography, it is not necessary to generate 10,000 individual mass spectra each second.

Scientists at the MSU/NIH Mass Spectrometry Facility have invented a *time-array detector* called the *integrated transient recorder* which can acquire the information from 10,000 transients each second[13]. Several consecutive transients are summed together to give an individual mass spectrum in the time domain. If 10,000 transients are generated by the time-of-flight mass spectrometer each second and 100 successive transients are integrated into one mass spectrum, this integration will reduce the mass spectral generation rate from 10,000 spectra/s to 100 spectra/s which is an excellent mass spectral generation rate for capillary GC/MS. Also the integration of the 100 individual transients will improve the signal-to-noise ratio of each spectrum by a factor of 10 which is the square root of the number of summed transients. Because the ion residence time in the ion source is about 2 μs, due to thermal motion of the ions, the 10,000 Hz extraction rate provides a sample utilization duty cycle of 2%, If the extraction rate were slower, the duty cycle would be even less.

1.2.3 Mass resolution of the time-of-flight mass spectrometer

1.2.3.1 Initial spatial and kinetic distribution

The mass resolving power can be calculated as the temporal distribution of a particular isomass ion packet at the detector position divided by its total flight time. Although the ion optical path and ion extraction electronics have major effects on the mass resolving power, they can be optimized, often leaving the initial kinetic energy and spatial distribution of the ions in the ion source as the two major factors which are limiting the mass resolution. The effects of these factors on the exit times and velocities for isomass ions are shown in Figure 1-1. The ideal situation, one that has zero initial spatial and velocity distribution, is shown in Figure 1-1(a). Isomass ions leave the ion source at the same moment with the same velocity. The effect of spatial distribution is shown in Figure 1-1(b). Isomass ions located at different source positions experience different extraction voltages. They leave the ion source with different velocities and at different times. The effect of the kinetic energy distribution is shown in Figure 1-1(c). The ions leave the ion source with different velocities and times because of their different initial velocities. An extreme case of Figure 1-1(c) is shown in Figure 1-1(d). Two ions have the same initial velocity but in opposite directions. These two ions leave the ion source with the same velocity but at different times. This time difference is called the *turn-around time*. The turn-around time causes a more significant detrimental effect to the isomass temporal distribution at the detector than the energy distributions in the same direction as shown in Figure 1-1(c), therefore, the turn-around effect has received greater attention as discussed in a later section.

1.2.3.2 Space focus plane and two stage extraction

The initial spatial distribution of the isomass ions in the ion source as shown in Figure 1-1(a) contributes significantly to the ion velocity difference of these isomass ions. If not corrected, this velocity difference will cause significant

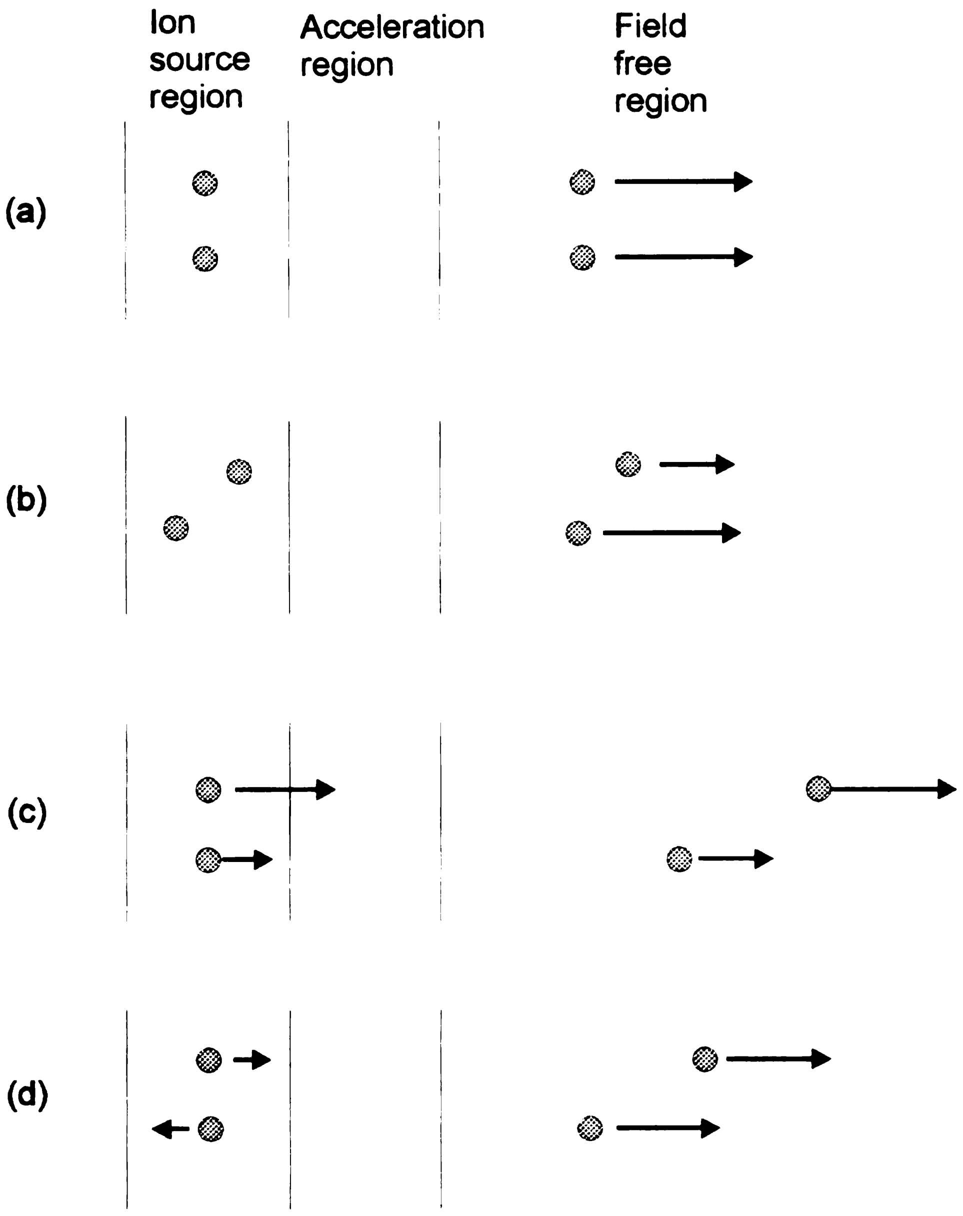

Figure 1-1. Schematic of four typical initial ion spatial and kinetic energy distributions and their effects on the ion temporal distributions. Arrows show the velocity vectors of ions with the same m/z. (a) Ideal situation with zero initial spatial and kinetic distribution in the ion source. (b) Initial spatial distribution but zero kinetic energy. (c) Initial kinetic energy distribution but zero spatial distribution. (d) Same kinetic energy in opposite directions but zero initial spatial distribution.

te
de
cou
reso
isom
linea
are e
sourc
near
They
less
along
catch
from c
at a p
focus
the ion
source
the flig
and acc
distribu
resolutio

temporal distribution at the detector position. In 1955, Wiley and McLaren defined the concept of the *Space Focus Plane* and introduced a way in which it could be moved to the surface of the detector, which significantly improved the resolution of time-of-flight mass spectrometry as shown in Figure 1-2. The isomass ions in the ion source are extracted from the ion source by applying a linear voltage across the ion source. The ions near the back of the ion source are extracted from a higher potential position. They spend more time in the ion source but gain more kinetic energy and exit with a higher ion velocity. The ions near the front side of the ion source are extracted from a lower potential position. They spend less time in the ion source and leave the ion source earlier but gain less kinetic energy and therefore have a lower ion velocity. At some position along the field-free flight path, the faster ions from the rear of the source will catch up to the slower ions starting from the front. Thus isomass ions originating from different positions in the ion source will form a minimal temporal distribution at a particular position along the flight path. This position is called the *space focus plane* (or *space focus position*) and it is independent of the m/z value of the ion. Wiley and McLaren added a second acceleration region to the ion source extraction field, so that the space focus plane could be set at the end of the flight path (the detector position) by adjusting the ratio of the extraction field and acceleration field. In this way, arrival time dispersion due to the initial spatial distribution is reduced and an improved mass resolution is obtained. The resolution of the mass spectrum recorded at the *space focus plane* is dependent

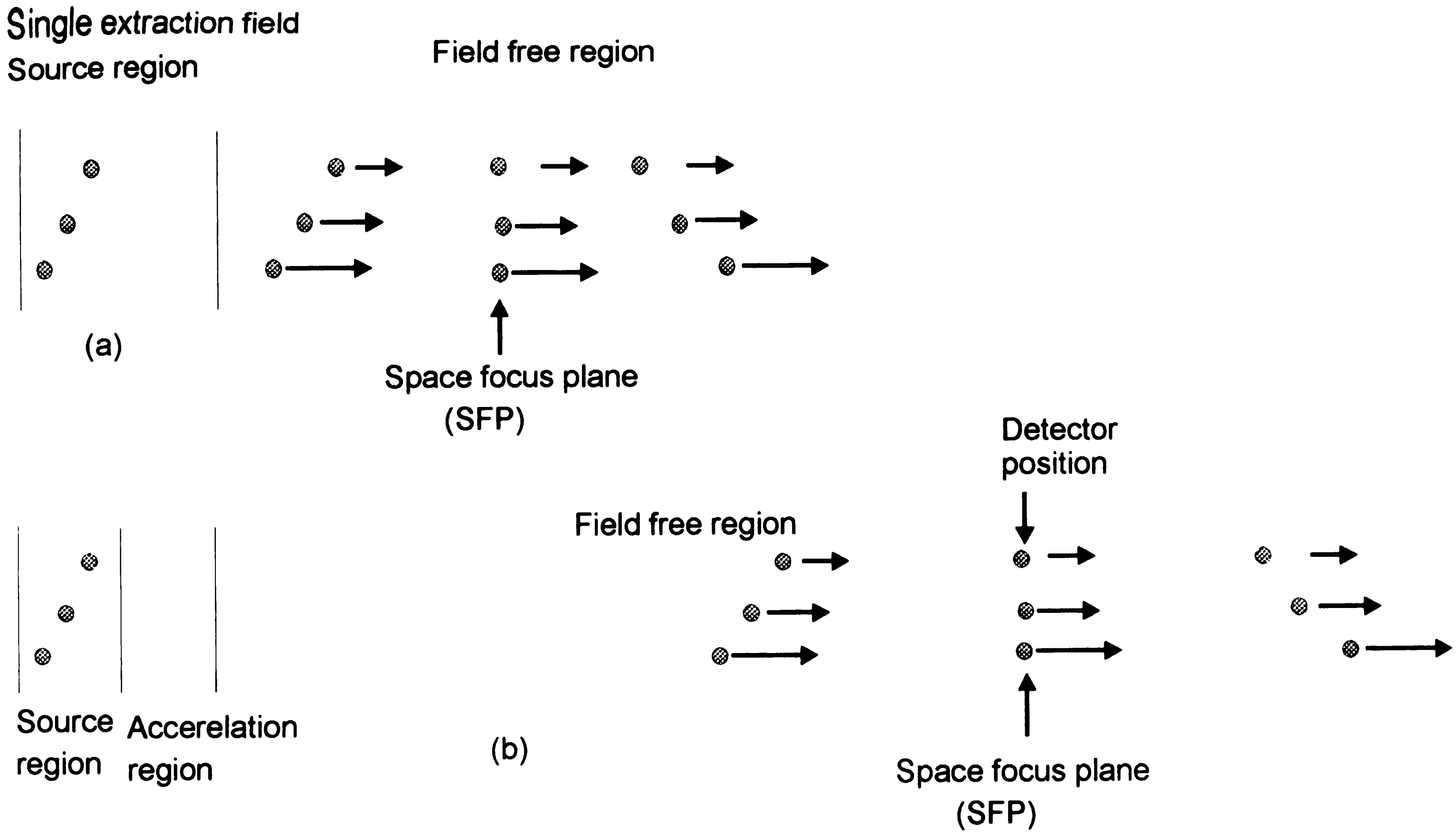

Figure 1-2. Representative schematic of the *Space Focus Plane* formed along the flight path due to initial isomass ion spatial distribution in (a) single field extraction, (b) two field extraction. Arrows show the velocity vectors.


Single extraction field
Source region
Field free region

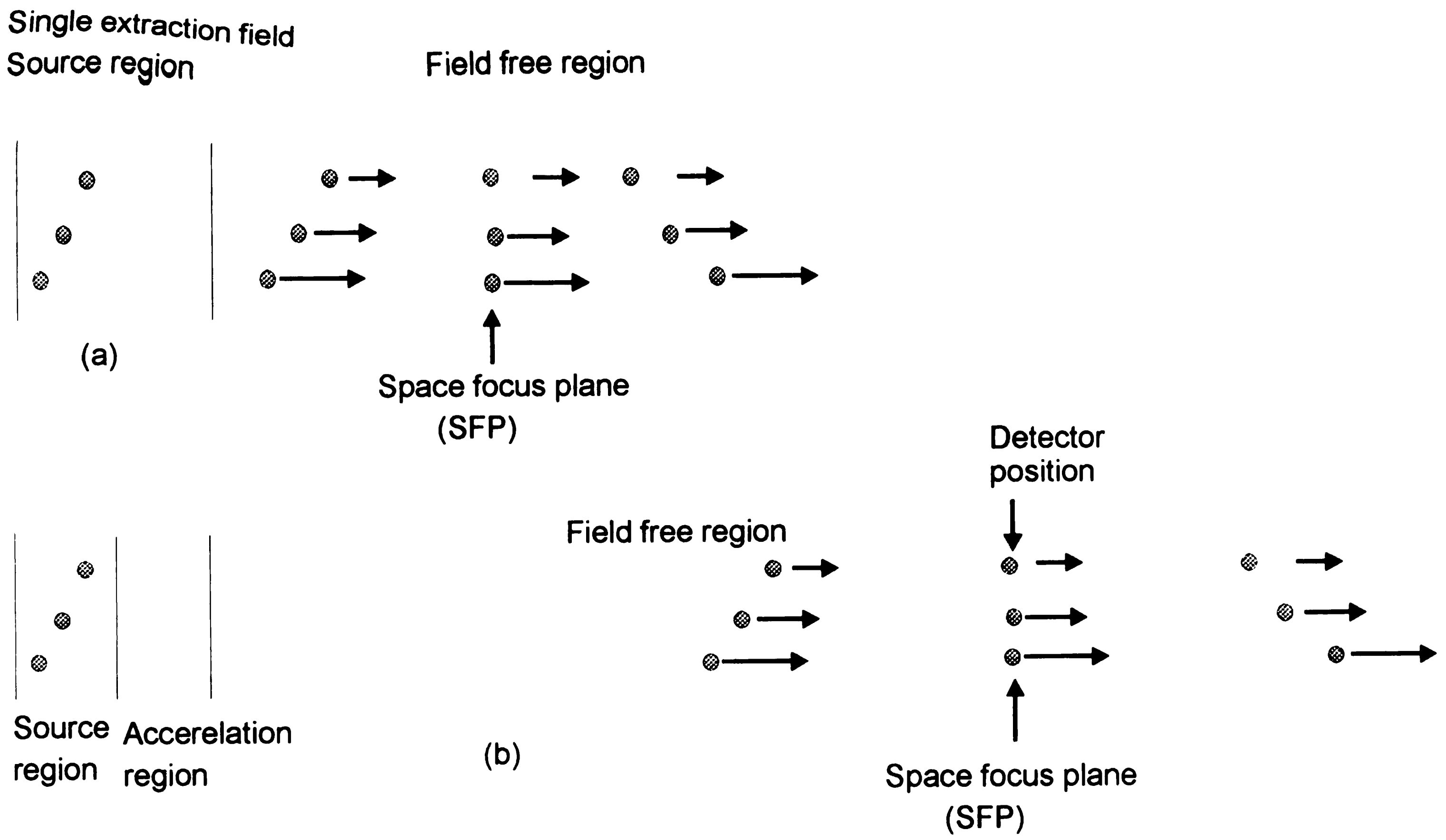

Figure 1-2. Representative schematic of the *Space Focus Plane* formed along the flight path due to initial isomass ion spatial distribution in (a) single field extraction, (b) two field extraction. Arrows show the velocity vectors.

on the ratio of the extraction voltage across the ion source to the acceleration voltage. As this ratio is increased, the resolution is decreased. A higher acceleration voltage results in better resolution[4].

1.2.3.3 Time lag focusing

Wiley and McLaren also developed a technique termed *time lag focusing* which is able to minimize the effect of the initial energy distribution as well as *turn-around time* (as shown in Figure 1-1(d)). Assume two isomass ions are generated at the same position in the ion source but have equal initial velocities in opposite directions. A time lag is applied between ion generation and ion extraction. During the time lag period, the ion moving toward the front extraction plate will move to a position where a lower extraction field will be experienced at the time that the ion extraction pulsed is applied. The ion moving backward will move to a new position where a higher extraction voltage will be experienced when the ion extraction pulse is applied. After the ion extraction pulse is applied, the ion turn around time of the ion moving backwards will be compensated by the higher velocity gained from the higher extraction voltage it experiences. The initial forward velocity of the forward-moving ion will be compensated by the lower extraction voltage. At some position along the flight path, the isomass ions will converge. The optimum lag period between ionization and extraction is dependent on the initial velocity of the ions and the m/z value of the ions. Only a limited fraction of the entire mass spectrum is focused for each value of the lag period[14].

1.2

In

spe

end

a ti

dots

The

elect

electr

direct

packe

increa

correc

of ion

at the

(simila

correct

nothing

1.2.3.5 D

Dynami

extracte

1.2.3.4 Reflectron

In 1973 Mamyrin introduced the electrostatic reflectron into time-of-flight mass spectrometry[15]. A reflectron is an assembly of electrodes located at the other end of the flight tube which acts as an ion mirror. The operation of a reflectron in a time-of-flight mass spectrometer is shown in Figure 1-3. The groups of red dots represent ion positions along the flight path in equal flight time increments. The green lines represent ion trajectories. The black lines represent the electrodes. Ions are initially placed in the ion source at different positions. The electric field of the reflectron decelerates incoming ions and changes their flight direction back into the flight tube. A reflectron is able to image isomass ion packets at the detector position while the total flight length and time are increased.

As discussed in more detail in Chapter Three, since a reflectron can correct only for energetic differences, it can theoretically give perfect correction of ion broadening due to the original spatial distribution (similar to the situation at the ion source shown in Figure 1-1(b)) or initial kinetic energy distribution (similar to the situation at space focus position). But a reflectron is not able to correct both initial energy and space distribution simultaneously and it can do nothing to correct the *turn-around time.*[16]

1.2.3.5 Dynamic focusing

Dynamic focusing is a technique which modifies the ion behavior after ions are extracted from an ion source. It could involve a change in some aspect of

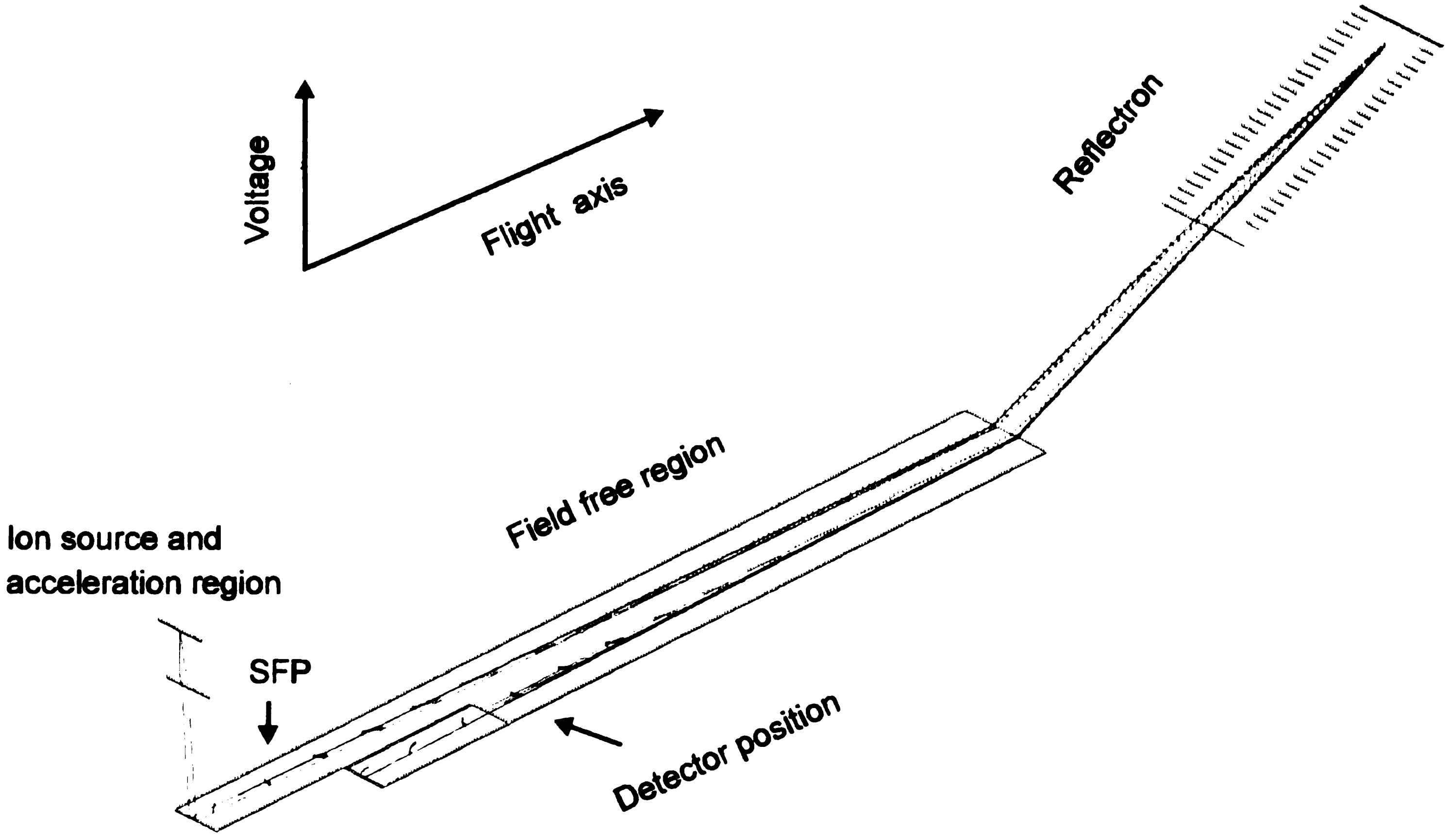

Figure 1-3. Computer simulated function of a reflectron in a time-of-flight mass spectrometer. The isomass ions in different positions in the ion source form a space focus plane in the field free region. This small temporal distribution is imaged to the detector position. The groups of red dots show the ion positions along the flight path in equal flight time increments.

dis

dy

inv

aft

afta

wit

A

affe

ter

pat

regi

dyn

acc

free

dyna

sim

mas

200

achie

cha

spect

distance, time, velocity or acceleration. Kinsel and Johnston introduced a dynamic focusing technique termed *post source pulse focusing*[17]. This method involves the application of a focusing voltage pulse to a short field region located after the source and acceleration regions. The pulse is timed so that it occurs after the ions of interest have entered this region. All the ions that are entirely within the dynamic field region will show a substantial improvement in resolution. All the ions which have already exited the acceleration region will not be affected.

Yefcheck, Enke and Holland developed a dynamic focusing technique termed *dynamic field focusing*[18]. Two field-free regions exist in the ion flight path. Ions are extracted from a single field source and enter the first field-free region. The space focus plane is located in the first-field free region. The dynamic field region is located between the field-free regions. Ions will be accelerated as they leave the first field-free region and enter the second field-free region. The acceleration is time-dependent because the voltage of the dynamic field region varies with time. The mathematical derivation and computer simulation indicated that concurrent space and energy focusing over a wide mass range is possible and unit resolving power can be achieved up to at least 2000 amu with typical gaseous source conditions. In practical terms, the achievement of the derived wave-shape for dynamic field operation would be challenging. This approach has never been implemented in an operational mass spectrometer.

1.2.4 Sample utilization efficiency

In 1989, Wollnik, Grix *et, al.,* introduced an ion source design which used electron impact ionization. The intention of Grix's source design was to generate a potential well by using two more negative voltage electrodes inside the ionization region[19]. However, experiments showed that the negative voltage applied to these electrodes did not generate a potential well as expected[20]. The potential well that was formed was generated by the electron beam which is focused into the ion source by an appropriate voltage setting to the source electrodes[21]. Different variations on the Grix ion source design were experimented with at the MSU/NIH Mass Spectrometry Facility to enhance the potential well formed by the electron beam. Because the electron beam shape is affected by very small changes in electrode configuration, repeatable experimental results were difficult to obtain.

Another idea that existed in Professor Enke's group for improving the sample utilization efficiency of the time-of-flight mass spectrometer was to improve the duty cycle by using a RF ion trap to continuously accumulate ions generated between extractions. This concept initiated the research project that is the basis of this dissertation.

1.3 Ion trap mass spectrometer

The quadrupole ion trap is an ion storage device which was first disclosed by Paul and Steinwedel in 1953 at the same time as the quadrupole mass filter. Subsequent interest followed two lines: selective ion storage for the study of

ion
tra
stu
has
mod
valu
beh
valu
have
of a
spect
m/z ra
been

ion sto
electro
chemica
atmosph
various
within th
the ion t
variety of

ionic species, and methods to obtain a mass spectrum of the ions stored in the trap. The long term storage of selected m/z values in the ion trap has allowed studies of ion spectroscopy and other ionic properties. A "scanning" technique has been developed by Stafford, *et. al.*[22] (mass-selective instability scanning mode) in which ion trajectories are destabilized in sequential order of their m/z values. A fraction of the destabilized ions pass through one of the end caps behind which is an ion detector. The plot of ion current as a function of the m/z value being destabilized is a mass spectrum. The capabilities of the ion trap have developed rapidly. This progress was greatly stimulated by the availability of a powerful commercial (Finnigan MAT, San Jose, CA) ion trap mass spectrometer (ITMS). Now in the hands of several innovative investigators, the m/z range of the ITMS has been extended to 70,000 Da/z[23], and the ITMS has been operated at resolutions (FWHM) in excess of 100,000[24].

Since the availability of the ITMS, many investigators have extended the ion storage capabilities to a wide range of ionization techniques. These include electron impact ionization[25,26], positive chemical ionization[27,28,29,30 31], negative chemical ionization[32], electrospray[33,34,35] ion spray[36], thermospray[37,38], atmospheric sampling glow discharge ionization[39], laser desorption[40,41,42], and various photoionization techniques[43,44,45,46]. Ionization is either performed within the trap, or outside the trap followed by ion injection into the trap. Thus, the ion trap is rapidly developing as a storage ion source adaptable to a wide variety of ionization methods.

The scan speed of the commercial ITMS instrument is 5,555 Da/s, or 117 ms per 650 Da scan. Full scan spectrum generation rates of greater than 5 spectra per second are difficult to achieve due to the need for ion generation, collisional damping, and mass scanning in each scan cycle. Higher scan rates are obtained only at the expense of mass resolution, mass range and sensitivity. There are thus inherent limitations and trade-offs with the mass-selective instability scanning method for achieving the mass spectra of the ions stored in the trap.

When the ion trap is combined with external TOF mass analysis, most of these trade-offs no longer apply. The mass resolution of the TOF system is not dependent on the precision of the quadrupole field as is the ITMS when operating in the mass-selective instability mode. Extraction pulses can be applied more frequently than can destabilizing sweeps. The extraction is complete in a few μs and a new ionization/storage cycle can begin simultaneously with the mass analysis of the previous batch. The resulting higher spectral generation rate has the potential to increase the dynamic range available and increase sample utilization efficiency by emptying the source before it becomes space-charge limited with analyte ions.

1.4 Quadrupole ion trap/ time-of-flight mass spectrometer

Pulsed ejection with subsequent mass analysis of trapped ions has been implemented before in several laboratories[47, 48, 49, 50]. Information on the velocity distribution of ions was obtained by this method, but work in this direction stopped in the late seventies in favor of the rapidly developing selective destabilization mode of mass analysis. The problem of achieving temporal focusing of ions having a significant distribution of starting velocities and positions is, if anything, exacerbated by the ion motion induced by the RF field oscillations. In fact, much of the early work was an exploration of the optimum phase angle of the RF field at the onset of the extraction [48, 49, 50]. Other studies explored the cessation of RF altogether prior to extraction[47].

Recently, the quadrupole ion trap was interfaced with time-of-flight mass spectrometry in Professor Lubman's Lab[51]. The quadrupole ion trap is used as an ion source for the preparation of ions to be analyzed by the time-of-flight mass spectrometer. Ions generated by an external ionization method are introduced into the quadrupole ion trap and accumulated in this ion source. This ion source is filled with collisional bath gas. Ions are trapped in this source up to several hundreds of milliseconds. The ion displacements and initial kinetic energies are minimized by collisional cooling with the bath gas during this period. A good mass resolution with time-of-flight mass analysis is achieved by extracting these "ion trap prepared" ions. Extensive collisional cooling is necessary because the nonuniform extraction field generated by the hyperbolic shaped electrodes of the ion trap is not compatible with the uniform, linear extraction field required for the time-of-flight mass analysis. Good mass resolution is only achieved by inserting an ion cooling operation in the spectrum generation cycle. This sacrifices the fast spectral generation advantage of time-of-flight mass spectrometry as well as the high sample utilization duty cycle.

1.5 Segmented ring ion trap storage source/reflectron/time-of-flight (SRS/TOF) mass spectrometer

To make a ion storage source that will increase the duty cycle of the time-of-flight mass spectrometer and meet the optical requirements of time-of-flight mass analysis, a segmented ring, ion storage ion trap has been developed. The theoretical development and computer simulation of this innovative ion source for time-of-flight mass analysis is discussed in Chapter Two. To minimize the detrimental effect due to the initial kinetic energy distribution, high extraction voltages synchronized with the appropriate RF phase angle are required. This is also discussed in Chapter Two. The development and the design considerations of a reflectron that is able to focus ions extracted from the ion source with a wide energy range distribution is discussed in Chapter Three. The instrument construction, control and timing system, static and dynamic voltage supplies, and the data acquisition and processing systems are described in Chapter Four. Instrument performance, characterization of the ion storage of this segmented ring ion trap, and the advantages of interfacing a gas chromatograph with this novel ion storage source/reflectron/time-of-flight mass spectrometer are discussed in Chapter Five.

References:

---

[1] Holland, J. F., Enke, C. G., Allison, J., Stults, J. T., Pinston, J. D., Newcome, B., and Watson, J. T.: Mass Spectrometry on the Chromatographic Time Scale: Realistic Expectations, Anal. Chem. 55, 997A-915A (1983)

[2] Gross, M. L., Rempel, D. L.: Science, 226, 261 (1984)

[3] Cameron, A. E. and Eggers, D. F. Jr., Rev. Sci Instrument., 19, 605 (1948)

[4] Wiley, W. C. and McLaren, I. H.: Time-of-Flight Mass Spectrometer with Improved Resolution. Rev. Sci. Instrument., 26, 1150, (1955),

[5] Gohlke, R. S., Anal Chem., 31, 535 (1959)

[6] Wollnik, H.: Time-Of-Flight Mass Analyzer. Mass Spectrometry Reviews, 12, 89-114 (1993)

[7] Ioanoviciu, D., Yechak G. E. and Enke C. G.: Second-Order Space-Time Transfer Matrix of The Two Stage Electrostatic Mirror. Int. J. Mass Spectrom. Ion Processes, 94, 281-291 (1989)

[8] Bosel, U., Weinkauf, R. And Schlag, E. W. : Reflectron Time-of-Flight Mass Spectrometry and Laser Excitation for the analysis of Neutrals, Ionized Moleclues and Secondary Fragments. Int. J. Mass Spectrom. Ion Processes, 111, 121-166 (1992)

[9] Walter, K., Boesl, U., and Schlag, E.W.: Mass Resolution of 10000 in a laser ionization time-of flight mass Spectrometer. Anal. Chem., 57, 1884-1889 (1985)

[10] Marable N. L. and Sanzone, G.: High -Resolution Time-of-Flight Mass Spectrometry Theory of The Impulse-Focused Time-of-Flight Mass Spectrometer, Int. J. Mass Spectrom. Ion Processes, 120, 97-100 (1993)

[11] Eckenrode, B. A., Watson, J. T., and Enke C.G. and Holland J. F.: Complete Mass Spectrometry/Mass Spectrometry Data Field Acquisition on the Chromatographic

---

Time Scale by Time-Resolved Ion Momentum Spectrometry with Time-Array Detection, Anal Chem. 62, 1362-1367 (1990)

[12] Ben-Itzhak, I., Carnes, K. D. And DePaola B. D.: Fast Timing Signal Sorter for Multiple Hit Coincidence Time-of-Flight Spectroscopy, Rev. Sci. Instrum. 63, 5780-5783 (1992)

[13] Holland, J. F., Newcombe, B., Tecklenburg, R. Jr , Davenport, M., Allison, J., Watson, J. T., Enke, C. G.: Design, Construction, and Evaluation of an Integrating Transient Recorder for Data Acquisition in Capillary Gas Chromatography/Time-of-Flight Mass Spectrometry. Rev. Sci. Instrum., 1991, 62, 69-76 (1991)

[14] Erickson, E. D., Yefchak, G. E., Enke C. G., and Holland J. F.: Mass Dependence of Time-Lag Focusing in Time-of-Flight Mass Spectrometry — An analysis. Int. J. Mass Spectrom. Ion Processes, 97, 87-106 (1990)

[15] a. Mamyrin, B. A., Karataev, V. I., Shmikk, D. V., and Zagulin V. A.: The Mass Reflectron, A New Nonmagnetic Time-of-Flight Mass Spectrometer with High Resolution. Sov. Phys. JETP, 37, 1, 45-48 (1973)

b. Mamyrin, B. A., and Shmikk, D. V.; The Linear Mass Reflectron. Sov. Phys. JETP 49, 5, (1979)

[16] Stein, R.: On Time Focusing and Phase Space Dynamics in Time-of-Flight Mass Spectrometer Design. Int. J. Mass Spectrom. Ion Processes, 132, 29-47 (1994)

[17] a. Kinsel, G. R. and Johnston, M. V.: Post Source Pulse Focusing : A Simple Method to Achieve Improved Resolution in a Time-of-Flight Mass Spectrometer, Int. J. Mass Spectrom. Ion Processes, 91, 157-176 (1989)

b. Kinsel, G. R., Mowry, C. D., McKeown, P. J. and Johnston, M. V.: Resolution Enhancement in Linear Time-of Flight Mass Spectrometry by Post-Source Pulse Focusing, Int. J. Mass Spectrom. Ion Processes, 91, 157-176 (1989)

[18] Yefchak, G. E., Enke, C. G. and Holland, J. F.: Models for Mass Independent Space and Energy Focusing in Time-of-Flight Mass Spectrometer. Inter J. Mass Spectrom. Ion Processes, 87, 313-330 (1989)

---

[19] Grix, R., Gruener, U., Li, G., Stroh, H. and Wollnik, H.: An Electron Impact Storage Ion Source for Time-of-Flight Mass Spectrometers. Int. J. Mass Spectrom. Ion Processes, 93, 323-330 (1989).

[20] Mary Ann Seeterlin, Ph. D. Dissertation, Michigan State University, 1993

[21] Studier, M. H.: Continuous Ion Source For a Time-of-Flight Mass Spectrometer. Rev. Sci. Instrum., 34, 1367-1370 (1963)

[22] Stafford, G. C. (Jr.), Kelley, P. E., Syka, J. E. P., Reynolds, W. E., and Todd, J. F. J.: Recent Improvements in and Analytical Applications of Advanced Ion Trap Technology. Int. J. Mass Spectrom. Ion Processes, 60, 85-98 (1984).

[23] Kaiser, R. E. (Jr.), Cooks, R. G., Stafford, G. C. (Jr.), Syka, J. E. P., and Hemberger, P. H.: Operation of a Quadrupole Ion Trap Mass Spectrometer To Achieve High Mass/Charge Ratios. Int. J. Mass Spectrom. Ion Processes, 106: 79-115 (1991).

[24] Williams, J. D., Cox, K. A., Cooks, R. G., Kaiser, R. E. (Jr.), and Schwartz, J. C.: High Mass-Resolution Using a Quadrupole Ion-Trap Mass Spectrometer. Rapid Commun. Mass Spectrom., 5, 327-329 (1991).

[25] Eckenrode, B. A., McLuckey, S. A., and Glish, G. L.: Comparison of Electron Ionization and Chemical Ionization Sensitivities in an Ion Trap Mass Spectrometer. Int. J. Mass Spectrom. Ion Processes, 106, 137-157 (1991).

[26] Louris, J. N., Amy, J. W., Ridley, T. Y., and Cooks, R. G.: Injection of Ions into a Quadrupole Ion Trap Mass Spectrometer. Int. J. Mass Spectrom. Ion Processes, 88, 97-111 (1989).

[27] Eckenrode, B. A., McLuckey, S. A., and Glish, G. L.: Comparison of Electron Ionization and Chemical Ionization Sensitivities in an Ion Trap Mass Spectrometer. Int. J. Mass Spectrom. Ion Processes, 106, 137-157 (1991).

[28] Mather, R. E., Lawson, G., and Todd, J. F. J.: The Quadrupole Ion Storage Trap (Quistor) as a Low-Pressure Chemical Ionization Source for a Magnetic Sector Mass Spectrometer. Int. J. Mass Spectrom. Ion Physics, 28, 347-364 (1978).

[29] Brodbelt, J. S., Louris, J. N., and Cooks, R. G.: Chemical Ionization in an Ion Trap Mass Spectrometer. Anal. Chem., 59, 1278-1285 (1987).

---

[30] Boswell, S. M., Mather, R. E., and Todd, J. F. J.: Chemical Ionization in the Ion Trap: A Comparative Study. Int. J. Mass Spectrom. Ion Processes, 99, 139-149 (1990).

[31] Eckenrode, B. A., Glish, G. L., and McLuckey, S. A.: Negative Ion Chemical Ionization in a Quadrupole Ion Trap Using Reagent Anions Injected From an External Ion Source. Int. J. Mass Spectrom. Ion Processes, 99, 151-167 (1990).

[32] Van Berkel, G. J., Glish, G. L., and McLuckey, S. A.: Electrospray Ionization Combined with Ion Trap Mass Spectrometry. Anal. Chem., 62, 1284-1295 (1990).

[33] Van Berkel, G. J., McLuckey, S. A., and Glish, G. L.: Electrospray Ionization of Porphyrins Using a Quadrupole Ion Trap for Mass Analysis. Anal. Chem., 63, 1098-1109 (1991).

[34] McLuckey, S. A., Van Berkel, G. J., Glish, G. L., Huang, E. C., and Henion, J. D.: Ion Spray Liquid Chromatography/Ion Trap Mass Spectrometry Determination of Biomolecules. Anal. Chem., 63, 375-383 (1991).

[35] Kaiser, R. E. (Jr.), Williams, J. D., Schwartz, J. C., Lammert, S. A., and Cooks, R. G.: Thermospray LC/MS with a Quadrupole Ion Trap and Recent Applications of Ion Injection. Presented at the 37th ASMS Conference on Mass Spectrometry and Allied Topics, 369-370 (1989).

[36] Kaiser, R. E. (Jr.), Williams, J. D., Lammert, S. A., Cooks, R. G., and Zakett, D.: Thermospray Liquid Chromatography-Mass Spectrometry with a Quadrupole Ion Trap Mass Spectrometer. J. Chromatog., 562, 3-11 (1991).

[37] McLuckey, S. A., Glish, G. L., and Asano, K. G.: Coupling of an Atmospheric-Sampling Ion Source with an Ion-Trap Mass Spectrometer. Analytica Chimica Acta, 225, 25-35 (1989).

[38] a. Van Berkel, G. J., Glish, G. L., and McLuckey, S. A.: Electrospray Ionization Combined with Ion Trap Mass Spectrometry. Anal. Chem., 62, 1284-1295 (1990).

[39] Todd, J. F. J., Mylchreest, I. C., Berry, A. J., Games, D. E., and Smith, R. D.: Supercritical Fluid Chromatography/Mass Spectrometry with an Ion Trap Detector. Rapid Commun. Mass Spectrom., 2, 55-58 (1988).

---

[40] Louris, J. N., Amy, J. W., Ridley, T. Y., and Cooks, R. G.: Injection of Ions into a Quadrupole Ion Trap Mass Spectrometer. Int. J. Mass Spectrom. Ion Processes, 88, 97-111 (1989).

[41] Heller, D. N., Lys, I., Cotter, R. J., and Uy, O. M: Laser Desorption from a Probe in the Cavity of a Quadrupole Ion Storage Mass Spectrometer. Anal. Chem., 61, 1083-1086 (1989).

[42] Goeringer, D. E., Glish, G. L., Asano, K. G., and McLuckey, S. A.: Applications of Laser Desorption in an Ion Trap Mass Spectrometer. Presented at the 37th ASMS Conference on Mass Spectrometry and Allied Topics, 1260-1261 (1989).

[43] Louris, J. N., Brodbelt, J. S., and Cooks, R. G.: Photodissociation in a Quadrupole Ion Trap Mass Spectrometer Using a Fiber Optic Interface. Int. J. Mass Spectrom. Ion Processes, 75, 345-352 (1987).

[44] Creaser, C. S., McCoustra, M. R. S., and O'Neill, K. E.: Combined Gas Chromatography/Tandem Mass Spectrometry Using Laser Photodissociation. Org. Mass Spectrom., 26(4), 335-338 (1991).

[45] Lifshitz, C.: Dissociative Photoionization in the Vacuum UV Region with Ion Trapping. Int. J. Mass Spectrom. Ion Processes, 106, 159-173 (1991).

[46] Goeringer, D. E., Glish, G. L., and McLuckey, S. A.: Fixed-Wavelength Laser Ionization/Tandem Mass Spectrometry for Mixture Analysis in the Quadrupole Ion Trap. Anal. Chem., 63, 1186-1192 (1991).

[47] Mosburg Jr., E. R., Vedel, M. Zerega, Y., Vedel, F. and Anere, J.: A Time-of-Flight Method for Studying the Properties of an Ion Cloud Strored in An RF Trap. Int. J. Mass Spectrom. Ion Processes, 77, 1-12 (1987).

[48] Waldren, R. M. and Todd, J. F. J.: The Quadrupole Ion Store (QUISTOR). Part III. Studies on Phase-Synchronized Ion Ejection; The Effects of Ejection Pulse Width and Detection Pulse Delay. Int. J. Mass Spectrom. Ion Phys. 29, 315-335. (1979)

[49] Lawson, G., Bonner, R. F. and Todd J. F. J.: The Quadrupole Ion Store(Quistor) as a Novel Source for a Mass Spectrometer, J. Physics E: Scientific Instruments, 6, 357-362 (1973)

---

[50] Brincourt, G., Catella, R., Zerega, Y. and Andre, J.: Time-of-flight Detection of Ions Ejected from a Radio Frequency Quadrupole Trap: Experimental Determination of Their f_z Secular Frequency, Chemical Physics Letters, 174, 6, 626-630 (1990)

[51] a. Michael, S. M., Chien, B. M., and Lubman, D. M.: An Ion Trap Storage /Time-of-Flight Mass Spectrometer. Rev. Sci. Instrum. 63, 4277-4284, (1992).

b. Chien, B. M., Michael, S. M. and Lubman, D. M.: Enhancement of Resolution in Matrix-Assisted Laser Desorption Using an Ion-Trap Storage/ Reflectron Time-of-Flight Mass Spectrometer. Rapid Comm. Mass Spectrom. 7,837-843 (1993).

c. Chien, B. M., Michael, S. M. and Lubman, D. M.: Plasma Source Atmospheric Pressure Ionization Detection of Liquid Injection Using an Ion Trap Storage/Reflectron Time-of Flight Mass Spectrometer. Anal. Chem. 65, 1916-1024 (1993).

d. Michael, S. M Chien, B. M., and Lubman, D. M.: Detection of Electrospray Ionization Using an Ion Trap Storage/Reflectron Time-of Flight Mass Spectrometer. Anal. Chem. 65, 2614-2620 (1993).

e. Chien, B. M., and Lubman, D. M.: Analysis of the Fragments from Collision Induced Dissociation of Electrospray-Produced Peptide Ions Using an Ion Trap Storage/Reflectron Time-of Flight Mass Spectrometer. Anal. Chem. 66, 1630-1636 (1994).

f. Qian, M.; Lubman, D. M.: Analysis of Tryptic Digests Using Michrobore HPLC with an Ion Trap Storage/ Reflectron Time -of-Flight Detector. Anal Chem. 67, 2870-2877 (1995)

g. Lee, H., Lubman, D. M.: Sequence-Specific Fragmentation Generated by Matrix-Assisted Laser Desorption/Ionization in a Quadrupole Ion Trap/ Reflectron Time-of-Flight Device. Anal Chem. 67, 1400-1408 (1995)

h. He, L., Liang, L., and Lubman, D. M.: Continuous-Flow MALDI Mass Spectrometry Using An Ion Trap/ Reflectron Time-of -Flight Detector. Anal Chem. 67 , 4127-4132 (1995)

Chapter 2 Theoretical development and computer simulation of the segmented ring ion trap source for time-of-flight mass spectrometry

2.1 Background

The concept of using an ion trap as an ion storage source for time-of-flight mass spectrometry has existed in Professor Enke's group for several years. In 1991, Paul Vlasak and Professor Enke submitted a grant application for the development of a quadrupole ion trap/time-of-flight mass spectrometry system as part of the NIH/MSU Mass Spectrometry Facility renewal proposal. During the summer of 1992, Professor Enke, Professor Holland and I started to work on a revised version of this grant application to be submitted as a independently-funded project. The idea of using a segmented ring ion trap storage source for the time-of-flight mass spectrometer was delineated at that time.

2.1.1 Quadrupole ion trap

A suitable electrode configuration for trapping ions is the quadrupole ion trap which is composed of a hyperbolic ring electrode located between two hyperbolic end caps. This arrangement was first proposed by Paul and Steinwedel in 1956[1].The general geometry of the device is described by the relationship

$$r_0^2 = 2z_0^2$$

wher

betw

and

can

$$\frac{d^2x}{dr^2}$$

in w

$a_z =$

$q_z =$

whe

volt

abo

fun

dia

par

whi

has

high

$\omega_r =$

where r_0 is defined as the radius of the ring electrode and $2z_0$ is the separation between two end-caps. A dynamic voltage is applied between the ring electrode and the end caps. The resulting ion motion, resolved into r and z components, can be represented by the Mathieu differential equation

$$\frac{d^2x}{dr^2} + (a_x + 2q_x \cos 2\gamma)_x = 0$$

in which $x = r$ or z and

$$a_z = -2a_r = -\frac{8eU}{mr_0^2\Omega^2}$$

$$q_z = -2q_r = -\frac{4eV}{mr_0^2\Omega^2}\omega t$$

where V is the RF voltage (zero to peak), Ω is the RF frequency and U is the DC voltage between the ring and cap electrodes. The parameters a and q defined above determine whether the ion trajectory is stable (bound) or unstable (unbounded). Regions of stability may be plotted in (a, q) space giving a stability diagram as shown in Figure 2-1[3].

Iso-β lines are also shown in Figure 2-1. The significance of the parameter β is that it is related to the frequencies of ion motion. β is a parameter which only depends on the value of a and q. It can be shown that the ion motion has a fundamental or “secular” frequency of oscillation ω_0 and a number of higher order components of frequency ω_n given by

$$\omega_n = (2n+\beta)\frac{\Omega}{2},\ n = 0,\ 1,\ 2\ldots\ldots$$

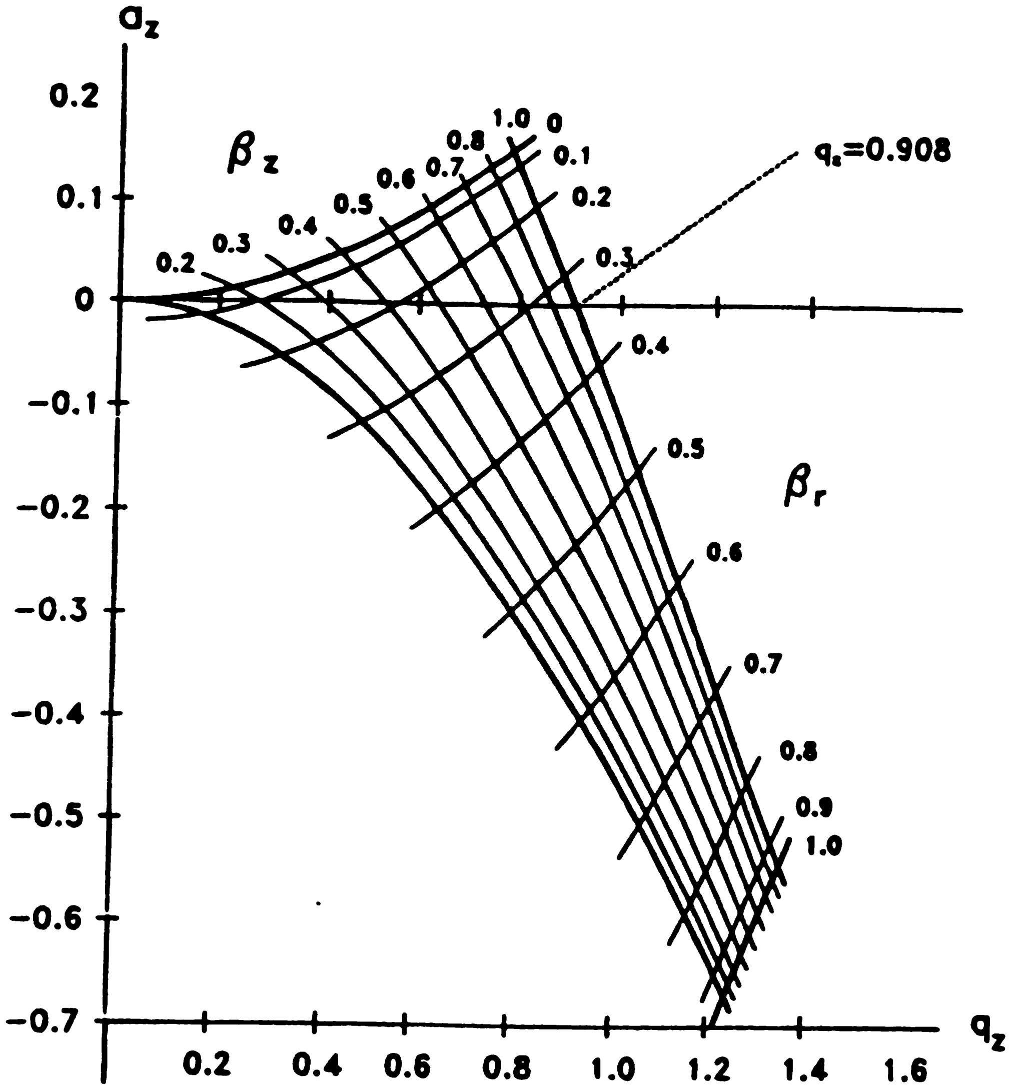

Figure 2-1. Stability diagram for the three-dimensional quadrupole ion trap.

Th

be

rep

an

two

the

pos

the t

desc

ripple

at se

D_z as

$D_z = $

$D_z = 2$

This m

trap w

$N_{max} = $

$N_{max} = $

The solution to the Mathieu equation allows stable motion only for β values between 0 and 1. Hence, the two sets of intersecting lines in Figure 2-1 represent frequencies of the ion motion along the two perpendicular *r* and *z* axes and are denoted by β_r and β_z which is related to the oscillating frequency in the two dimensions ω_z, ω_r.

The Mathieu equation assumes that there is only one ion in the trap. Also the equation assumes that the hyperbolic electrodes are perfectly shaped and positioned. In practical cases, a considerable amount of space charge exists in the trap and this alters the potential field within the ion trap.

Dawson and coworkers[2] developed a pseudopotential-well method describing the ion motion in the quadrupole ion trap. Disregarding the trajectory ripple arising from higher order oscillations, ions exhibit simple oscillatory motion at secular frequencies ω_{0z}, ω_{0r} in a so-called pseudopotential well of depth D_z and D_r as described in Figure 2-2.

$$D_z = -\frac{eV^2}{4mz_0^2\Omega^2}$$

$$D_z = 2D_r$$

This model has been used to calculate the maximum ion density N_{max} in the ion trap when the space charge effect is considered[3].

$$N_{max} = \frac{3}{64\pi}\left(\frac{m\Omega^2}{e^2}\right)q_z^2$$

$$N_{max} = \frac{3}{4\pi}\left(\frac{V^2}{m\Omega^2 r_0^4}\right)$$

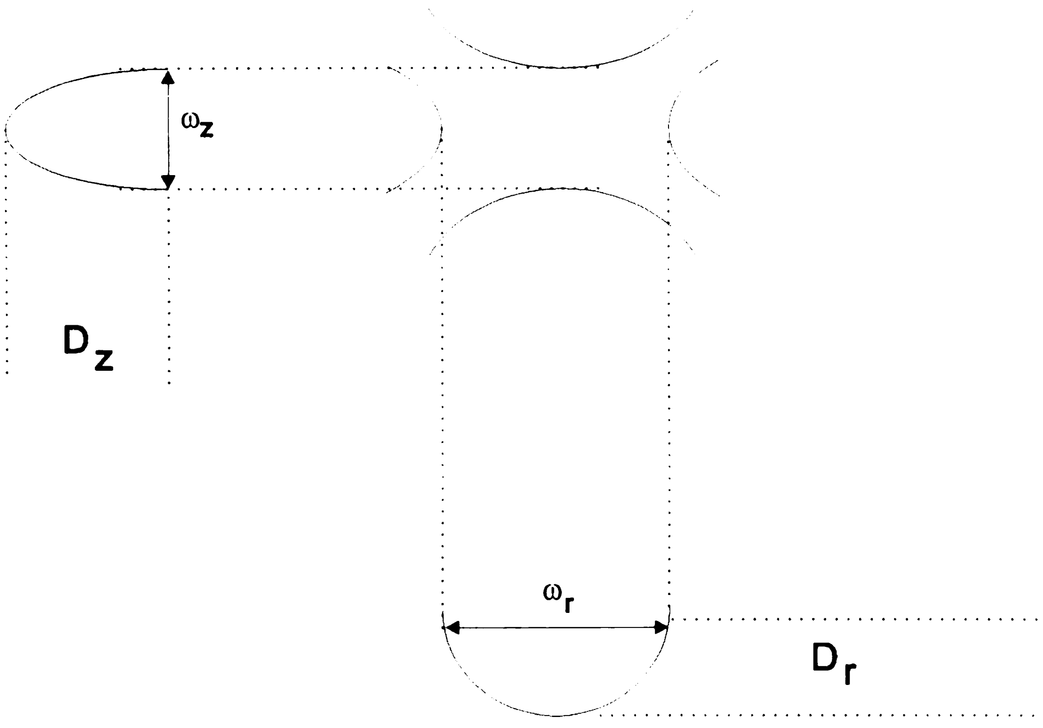

Figure 2-2. Representative diagram of the parabolic pseudopotential well D_r and D_z.The respective secular frequencies of ion oscillation within the wells are ω_z and ω_r.

If t

ma

kep

freq

2.1

An

elec

and

qua

mini

is 2z

With

ionic

with

$\alpha = a$

The

$r_i^2=2z$

Rung

quadr

for the

on a a

If the ion trap is operated under conditions which maintain a constant V, the maximum ion density is inversely proportional to the mass and frequency. If q_z is kept constant, the maximum ion density is proportional to the mass and the RF frequency.

2.1.2 Cylindrical ion trap

An ion storage device of cylindrical geometry is one in which a cylindrical barrel electrode of radius r_1 replaces the hyperbolic surface ring electrode of radius r_0 and two planar disk (end cap) electrodes replace the end-cap electrodes of the quadrupole ion trap. The distance between the planar disks is $2z_1$, while the minimum separation between the end-cap electrodes of the quadrupole ion trap is $2z_0$. A patent for a cylindrical ion trap was issued to Langmuir et al. in 1962[4]. With some mathematical approximations, Benilan and Audoin[5] deduced that ionic motion in the cylindrical ion trap may be described by the Mathieu equation with *a* and *q* replaced by α and χ, given by

$$\alpha = a_z\left(\frac{r_0}{r_1}\right)^2, \chi = q_z\left(\frac{r_0}{r_1}\right)^2$$

The theoretical stability diagrams of the two different geometries $r_1 = z_1$, and $r_1^2 = 2z_1^2$, were obtained by numerically calculating ion trajectories, using the Runge-Kutta method of integration, and were compared with that of the quadrupole ion trap. These stability diagrams involving the α and χ parameters for these two cylindrical ion traps are very similar to the stability diagram based on *a* and *q* for the quadrupole ion trap[5]. Bonner et al.[6] discussed the theoretical aspects of the cylindrical ion trap with RF applied to the ring electrode and presented first experimental evidence of ion storage in a cylindrical ion trap. For a cylindrical ion trap with the geometric relationship $r_1^2 = 2z_1^2$, the potential distribution is

$$\varphi(r,z) = 4V_0 \sum_n \frac{(-1)^n}{(2N+1)\pi} \frac{I_0(P_n r)}{I_0(P_n r_1)} \cos(p_n z)$$

$$p_n = \frac{(2n+1)\pi}{2z_1}$$

where I_0 is a zero-order modified Bessel function of the first kind. In the case of the quadrupole ion trap, the electric fields in the r and z direction depend only on r and z respectively; thus the fields and the equations of the ion motion are uncoupled. In the case of cylindrical ion trap, both the fields and the equations of the ion motion are coupled. However, by a numerical calculation method, Bonner et al. found that the equipotential fields between the quadrupole ion trap and the cylindrical ion trap were quite similar. This provided an explanation for the ion storage characteristic within the cylindrical ion trap. Mather et al.[7] determined experimentally the stability diagrams of three cylindrical ion traps with the geometric ratios of r_1^2/z_1^2 of 1.476, 1.966, and 1.766. The RF frequency was fixed. The boundary RF voltages with regard to different DC offset voltage settings were determined according to the existence of Ar^+ stored in these cylindrical ion traps. They concluded that the experimental results were in broad agreement with theoretical calculations allowing for some possible distortion due to the space charge effect caused by multiple ions present in the trap.

2.1.3 Segmented ring ion trap

The segmented ring ion trap is developed to be an ion storage source for the time-of-flight mass spectrometer[8]. It consists of two flat end plates and a stack of ring diaphragms instead of one center ring electrode as in the quadrupole ion trap or cylindrical ion trap. Each of the end plates has a center hole space covered with a mesh screen to allow ion transmission. The inside diameter of the ring electrode is defined as $2r_2$ and the distance between two end plates is defined as $2z_2$. Theoretically, the potential field of the cylindrical ion trap could be achieved perfectly by the segmented ring ion trap as the space between each diaphragm is decreased and the number of ring diaphragms is increased. For electronic circuit simplicity, the number of ring diaphragms composing the ring electrode in our segmented ring ion trap is minimized to two. The ion storage characteristics and the time-of-flight mass analysis characteristics of this segmented ring ion trap source were first examined by computer simulation.

2.1.4 Computer simulation

In 1968, a numerical calculation was used by Dawson and Whetten[9] to analyze single ion trajectories in the quadrupole ion trap. Benilan and Audoin[5] used a numerical method to solve the Laplace equation to calculate the potential field of cylindrical ion traps and an ion trap with spherical end caps and a ring electrode of circular cross section. Since then, computer simulation has been widely used to simulate the behavior of ion storage, mass selective isolation, ion collisions with the bath gas and the effect of nonlinear resonance in the quadrupole ion trap. March et al.[10] developed a computer simulation program called SPQR (specific program for quadrupole resonance) which uses a field interpolation method and is able to simulate the mass selective isolation and resonance excitation of ions stored in the quadrupole ion trap. The ITSIM simulation program[11] developed at Purdue University is able to simulate the behavior of a large number of ions in the different ITMS operation modes. The effects of space charge and bath gas collision are considered. The imperfection of the electrode geometry of a real ion trap mass spectrometer is accounted for by expanding electric field equations to also include higher-order terms based on Legendre polynomials. Franzen[12] simulated ion behavior when multipole fields are superimposed on the quadrupole field.

SIMION[13] is a computer program developed by Dahl and Delmore. Iterated numeric calculation gives the ion trajectories under the electric field generated by any specified arrangement of electrodes. Ma et al.[14] demonstrated the application of SIMION for the simulation of quadrupole ion trap operation.

The electric field resulting from a cylindrical ion trap or the segmented ring ion trap is much more complex than the quadrupole field. The superimposed multipole field of the segmented ring ion trap is difficult to describe or solve mathematically. SIMION can generate the electric field directly from the electrode geometry. For the development of the segmented ring ion trap, SIMION was used to compare the ion storage characteristics of the quadrupole ion trap, the cylindrical ion trap and the segmented ring ion trap. SIMION was also used to simulate the time-of-flight behavior of ions extracted from these different ion trap geometries.

2.2 Theoretical development and computer simulation of the segmented ring ion trap as an ion trap storage device

The electrodes of ion trap are represented by a set of point electrodes in SIMION. The distance between the two flat end plates of the segmented ring ion trap (SRIT) is 94 grid units which represents 9.4 mm ($2r_2$ = 9.4 mm). The conversion factor is 0.1 mm/grid. A cylindrical ion trap and a quadrupole ion trap were also simulated. The cylindrical ion trap has the same conversion factor and dimensions as the segmented ring ion trap. For the quadrupole ion trap, the distance between the end caps is 57 grid units. A conversion factor of 0.1649 mm/grid was used to obtain the same 9.4 mm distance between two end caps. The geometric configurations are $z_0^2=2\,r_0^2$, $z_1^2=2\,r_1^2$ and $z_2^2=2\,r_2^2$ for these three kinds of ion trap. A user program from David Dahl was modified to apply a cosine function dynamic voltage and a DC offset to the ring electrodes. The end caps (end plates) were set to 0 V. The time interval between each calculation is less than 1 ns of ion motion. A time interval of 0.1 ns was employed in a few instances for comparison. No significant difference in the ion trajectories was noticed except the calculation time was increased dramatically.

2.2.1 Computer simulation of the equipotential field of the ion traps

The SIMION program was used to obtain the equipotential field lines of the ion traps. The voltage of both ring electrode elements was set at 300 V (Figures 2-4, and 2-3(a)) or 350 V (Figure 2-3(b)). The end caps (end plates) were set at 0 V. The equipotential lines (red lines) are voltages starting at 25 V and increasing in 25 V intervals. The equipotential lines are quite similar for the cylindrical ion trap and the quadrupole ion trap. Because of the potential lines leaking into the space between the two ring electrode elements, the potential lines inside the ion trap are less dense for the segmented ring ion trap (Figure 2-3(a)) than for the quadrupole ion trap(Figure 2-4 (b)) and the cylindrical ion trap (Figure 2-4(a)) when same amplitude of RF voltage is applied. This situation can be compensated for by applying a higher voltage to the ring electrode elements in the segmented ring ion trap. The potential lines generated in the segmented ring ion trap with 350 V applied to the ring electrode elements (Figure 2-3(b)) are quite similar to those in the cylindrical ion trap with 300 V applied (Figure 2-4(a)).

2.2.2 Computer simulation of ion trajectories

Ion trajectory simulations were obtained by using SIMION with a modified user program from Dahl[13]. The initial ion position was set at $r=0.2r_2$ and $z=0.2z_2$. The initial kinetic energy was set to 0 eV. The collision factor (MFP) was set to 4 x10^6 mm. The cosine wave RF frequency is 1.2 MHz and the RF voltage 300 V (zero to peak). The positions in the r and z dimensions of an ion with m/z 100 in the

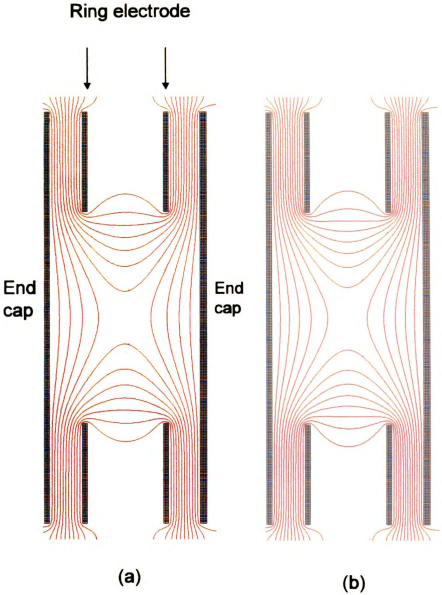

(a) (b)

Figure 2-3. Equipotential contours of the segmented ring ion trap. The red lines are equipotential lines starting 25 V in 25 V increments. The endplates are 0 V and ring electrode is 300 V (a) and 350 V (b).

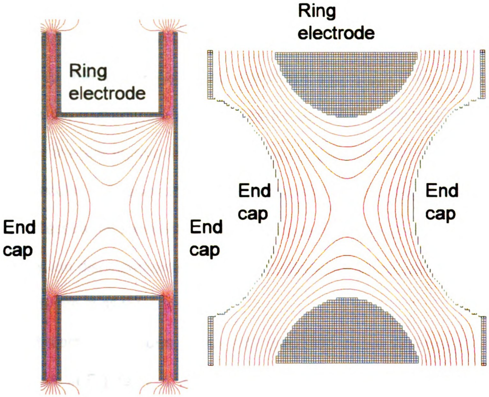

(a) (b)

Figure 2-4. Equipotential contours of (a) Cylindrical ion trap (b) Quadruple ion trap.The red lines are equipotential lines from 25 V to 275 V in 25 V intervals.
The end caps are 0 V and ring electrodes are 300 V.

se

tim

mr

the

tra

io:

0.

fre

0.2

Th

the

co

mr

tra

tra

2.2

Th

seg

ver

$\pi/4$

the

segmented ring ion trap, cylindrical ion trap and quadrupole ion trap vs. storage time are shown in Figures 2-5, 2-6, and 2-7. Although different degrees of multipole fields exist in the cylindrical ion trap and the segmented ring ion trap, the simulations clearly show that the ion motion characteristic of stable ion trajectories are quite similar in all three ion traps. The fundamental frequency of ion motion in the r dimension is 0.097 MHz for the segmented ring ion trap and 0.11 MHz for the quadrupole and cylindrical ion traps. The fundamental frequency in the z dimension is 0.17 MHz for the segmented ring ion trap and 0.21 MHz for the quadrupole and cylindrical ion traps (Figures 2-5, 2-6, and 2-7). The lower secular frequency of the segmented ring ion trap(Figure 2-5) is due to the lower effective field strength in the trap as represented in the equipotential contour. The ion displacements in the *z* and *r* dimensions are approximately 1.5 mm and 1.25 mm in all three ion traps.

The trajectories of ions of m/z 100 and 2000 in the segmented ring ion trap are shown in Figures 2-8, and 2-9. The ion motion characteristic of this ion trap is quite similar to that of the quadrupole ion trap.

2.2.3 Effect of initial phase angle of RF field on the ion motion

The effect of the RF phase applied when an ion was initially placed in the segmented ion trap was examined. The ion position in the *r* and *z* dimensions versus the ion storage time is shown for four different initial RF phase angles, 0, $\pi/4$, π and $3\pi/4$, as represented in Figures 2-10, and 2-11. The displacement in the *z* dimension is about 2.5 mm for initial phases of $\pi/4$ and $3\pi/4$, 1.5 mm for

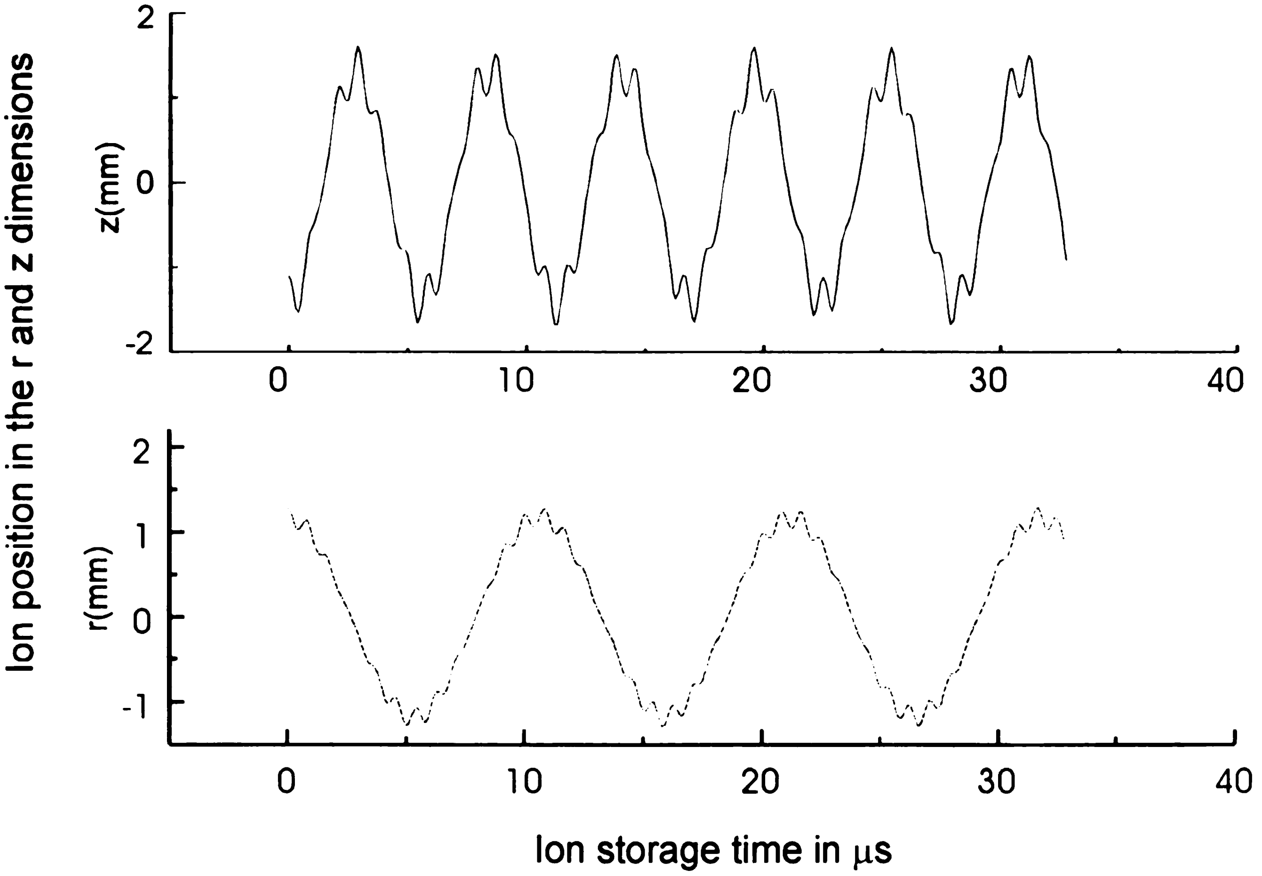

Figure 2-5 .The relationship between the ion storage time and the ion position in the r and z dimensions in the segmented ring ion trap.

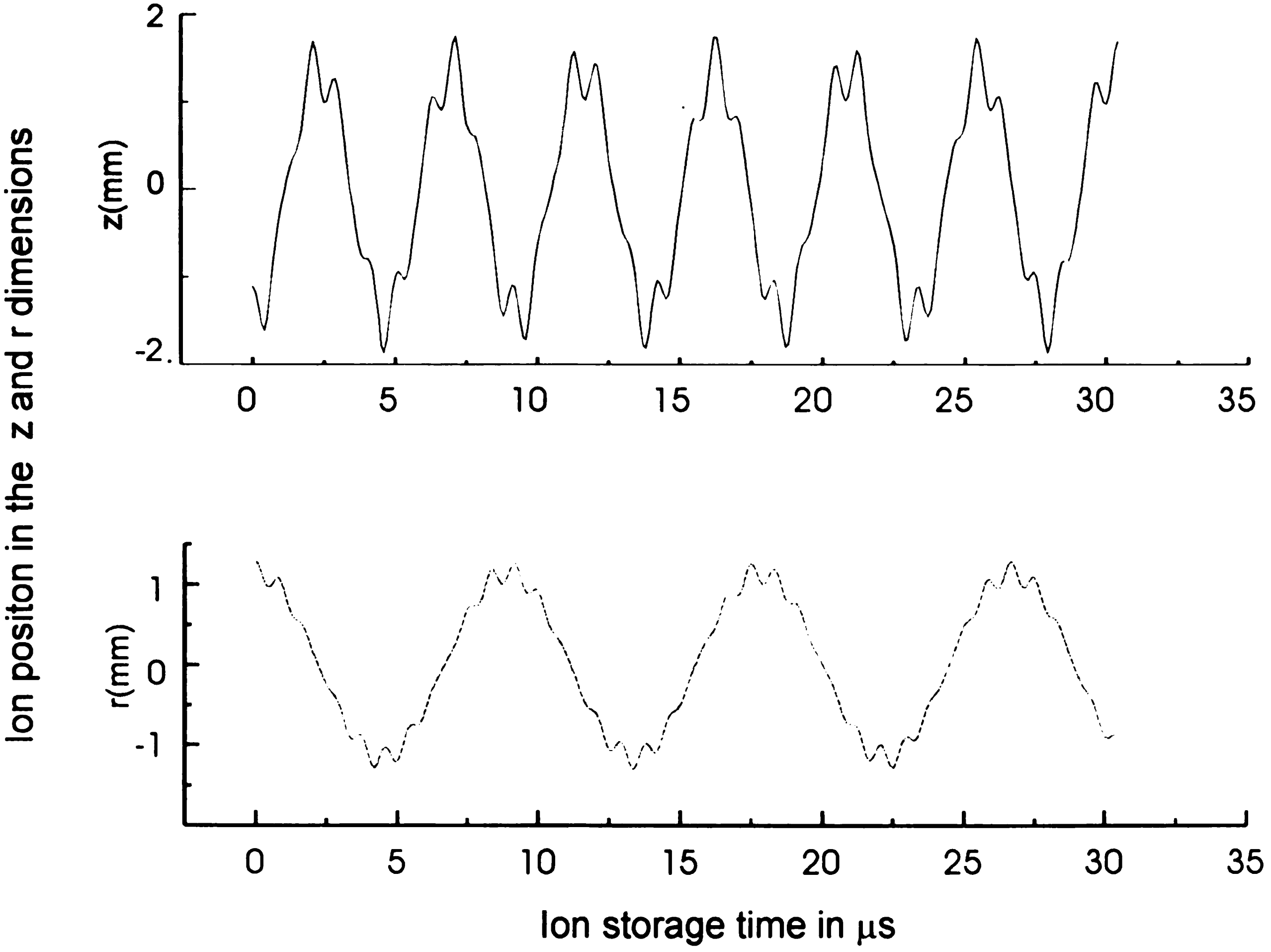

Figure 2-6. The relationship between the ion storage time and the ion position in the r and z dimensions in the cylindrical ion trap.

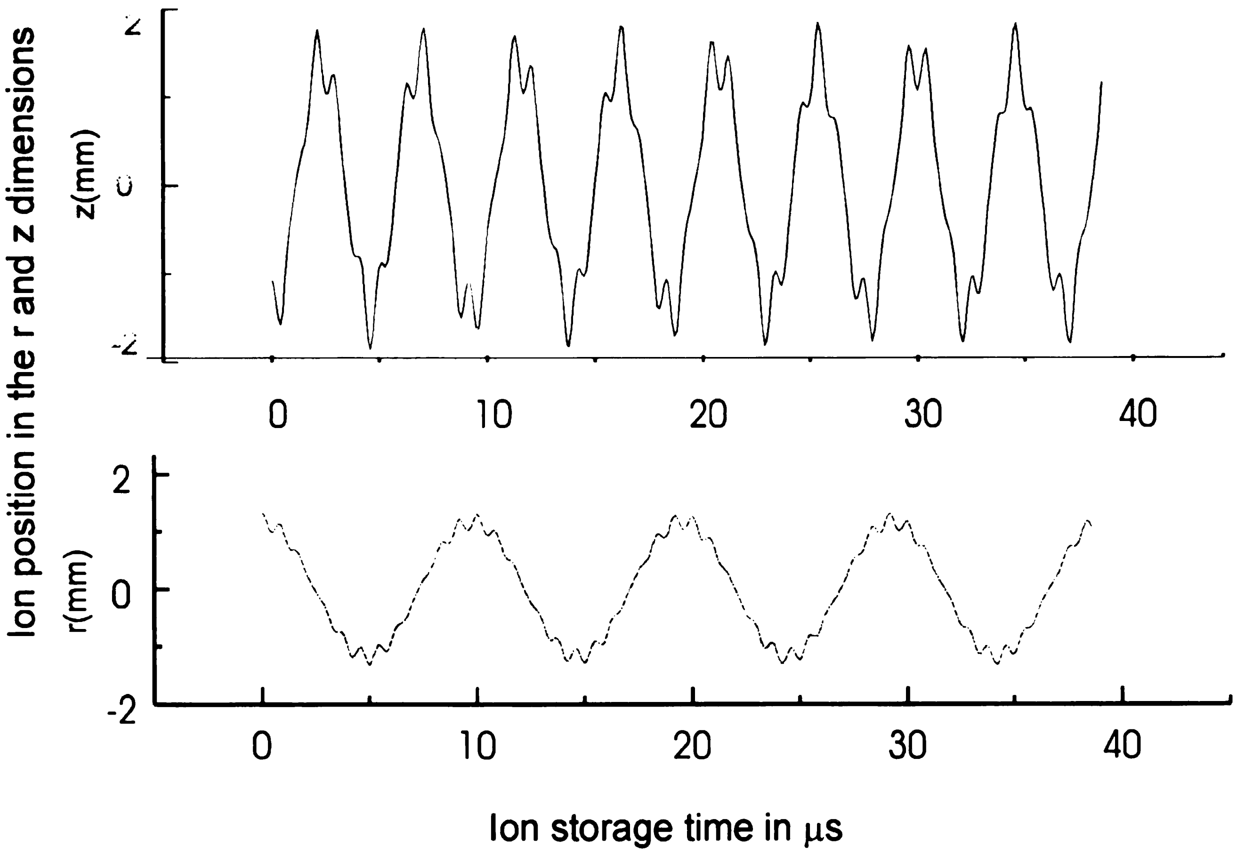

Figure 2-7. The relationship between the ion storage time and the ion position in the r and z dimensions in the quadrupole ion trap.

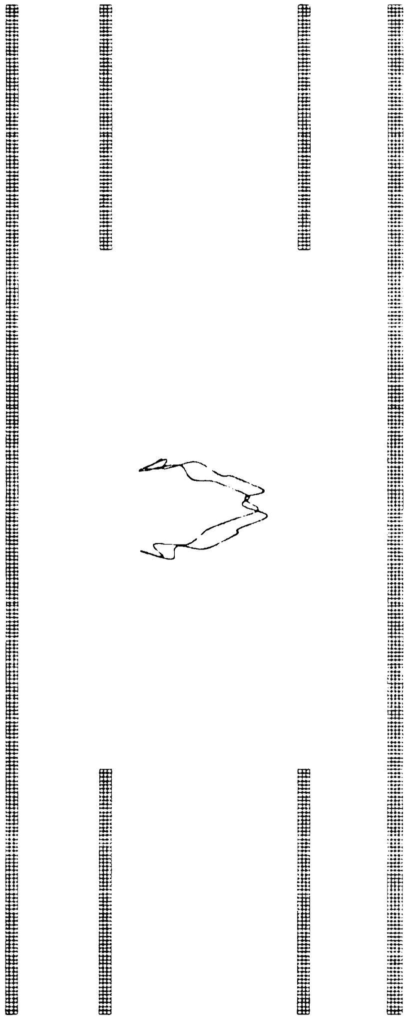

Figure 2-8. Computer simulated ion trajectory of an ion of m/z 100 for an RF of 1.2 MHz and 300 V (zero to peak) in the segmented ring ion trap

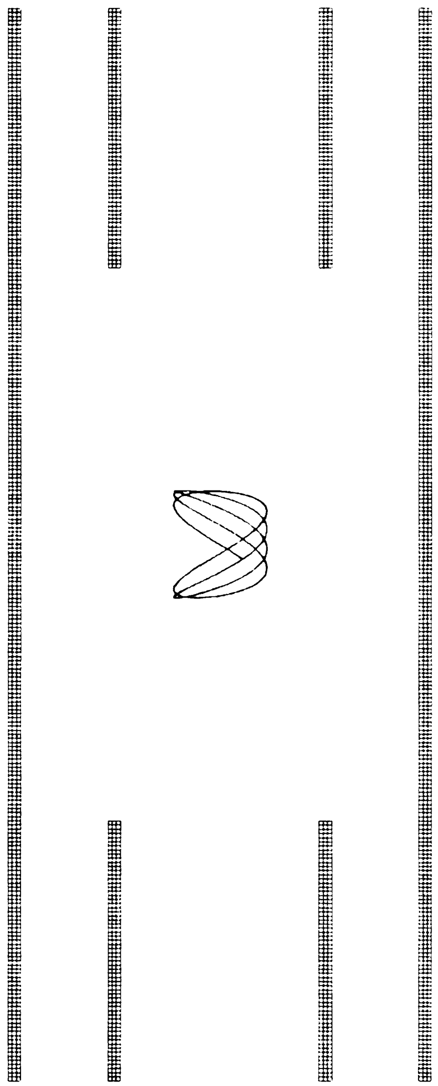

Figure 2-9. Computer simulated ion trajectory of an ion of m/z 2000 for an RF of 1.2 MHz and 300 V (zero to peak) in the segmented ring ion trap

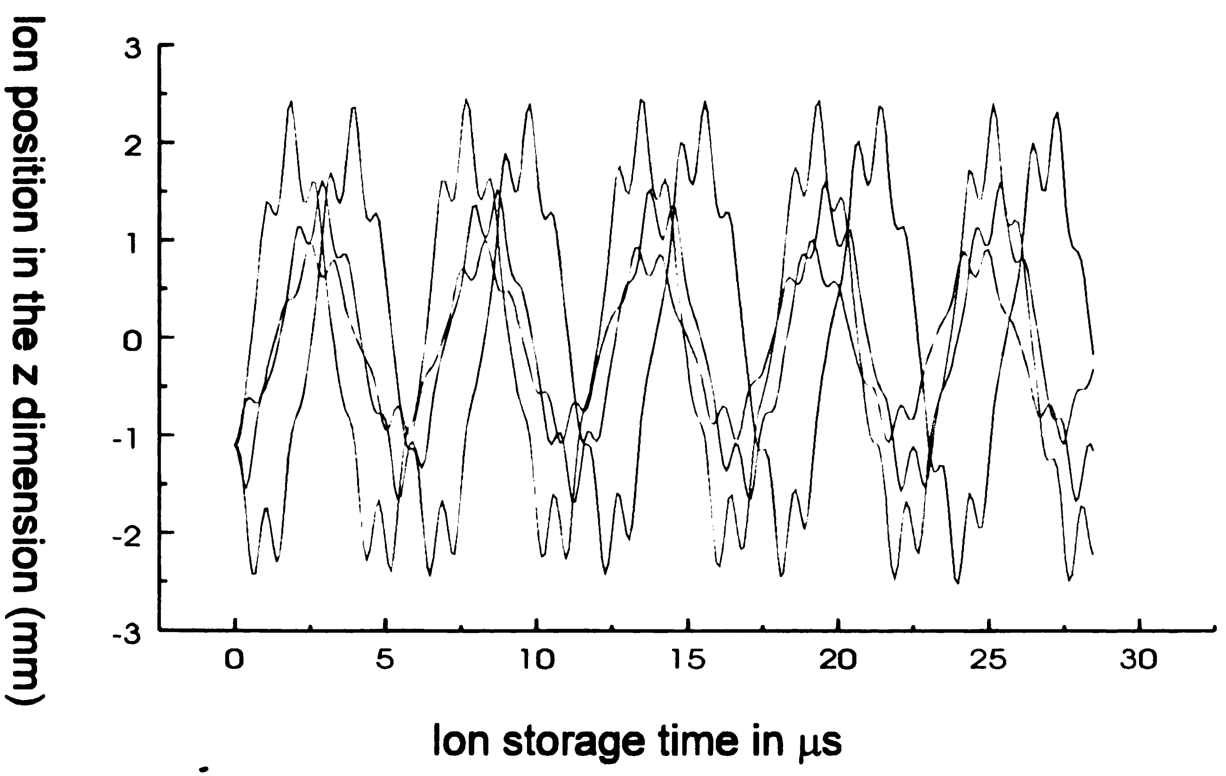

Figure 2-10. The ion position in the z dimension vs. the ion storage time for ions generated at four different RF phase angles. The RF phases for black, red, green blue lines are 0, π/2, π, 3π/4.

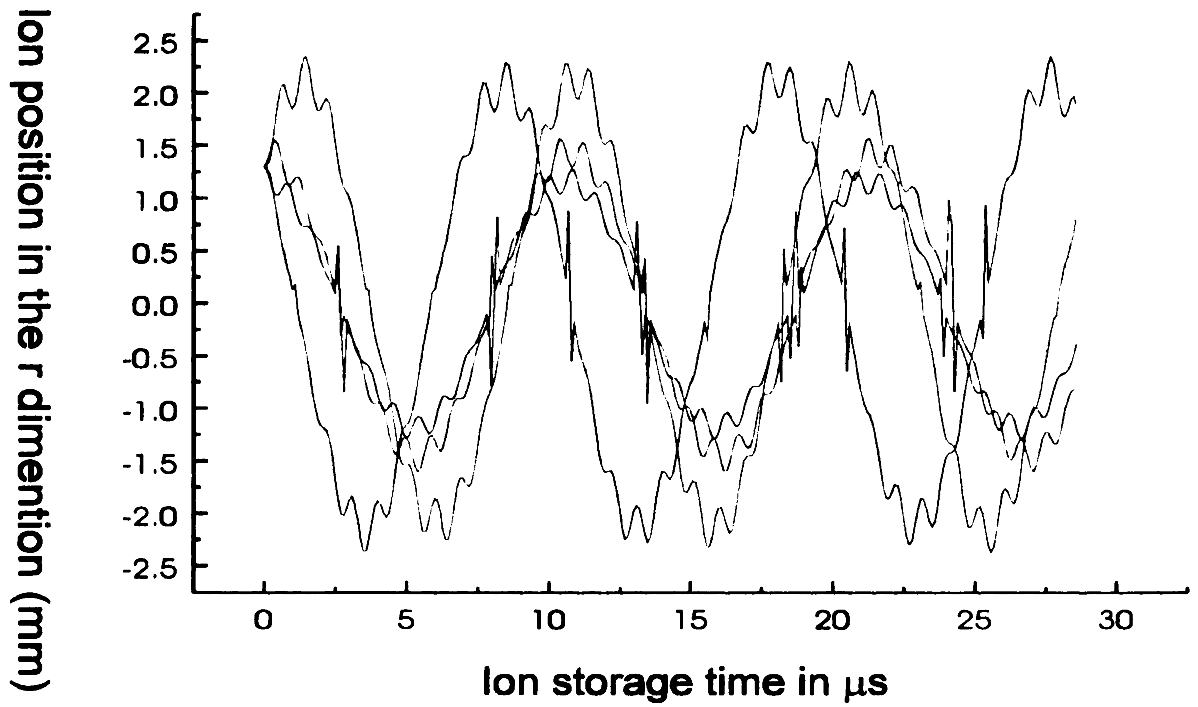

Figure 2-11. The ion position in the z dimension vs. the ion storage time for ions generated at four different RF phase angles. The RF phases for black, red, green blue lines are 0, $\pi/2$, π, $3\pi/4$.

that of 0, and 1.0 mm for that of π. The displacement in the *r* dimension is 2.5 mm for initial phases of π/4 and 3π/4 and 1.25 mm for that of 0, and 1.0 mm for that of π. The fundamental frequency of ion motion is 0.17 MHz in the *z* dimension and 0.097 MHz in the *r* dimension for all four initial phases. These responses to the RF phase angle at the time of ion generation are similar to those in the quadrupole ion trap[7].

2.2.4 Relationship between the ion kinetic energy and the RF phase

The ion's kinetic energy variations with the RF phase during the ion storage time are shown in Figure 2-12. The ions that were generated at the cosine function wave phases of π/2 and 3π/4 (red line and blue line) have more kinetic energy variation than ions generated at the RF phases of 0 and π (black and green lines). Ions generated at the RF phases of π/2 and 3π/4 normally have a kinetic energy valley at the RF phases of n+(1/2)π and a kinetic energy peak at the RF phase of nπ. Ions generated at RF phases of 0 and π normally have a kinetic energy valley at the RF phase of nπ and a peak at the RF phase of n+(1/2)π.

Since the sample introduced into the segmented ring ion trap ion source will remain in the source longer than the time period of one RF cycle, the sample introduced over the entire RF cycle period can be ionized even through the ionization occurs only during a fraction of the RF cycle period. Ions that are generated in the ion source at a particular RF phase and analyzed at a related RF phase, will be in their lowest kinetic energy position at the mass analysis moment. To ionize the sample at a specific RF phase, the ionization energy

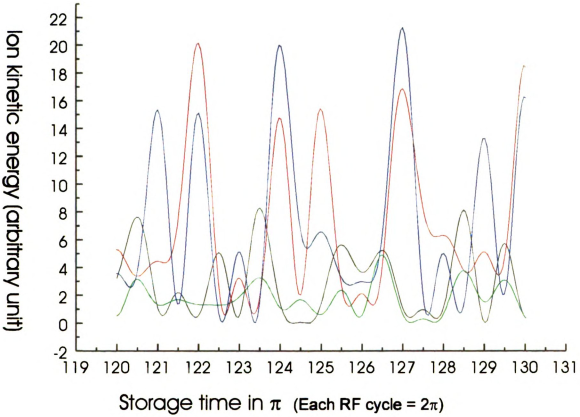

Figure 2- 12. The relationship between the ion kinetic energy and the RF phase for ions generated at four different initial phases.

The black, red, green, and blue represent initial rf phases of 0, π/2, π, 3π/4 degrees could come from a pulsed laser beam or a pulsed electron beam. For the segmented ring ion trap source with electron impact ionization design as discussed in Chapter 4, electrons can only enter the ion source during half the RF cycle. The effect of this "pulsed" ionization on the optimum RF phase at which ions are extracted for TOF analysis will be discussed further in Chapter 5.

2.2.5 Stability diagram of the segmented ring ion trap

The stability diagram of the segmented ring ion trap was constructed by computer simulation following the same procedure which Mather et al.[2] used to determine the stability diagram of a cylindrical ion trap. An ion with m/z 100 was placed in the segmented ring ion trap. The initial ion position was set at r=0.2r_2 and z=0.2z_2. The dimensions of the ion trap are 2z_2=9.4 mm and $r_2^2 = 2z_2^2$. The initial ion kinetic energy and initial RF phase were set to zero. The ion trajectory was considered stable if the ion remained in the segmented ring ion trap for 100 μs. Ions that hit the electrode were considered unstable. The end plates were set to 0 V. The DC offset applied to the ring electrode elements was varied from -50 to 250 V. For each DC offset, the boundary RF voltage for a stable trajectory was found using computer simulation.

The stability diagram expressed in DC offset voltage and RF voltage is shown in Figure 2-13. For comparison, the equation used to calculate the a_z and q_z value for the quadrupole ion trap was used to calculate the stability diagram of the segmented ring ion trap in a_z and q_z coordinates. The resulting stability diagram is shown in Figure 2-14. The shape of the stability diagram is quite

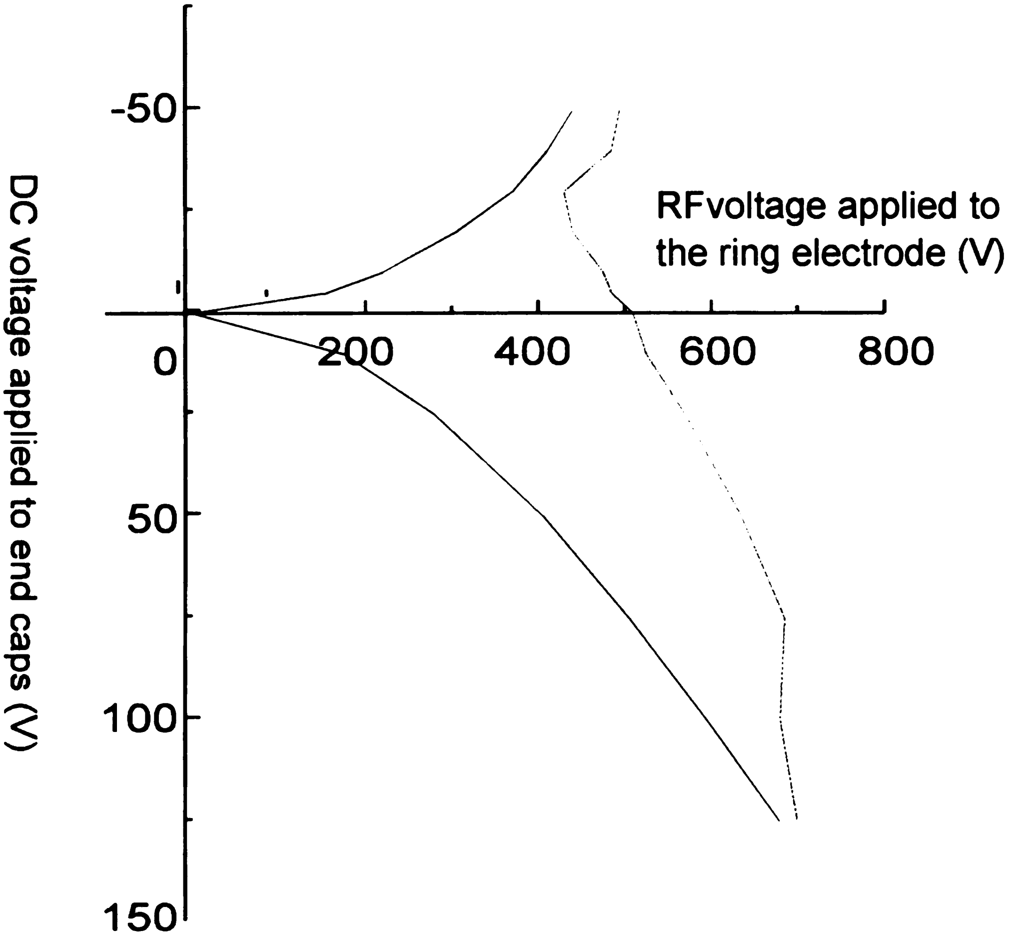

Figure 2-13. Stability diagram of the segmented ring ion trap constructed by computer simulation. The x axis and y axis show the RF and DC values of the voltage applied between the ring electrode and the end plates.

Fig
con
eq

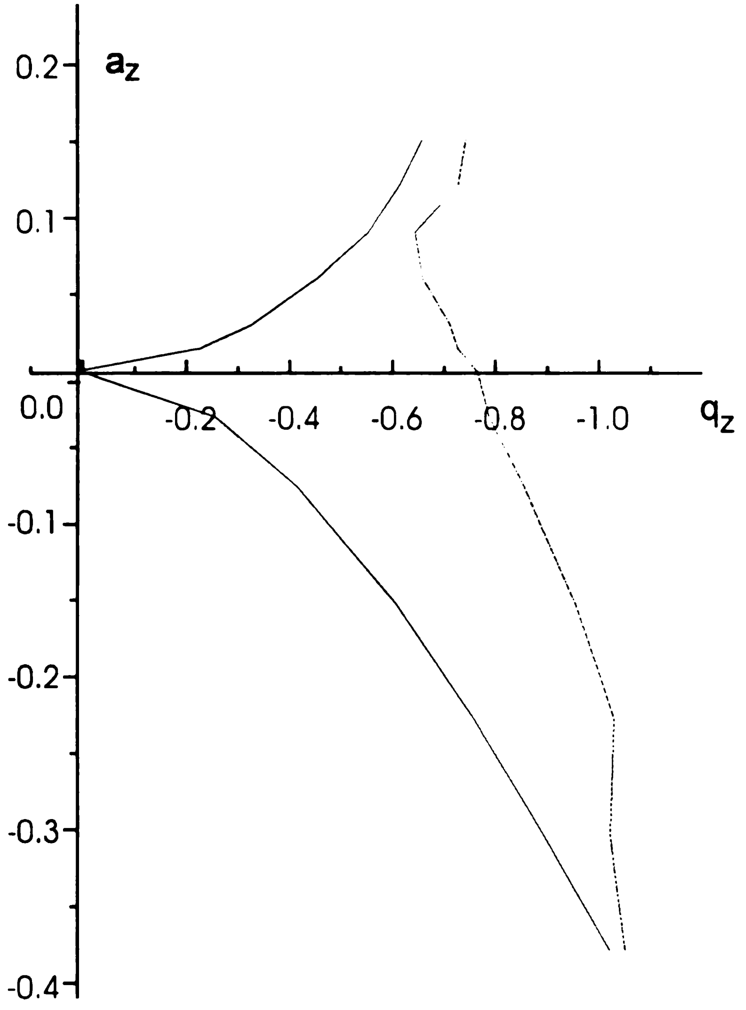

Figure 2-14. Stability diagram of the segmented ring ion trap constructed by computer simulation. The a_z and q_z values were calculated using the same equation as that for the quadrupole ion trap.

similar to that of the quadrupole ion trap (Figure 2-1). When the DC offset of the ring electrode elements is zero, the maximum boundary value of q_z for the segmented ring ion trap is 0.77 but for the quadrupole ion trap, the maximum value of q_z is 0.908. This difference indicates that the stable mass range of the segmented ring ion trap is likely to be smaller than that of the quadrupole ion trap when zero DC offset is used.

2.2.6 Effect of bath gas collisional cooling

For the development of a new ion storage device for a time-of-flight mass spectrometer, the capability of ion storage is of greatest concern. The m/z range of ions having stable trajectories is quite dependent on the actual physical device and on the initial conditions when the ion is generated. These initial conditions include the initial ion position in the ion trap, the initial ion kinetic energy, initial direction of ion motion, and the initial RF phase when the ion is generated. The space charge and collisional cooling effects play an important role in ion stabilization. The collisional cooling effect of He bath gas was simulated by SIMION with the user program. The program only simulates the single ion situation. The collision frequency is determined by the mean free path. The mean free path is generated from the random variation of a specified mean free path factor which is pressure related. Collisions are assumed to be elastic. After each collision, the ion loses a part of its kinetic energy; the fraction lost depends on its own mass and the mass of the collision bath gas. Because the source pressure is normally set at 1 x 10^{-6} torr, the mean free path factor was set at $4x10^4$ mm which is approximately the mean free path value of a single ion at room temperature when only thermal motion is considered. The collisonal frequency is approximately 10 Hz at this pressure. However, the use of this value only provides an idea of the effect of the bath gas collision and does not necessarily represent the exact behavior at this pressure. During each collision part of the ion's kinetic energy is transferred to the bath gas molecule.

The effects of collisional cooling on the ion position in r and z dimensions vs. the ion storage time are shown in Figures 2-15 and 2-16. The RF voltage is 300 V (zero to peak) and 1.2 MHz. The initial ion position is r=$0.2r_2$ and z=$0.2z_2$. The collision frequency is controlled by adjusting the mean free path factor. The r and z dimension displacements decrease when the mean free path factor decreases from $4x10^3$ to 40 mm which brings the mean time between collision to around 10 μs. As the mean free path factor decreases from $4x10^4$ mm to $4x10^3$ mm (which corresponds to a mean time between collision of 1000 μs), there is no significant effect on the ion trajectory during 100 μs storage period. This shows that it is not possible to use the collision cooling effect to decrease the ion displacement in the ion trap on the 100 μs time scale. To achieve multiple collisions within this interval would required an impractical high pressure. Even then, ions generated late in the storage cycle would still not be cooled.

2.2.7 Conclusion

The computer simulation studies of the segmented ring ion trap have shown that the segmented ring ion trap has ion storage characteristics similar to the

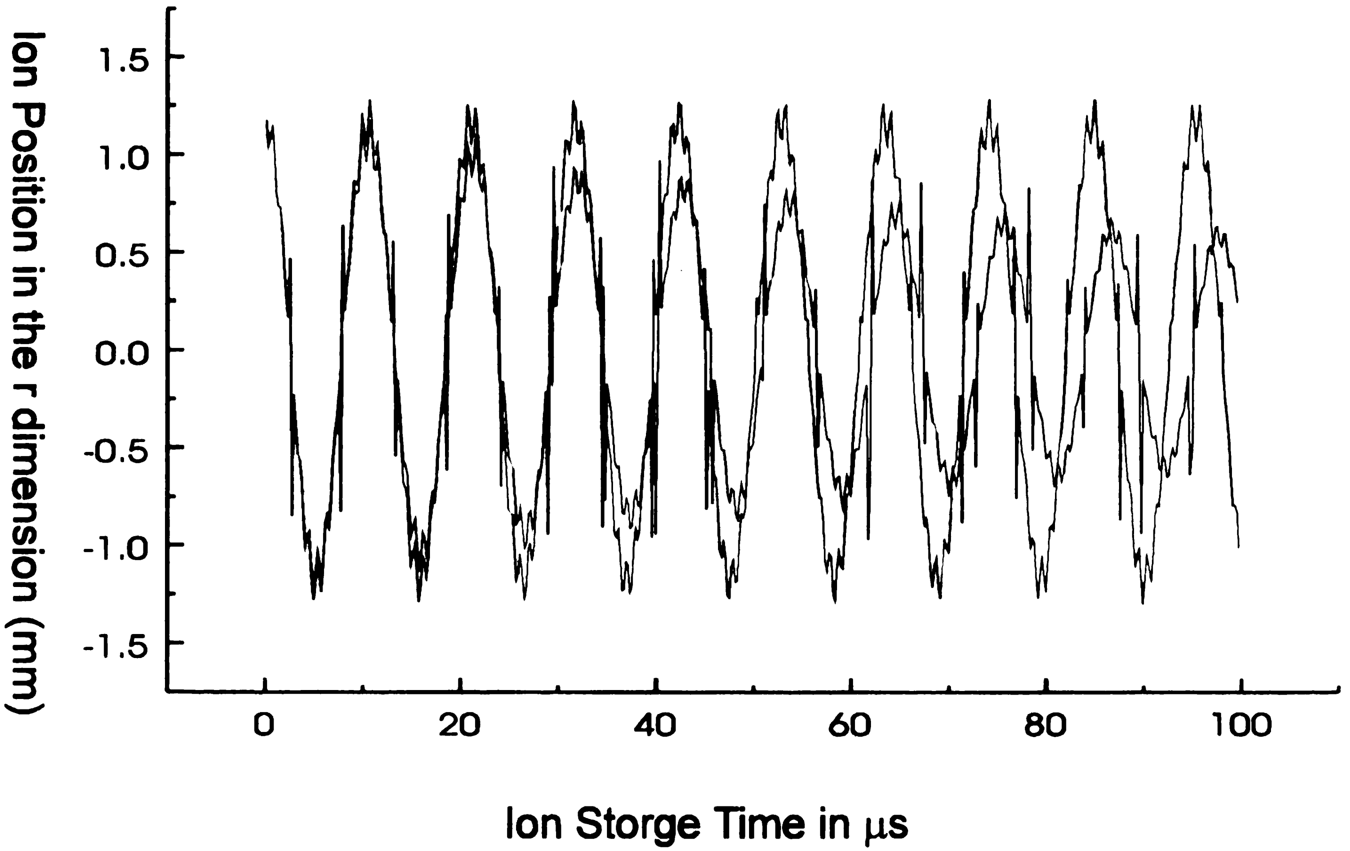

Figure 2-15. Ion position in the r dimension vs. ion storage time. The green line is for a mean free path factor of $4x10^4$ mm or $4x10^3$ mm, the black line is for that of 40 mm.

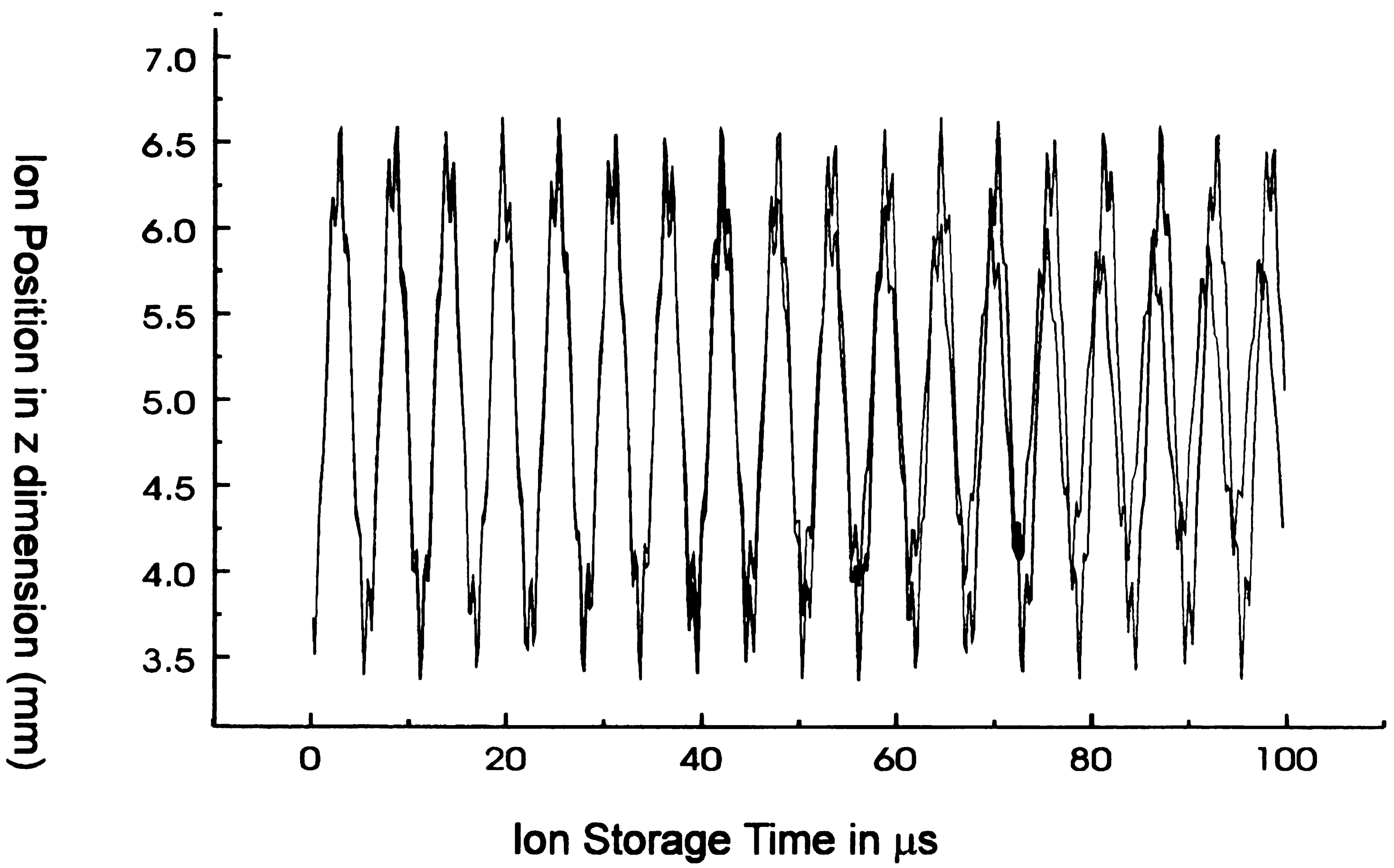

Figure 2-16. Ion position in the z dimension vs. ion storage time. The green line is for a mean free path factor of 4×10^4 mm or 4×10^3 mm, the black line is for 40 mm.

quadrupole ion trap. The storage mass range may be somewhat smaller than that of the quadrupole ion trap due to both the distortion of the quadrupole field and a less effective RF field inside the trap. Nevertheless it appears likely that an ion trap with this simple geometry will provide ion storage for subsequent time-of-flight mass analysis.

2.3 Development and computer simulation of the segmented ring ion trap as an ion source for time-of-flight mass spectrometry

For the ion trap to be used as an ion storage source for time-of-flight mass spectrometry, a pulsed voltage is applied to the end caps (and/or ring electrode) during the ion extraction for the time-of-flight analysis event. The extraction field generated in the ion trap source is one of the key factors affecting the sensitivity and resolution of time-of-flight analysis. To develop an effective ion source for time-of-flight mass spectrometry, computer simulation was used to evaluate the ion extraction characteristics of the segmented ring ion trap and the quadrupole ion trap.

2.3.1 Computer simulation of ion extraction from the quadrupole ion trap storage source for time-of-flight mass analysis.

The characteristics of ion extraction from a quadrupole ion trap were examined with SIMION. The ion trajectories (green lines) for ions extracted from the quadrupole ion trap as well as the equipotential contours (red lines) when an 800 V extraction pulse was applied between the rear and front caps of these ion traps are shown in Figures 2-17, 2-18, and 2-19. When a 400 V pulse was also applied to the ring electrode as shown in Figure 2-18, a set of a collimated ion trajectories was obtained from the ions located in the back half of the ion trap at the time of extraction. When the ring electrode voltage is 800 V (Figure 2-17) or 0 V (Figure 2-19), a set of very dispersed ion trajectories resulted. The lens effect of the curved extraction fields is the major reason for the dispersed ion trajectories. The unbalanced extraction voltages applied to the ring electrodes in Figure 2-17 and Figure 2-19 result in a much more severe lens effect than in Figure 2-18. The large ion trajectory dispersion will result in a high proportion of ion loss during the time-of-flight mass analysis period.

The patterns of ion extraction trajectories vary with the RF applied to the ring electrode. If the RF is not blocked at the time of extraction, a large percentage of ion loss during the time-of-flight mass analysis is expected. In the grant proposal for this project to NIH in 1991, we proposed that for time-of-flight analysis from the quadrupole ion trap storage source, the best results will be obtained by setting the ring extraction potential at a potential half way between the extraction potential of two end caps.

This most favorable situation for ion extraction from the quadrupole ion trap was modeled in more detail as shown in Figure 2-20. The distance between the two end caps of the quadrupole ion trap is 20 grid units and the conversion factor is 1.0 mm/grid (Figure 2-20). Several additional electrodes were added at the front of the ion trap to simulate the ion acceleration and focusing electrodes.

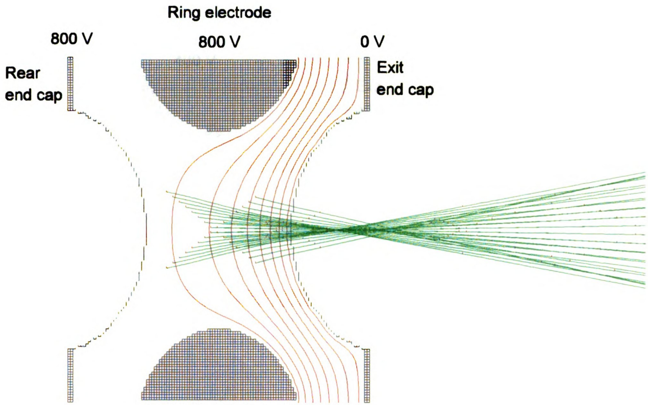

Figure 2-17. Equipotential contours of a quadrupole ion trap during ion extraction. Electrodes are in black, the red lines are equipotential lines from 50 V to 750 V in 100 V intervals.
The green lines are trajectories of the ions extracted from the ion trap under the indicated extraction voltages.

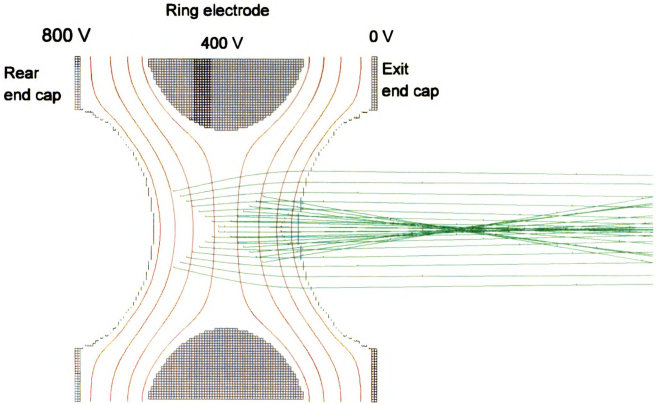

Figure 2-18. Equipotential contours of a quadrupole ion trap during ion extraction. Electrodes are in black, the red lines are equipotential lines from 50 V to 750 V in 100 V intervals.
The green lines are trajectories of the ions extracted from the ion trap under the indicated extraction voltages.

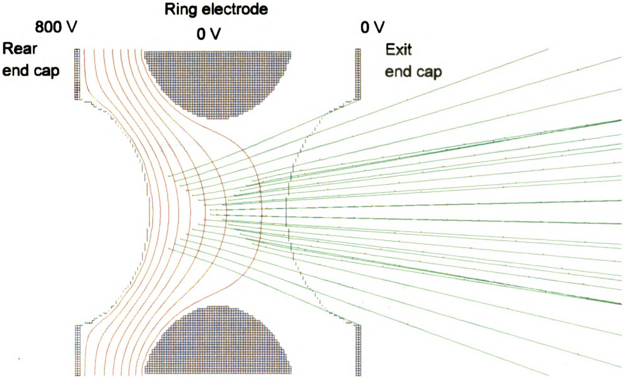

Figure 2-19. Equipotential contours of a quadrupole ion trap during ion extraction. Electrodes are in black, the red lines are equipotential lines from 50 V to 750 V in 100 V intervals.
The green lines are trajectories of the ions extracted from the ion trap under the indicated extraction voltages.

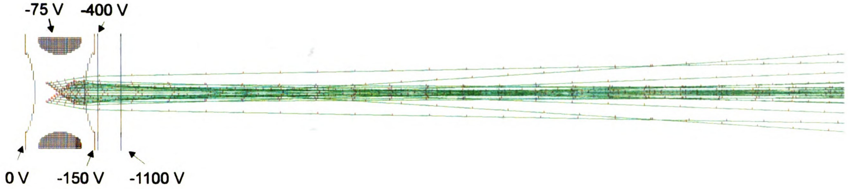

Figure 2-20. Trajectories of ions extracted from a quadrupole ion trap. The green lines are the ion trajectories.
The red dots are ion positions along the flight path at 0.5 μs intervals.
The m/z 100 ions are initially placed in the segmented ring ion trap source in an X pattern.
The voltages applied to the electrodes are indicated.

Ions of m/z 100 are initially placed in the quadrupole ion trap in an X pattern. The green lines are the ion trajectories. The ion positions at every 0.5 μs interval of flight time are represented by the red dots. The field along this flight path is produced by the ion trap extraction potential and a second acceleration electrode as in the design of Lubman[15]. The progression of the groups of dots representing the same flight time and relative distance over which they are spread clearly indicates that a spatially compact ion bunch is not achieved. Computer simulation shows that it is not possible to find a position along the flight path where the flight time of isomass ions is closely the same. The convergence position of ion trajectories depends on the position of the ion in the source at the moment of application of the extraction pulse. The minimum ion package temporal dispersion is approximately 500 ns.

As discussed in chapter one, a small minimum value of temporal dispersion of isomass ions at the space focus plane is critical to achieve good mass resolution with time-of-flight mass analysis. The simulation above clearly indicates that good mass resolution could not be achieved by extracting ions from the quadrupole ion trap unless the ions are initially located very close to the center region of the trap when the extraction pulse is applied. This initial condition could be achieved by using extensive collisional damping with He bath gas but this will require many milliseconds of cooling time[15]. Thus good resolution is only obtained by sacrificing the advantage of the high spectral generation rates that can be provided by the time-of-flight mass spectrometer.

2.3.2 Computer simulation of ion extraction from the segmented ring ion trap

For ion extraction from the segmented ring ion trap, the ring electrode elements and the rear cap are given extraction voltages linearly proportional to their distances from the exit cap. The equipotential contours of the segmented ring ion trap when the extraction voltages are applied are shown in Figure 2-21. The uniform extraction field allows ions at different radial positions to experience the same extraction field profile. The ion trajectory simulation of the ions extracted from the segmented ring ion trap is shown in Figure 2-22. The distance between the rear cap and the exit cap for the segmented ring ion trap is 40 grid units which represents a practical geometry of 9.4 mm separation; the conversion factor is 0.235 mm/ grid. One additional electrode was placed in the front of the ion trap to provide an ion acceleration voltage. In this case, the field along the flight path consists of the linear ion extraction field generated inside the segmented ring ion trap and the accelerating field experienced by ions exiting the ion trap. The extraction field and acceleration field strengths are the same so they form a single uniform extraction field. The ions are initially placed in the trap in an X pattern. The green lines are ion trajectories and the groups of red dots are ion positions as ions move along their flight path every 0.05 μs. The isomass ions are extracted from different initial positions in the segmented ring ion trap but they converge to a very close pattern, spatially and temporally, at the space focus plane (SFP). A minimum temporal dispersion of approximately 8 ns is

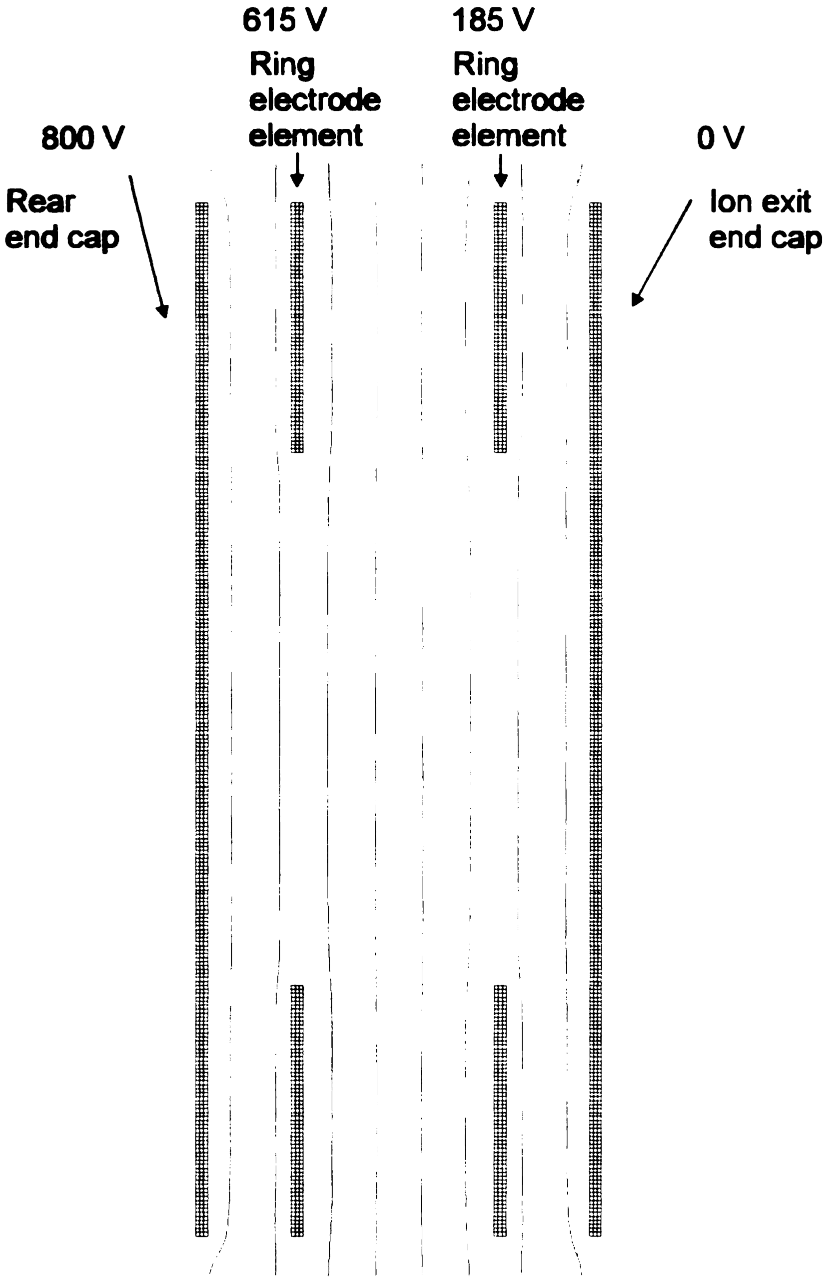

Figure 2-21. Equipotential contours of the segmented ring ion trap during the ion extraction. Electrodes are in black, the red lines are equipotential lines from 50 V to 750 V in 100 V intervals.

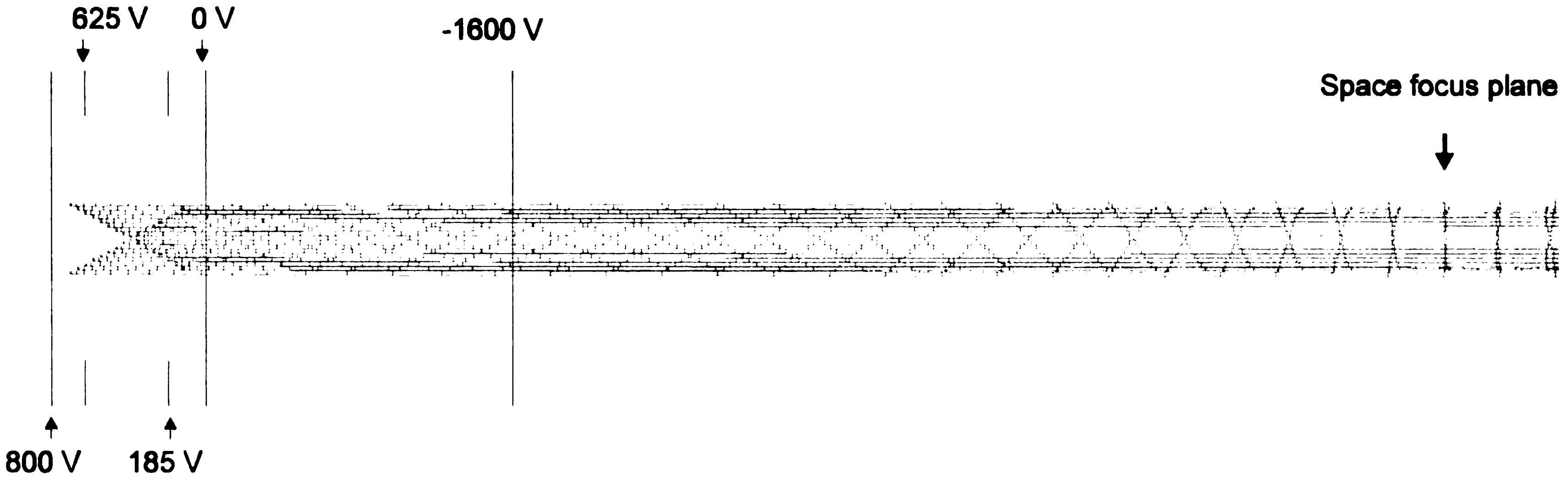

Figure 2-22. Trajectories of ions extracted from the segmented ring ion trap.The green lines are trajectories.
The red dots are ion positions along the flight path at 0.05 μs intervals.
The m/z 100 ions are initially placed in the segmented ring ion trap source in an X pattern.

obtai
good

2.3.3
spec

2.2.3.

The
extra
contr
the i
extra
the s
used
high a

2.3.3.2

The
deterr
energ
also a
phase.
at RF
energy

obtained. This small temporal dispersion at the space focus plane will result in good resolution for time-of-flight mass analysis.

2.3.3 Proposed energy focusing method for time-of-flight mass spectrometer analysis from the ion trap storage source

2.2.3.1 Strong extraction field

The extraction simulation above assumes a zero initial kinetic energy of the ion extracted for time-of-flight mass analysis. As discussed in chapter one, another contribution to the temporal ion spread at the SFP is the ion turn-around time in the ion source. In order to minimize the ion turn-around time, a strong ion extraction field is required. For a conventional time-of-flight mass spectrometer, the space between the extraction grids is 2-4 mm and the extraction voltage used is 200 to 400 V. For the segmented ring ion trap, an extraction voltage as high as 800 V is required to achieve the same ion extraction field strength.

2.3.3.2 Synchronized ion extraction with RF phase

The kinetic energy of the ion at the time the ion extraction pulse is applied determines the initial ion kinetic energy for time-of-flight analysis. The kinetic energy of ions in the segmented ring ion trap varies with the RF phase and is also a function of the phase at the time of ion generation. The ions at the RF phases of $\pi/2$ and $3\pi/4$ have wider kinetic energy variation than ions generated at RF phases of 0 and π as shown in Figure 2-12. For minimum ion kinetic energy, the extraction pulse should be applied at the moment of lowest initial kine

kine

and

3π4

If ion

applie

discus

fractio

which

2.3.3.3

In mas

tempo

Becau

same p

is built

focus p

segme

by mos

center

during

during

Thus, f

kinetic energy for ions generated at RF phases of π/2 and 3π/4. The valley of the kinetic energy of ions generated at RF phases π/2 and 3π/4 is at RF phases π/2 and 3π/4 degrees. So the extraction pulse should be applied at RF phases π/2 or 3π/4 if ions are generated throughout the RF cycle.

If ions are generated at a particular RF phase, then ion extraction should be applied at the RF phase when the ions are at their lowest kinetic energy. As discussed in Chapter 4 and Chapter 5, ions are generated only during some fraction of the RF cycle and the mass resolution is related to the RF phase at which the extraction voltage is applied.

2.3.3.3 Broad range energy focusing reflectron

In many time-of-flight mass spectrometers, a reflectron is used to image the temporal ion package at the space focus plane on the surface of the detector. Because of the reflectron, the total flight time is increased 2 to 4 fold within the same physical dimensions of the vacuum chamber. The conventional reflectron is built with a one or two stage linear static fields and the ion packet at the space focus plane has a small kinetic energy variation. For ions extracted from the segmented ring ion trap, a broader kinetic energy distribution than that produced by most time-of-flight sources is expected. The ions generated away from the center of the ion trap will have substantial energy due to the RF field applied during the ion storage period and also the ions gain a broader extraction energy during the ion extraction process due to the higher extraction voltage applied. Thus, for time-of-flight mass analysis from the segmented ring ion storage sourc

ions a

energ

Refer

---

[1]

naturf

[2]

Amste

[3]

Wiley

[4] I

3.065

[5] I

D'ions

421-43

[6] I

Ion Tr

(1977)

[7] M

Charac

Geome

[8] J

Storage

on Mas

[9] D

[10] a

Ion Tra

source, It was necessary to develop a reflectron which could image the isomass ions at the surface of the ion detector, and which would have a broader kinetic energy tolerance. The reflectron development is described in the next chapter.

References:

---

[1] Paul, W., Steinwedel, H.: A new Mass Spectrometer without a Magnetic Field. Z. naturforsch. 8a, 448-50 (1953)

[2] Dawson, P. H.: Quadrupole Mass Spectrometry and Its applications, Elsenver-Amsterdam, Chapter 4, (1976)

[3] March, R. E., Hughs, R. J.: Quadrupole Storage Mass Spectrometry, p192. John Wiley and Sons, New York (1989)

[4] Langmuir, D. B., Langmuir, R. V., Shelton, H. and Wuerker R. F., U.S. Patent No. 3, 065640 (1962)

[5] Benilan, M. -N. and Audoin, C., Int. J. Mass Spectrom. Ion Phys.: Confinement D'ions Par Un Champ Electrique De Radio-frequence Dans Une Cage Cylindrique. 11, 421-432 (1973)

[6] Bonner, R. F., Fulford, J. E., March, R. E., and Hamilton, G. F.: The Cylindrical Ion Trap. Part I. General Introduction. Int. J. Mass Spectrom Ion Phys. 24, 255-269 (1977)

[7] Mather, R. E., Waldren, R. M., Todd, J. F., and March, R. E.: Some Operational Characteristics of a Quadrupole Ion Storage Mass Spectrometer Having Cylindrical Geometry. Int. J. Mass Spectrom. Ion Phys., 33, 201-231 (1980)

[8] Ji, Q., Vlasak, P. R., Holland, J. F., and Enke, C. G.: A Segmented Ring Ion Trap Storage Time-of-Flight Mass Spectrometer. (Proceedings of the 42nd ASMS Conference on Mass Spectrometry and Allied Topics, Chicago, IL, May 29 - June 3, p. 1042, (1994)

[9] Dawson, P. H. and Whetten, N. R.: J. Vac. Sci. Technol., 5, 1 (1968).

[10] a. Londry, F. A., Roland, L. A. and March R. E.: Computer Simulation of Single Ion Trajectories in Paul-Type Ion Traps. J Am Soc. Mass Spectrom. 4, 687-705 (1992)

---

b.

Selecti

Mass S

c.

of Ions

Isolatio

d.

Vedel

Introdu

Process

e.

J. F., V

Further

f.

Resona

Study.

[11]

Simula

Proces

b.

Motion

JASMS

[12]

Int. J. M

[13]

[14] M

Three-D

[15] M

Flight M

---

b. March, R. E., Londry, F. A., Alfred, R. L., Franklin, A. M. and Todd J. F.: Mass-Selective Isolation of Ions Stored in a Quadrupole Ion Trap: A Simulation Study. Int. J. Mass Spectrom Ion Processes. 112, 247-271 (1992)

c. March, R. E., Tkacyzk, M., Londry, F. A., Alfred, R. L.: Mass-Selective Isolation of Ions Stored in a Quadrupole Ion Trap. Part 2. A Simulation Study of Consecutive Isolation. Int. J. Mass Spectrom Ion Processes. 125, 9-32 (1993)

d. March, R. E., Londry, F. A., Alfred, R. L., Todd, J. F., Penman A. D. Vedel F. and Vedel M.: Resonance Excitation of ions stored in a Quadrupole Ion Trap Part III Introduction to the Field Interpolation Simulation Method. Int. J. Mass Spectrom Ion Processes. 110, 159-178 (1991)

e. March, R. E., McMaon, A. W., Allinson, E. T., Londry, F. A., Alfred, R. L., Todd J. F., Vedel F.: Resonance Excitation of Ions Stored in a Quadrupole Ion Trap Part II. Further Simulation Studies. Int. J. Mass Spectrom Ion Phys, 99, 109-124 (1991)

f. March, R. E., McMaon, A. W., Londry, F. A., Alfred, R. L., Todd, J. F., Vedel F.: Resonance Excitation of Ions Stored in a Quadrupole Ion Trap Part I. A Simulation Study. Int. J. Mass Spectrom Ion Proc., 95, 119-156 (1989)

[11] a. Reiser Hans-Peter, Julian, R. K. and Cooks, R. G.: A Versatile Method of Simulation of the Operation of Ion Trap Mass Spectrometer. Int. J. Mass Spectrom Ion Processes. 121, 49-63 (1992)

b. Julian, R. K., Nappi, M., Well C. and Cooks, R. G.: Multiparticle Simulation of Ion Motion in the Ion trap Mass Spectrometer: Resonant and Direct Current Pulse Excitation. JASMS, 6, 51-70 (1995)

[12] Franzen, J.; Simulation Study of an Ion Cage with Superimposed Multipole Fields. Int. J. Mass Spectrom Ion Processes. 106, 63-78 (1991)

[13] SIMION 4.0 Dahl, D. A., and Delmore J. E. , EG&G Idaho, Inc

[14] Ma C., Lee H. and Lubman D. M.: Computer Simulation of The Operation of a Three-Dimensional Qudrupole Ion Trap. Applied Spectroscopy, 46, 12, 1769-1779 (1992)

[15] Michael, S. M Chien, M., and Lubman, D. M.: An Ion Trap Storage /Time-of-Flight Mass Spectrometer. Rev. Sci. Instrum. 63, 4277-4284, (1992).

C

br

sp

3.1

As

refl

dist

sou

pen

diffe

time

solu

spec

I fou

a re

distri

the t

obtai

for the

detecto

Chapter 3 Theoretical development and computer simulation of a broad energy range focusing reflectron for a time-of-flight mass spectrometer

3.1 Background

As discussed in chapter two, it was realized that it was necessary to design a reflectron that is able to focus isomass ions with a broad kinetic energy distribution that results from using the segmented ring ion trap as the ion storage source. Rockwood[1] postulated that a reflectron with a hyperbolic field will give a perfect temporal focus for isomass ions starting at the same position with different initial kinetic energies. This hypobolic reflectron field only applies to a time-of-flight mass spectrometer with no field-free region. The mathematical solution of the voltage profile for a reflectron in a time-of-flight mass spectrometer with a field-free region is difficult to derive. In the summer of 1993, I found an alternative numerical method to obtain a reflectron voltage profile for a reflectron that can temporally focus isomass ions with a broad energy distribution. Using this design approach, Paul Vlasak developed a reflectron for the tandem time-of-flight mass spectrometer in Professor Enke's lab and obtained experimental verification[2].

An electrostatic reflectron system was first introduced by Mamyrin et al.[3] for the time-of-flight mass spectrometer to focus an isomass ion bunch at the detector position. The most commonly used reflectron has one or two linear reflec

respe

betw

stag

thes

FWH

using

at th

two-s

trajec

cons

studi

used

stron

multi

so th

easily

desig

been s

mainta

reflectron fields, and provides first order or second order energy compensation, respectively. Homogeneous electric fields are generated by using mesh screens between regions of different field strength. The mathematics of the one or two-stage reflectron is well defined when only the initial kinetic energy distribution of these isomass ions was considered[3, 4]. A high mass resolution (over 10000 FWHM) for a reflectron time-of-flight mass spectrometer has been obtained by using laser ionization to achieve a minimal space and energy distribution of ions at the moment of ion generation[5].

The use of mesh screens to generate homogeneous fields for a one or two-stage reflectron reduces ion transmission and can cause deviation in ion trajectories. When an acceleration field was introduced into the reflectron construction, the ion transmission was improved about 20%[6]. Wollnik et al. studied the field distortion near the aperture of the mesh screen when a grid is used to split two regions of different field strengths along the ion flight path. The strong electric field reaches through the meshes of the grid generating a multitude of small lenses. These small lenses modify an incoming parallel beam so that some of the ion trajectories are strongly inclined to the beam axis and easily miss a final ion detector[7]. Several grid-free reflectrons have been designed and a mass resolution about 10000 has been achieved[8].

A reflectron with a single stage and a single grid at the front electrode has been shown to be able to focus isomass ions with a 7% energy distribution while maintaining a the resolving power up to a few thousand[9]. An energy range gra

tim

foo

ma

to

ele

ref

pro

eac

Der

fiel

dist

refle

with

field

profi

prac

ion e

greater than 10% has been temporally focused with a gridless reflectron in a time-of-flight mass spectrometer[10]. Recently, because of the requirement for focusing both precursor ion and secondary ions for the tandem time-of-flight mass spectrometer, the energy range that needs to be focused has increased up to 50% and more[12]. Cotter et al. have constructed a reflectron with 68 electrodes, the front electrode made of 90% transmission mesh screen. This reflectron is able to focus all of the product ions simultaneously. The voltage profile was determined experimentally by tuning the potentiometers between each electrode and a curved voltage profile was obtained experimentally[11]. Derrik et al. discussed theoretically the fundamental limitations of the quadratic-field reflectron for the temporal focusing of fragment ions with a broad energy distribution[12]. Actually, the reflectron profile they discussed is the same as the reflectron profile proposed by Rockwood in 1986, so it, too, requires a flight path with no field free region.

The method of reflectron design I conceived is to calculate the reflectron field numerically rather than to obtain a mathematical solution of the voltage profile. This method allows an high orders of energy focus according to the practical design parameters such as the length of the field free flight region, the ion energy range needed, and the length of the reflectron.

3.2. Ma

3.2.1 T

have

The g

increa

at the

differe

each

equati

$T_{tot}=T_{n}$

The te

spends

We w

accom

reflect

all of th

ion sto

now rec

single p

position

energy i

3.2. Mathematical considerations

3.2.1 Temporal focusing of isomass ions that start at the same position but have different kinetic energies.

The goals for using a reflectron in the time-of-flight mass spectrometer are to increase the total flight time as well as to get isomass ions to reach the detector at the same time. For the isomass ions that start at the space focus plane with different initial kinetic energies (different initial velocities), the total flight time for each ion to reach a detector position should be equal. The mathematical equation describing the total flight time is

$$T_{tot}=T_{ff}+T_r \tag{3.1}$$

The term T_{tot} is the total flight time of a single ion, T_{ff} is the flight time the ion spends in the field-free region and T_r is the flight time of the ion in the reflectron. We want T_{tot} to be the same for ions with the same m/z value. This is accomplished by choosing an appropriate potential profile for the reflectron.

An ion with a given kinetic energy will be slowed down after it enters the reflectron. The kinetic energy of the ion is converted into potential energy. When all of the kinetic energy of the ion has been converted into potential energy, the ion stops. Then it is accelerated in the reverse direction. Its potential energy is now reconverted into kinetic energy. For the following discussion, an ion with a single positive charge is used. As described in Figure 3-1, an ion that stops at position x_m in the reflectron will have a maximum potential $E(x_m)$. This potential energy is equal to the initial kinetic energy of the ion. After reconversion into

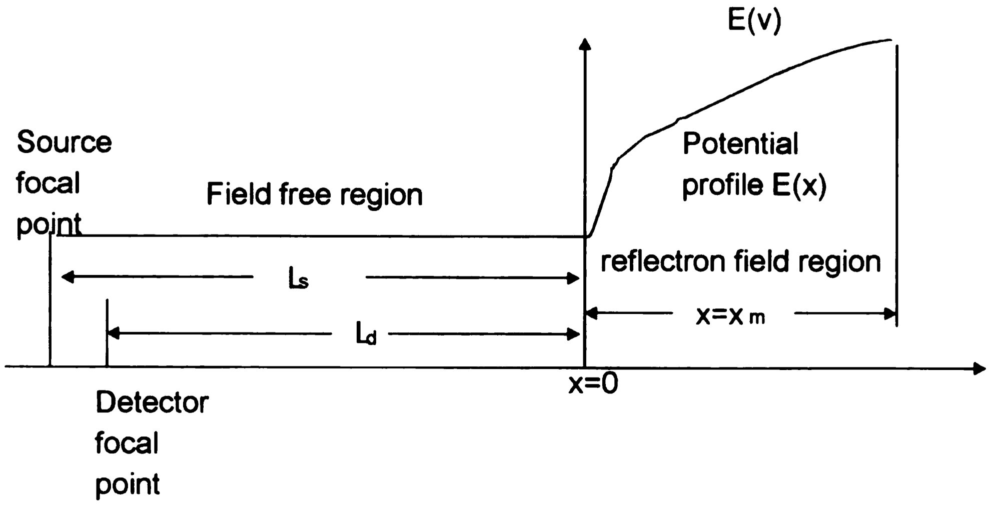

Figure 3-1. Schematic of potential profile of a reflectron and field free region.

kinetic

energy

$T_r = 2$

where

$v_z =$

The fl

$T_{ff} =$

where

and L

the re

$v_m =$

So th

$T_{tot} =$

$T_{tot} =$

the s

energ

kinetic energy, the ion is returned to the field free region with its initial kinetic energy, only the directional vector has been altered.

The flight time the ion spends in the reflectron is

$$T_r = 2\int_0^{x_m} \frac{dx}{v_x} \tag{3.2}$$

where v_x is the ion velocity at position x in the reflectron and m is the ion mass,

$$v_x = \sqrt{\frac{2}{m}[E(x_m) - E(x)]} \tag{3.3}$$

The flight time in the field-free flight region is

$$T_{ff} = \frac{L_s + L_d}{v_m} = \frac{L_{ff}}{V_m} \tag{3.4}$$

where v_m is the initial velocity of the ion and its velocity in the field-free region and L_{ff} is the total length of the field-free region both before (L_s) and after (L_d) the reflectron.

$$v_m = \sqrt{\frac{2e}{m}E(x_m)} \tag{3.5}$$

So the total flight time is

$$T_{tot} = T_{ff} + T_r \tag{3.6}$$

$$T_{tot} = 2\int_0^{x_m} \frac{dx}{v_x} + \frac{L_s + L_d}{v_m} \tag{3.7}$$

Mathematically, we need to find a reflectron field $E(x)=f(x)$ that will give the same constant T_{tot} for isomass ions over a wide range of initial kinetic energies.

pote

For

$T_{\alpha} =$

$T_{\alpha} =$

$T_{\alpha} =$

$T_{\alpha} =$

The

the h

ener

regi

by

illus

has

and

One special case is when there is no field-free region (L_{ff}=0), Then a potential profile with an hyperbolic function will give a satisfactory solution.

For $E(x)=ax^2+b$, and L_{ff}=0

$$T_{tot}=2\int_0^{x_m}\frac{dx}{v_x} \tag{3.8}$$

$$T_{tot}=2\int_0^{x_m}\frac{dx}{\sqrt{\frac{2e}{m}[E(x_m)-E(x)]}} \tag{3.9}$$

$$T_{tot}=2\int_0^{x_m}\frac{dx}{\sqrt{\frac{2e}{m}[(ax_m^2-b)-(ax^2-b)]}} \tag{3.10}$$

$$T_{tot}=\frac{\pi}{\sqrt{2a\frac{e}{m}}} \tag{3.11}$$

The total flight time T_{tot} only depends on the ion mass m and the magnitude of the hyperbolic field applied to the reflectron. It is independent of the initial kinetic energy of the ions.

For the situation of a time-of-flight mass spectrometer with a field-free region, we have obtained a solution for the potential profile of the reflectron *E(x)* by a numerical method rather than a mathematically derived equation as illustrated by following discussion and Figure 3-2.

Assume that the ion with the lowest kinetic energy that has to be focused has the kinetic energy V_1 in electron volts. The first grid of the reflectron is 0 V and the next grid needs to be set at the voltage of V_1 in order to stop this ion.

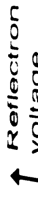
Reflectron
voltage

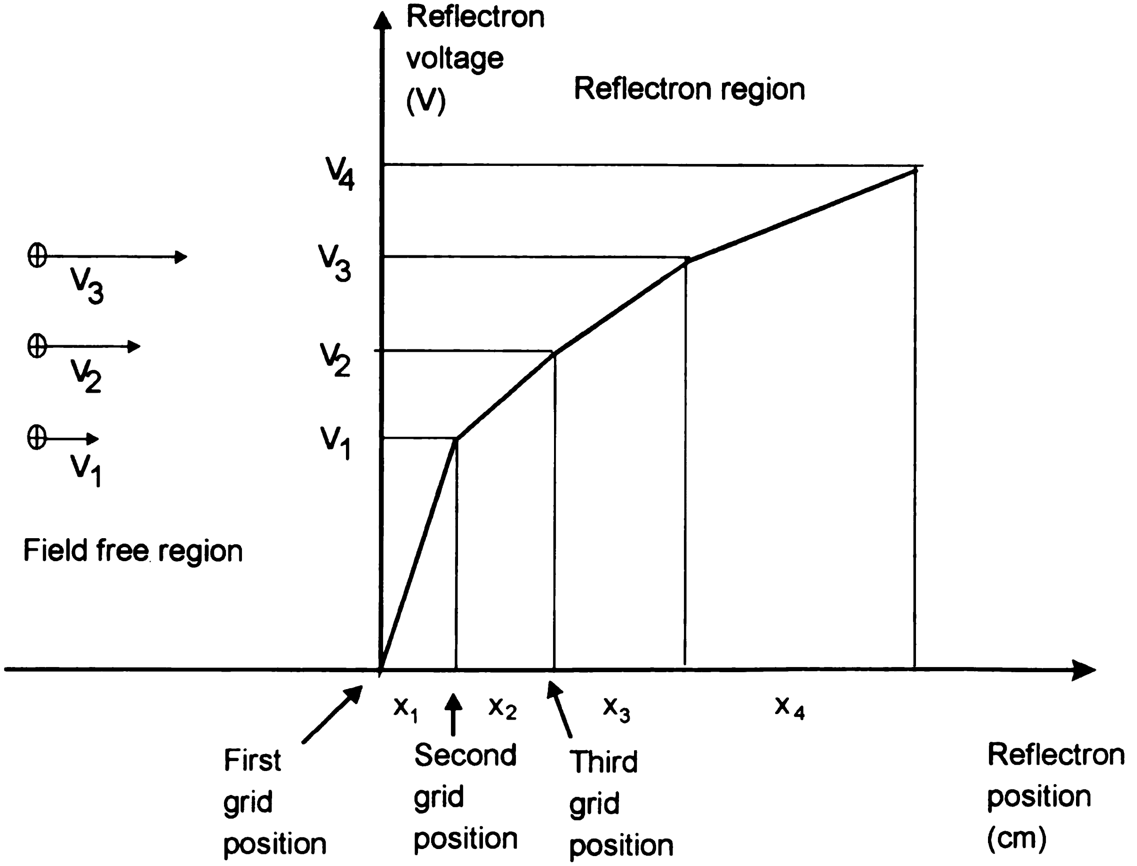

Figure 3-2. A representative diagram of a numerically constructed reflectron profile. Isomass ions with increasing kinetic energy are stopped at later reflectron grid positions.

Th

fie

U_1

so

an

fre

T_{bv}

the

bac

wi

and

to le

ion,

from

posi

is U_2

$(U_1^{(2)}$

This second grid is set x_1 cm away from first grid. The velocity of this ion in the field-free flight region and at the first grid position is

$$U_1^{(1)} = \sqrt{2\frac{V_1}{m}},$$

so the average speed of the ion in the region between the first reflectron grid and the second reflectron grid is $U^{(1)}{}_1/2$. The total flight time of this ion in the field free region as well as in the reflectron up to the turn around point x_1 is

$$T_{tot} = T_{ff} + T_r = \frac{L_{ff}}{U_1^{(1)}} + 2\frac{2x_1}{U_1^{(1)}} \qquad (3.12)$$

the factor 2 is added in second term because the ion travels both forward and back backward through the reflectron.

Consider now a second ion with a kinetic energy $V_2=V_1+dV$ (eV). This ion will pass the second reflectron grid, a third reflectron grid needs to be introduced and set at the voltage of V_2 in order to stop the ion at that grid position. In order to let the second isomass ion arrive at the detector at the same time as the first ion, the distance between the second grid and the third grid must be set as x_2 from the following calculation.

The velocity of the second ion at the field-free region and at the first grid position is $U_1^{(2)} = \sqrt{2\frac{V_2}{m}}$.The velocity of the second ion at the second grid position is $U_2^{(2)} = \sqrt{2\frac{dV}{m}}$ and the average velocity of the second ion after the first grid is $(U_1^{(2)} + U_2^{(2)})/2$ and after the second grid is $U_2^{(2)}/2$.

The flight time of the second ion at the turn around point is

$T_{tot} =$

so th

$x_2 = [$

increa

$V_n = V$

Its ve

$U_1^{(n)} =$

and a

$U_2^{(n)} =$

and a

$U_i^{(n)} =$

So the

$x_n = [T$

In this

energy

is there

$$T_{tot} = \frac{L_{ff}}{U_1^{(2)}} + 2\frac{2x_1}{U_1^{(2)} + U_2^{(2)}} + 2\frac{2x_2}{U_2^{(2)}} \tag{3.13}$$

so the value for x_2 could be determined by solving

$$x_2 = [T_{tot} - (\frac{L_{ff}}{U_1^{(2)}} + 2\frac{2x_1}{U_1^{(2)} + U_2^{(2)}})]\frac{U_2^{(2)}}{4} \tag{3.14}$$

This process can be continued for ions of a still higher energies, increasing in increments of dV. For the nth ion, which has a kinetic energy of

$V_n = V_1 + (n-1)dV$,

Its velocity at the first grid position is

$$U_1^{(n)} = \sqrt{2\frac{V_n}{m}} \tag{3.15}$$

and at the second grid position is

$$U_2^{(n)} = \sqrt{2(n-1)\frac{dV}{m}} \tag{3.16}$$

and at the 3rd to the nth grid positions is

$$U_i^{(n)} = \sqrt{2[(n-i)+1]\frac{dV}{m}}\ ;\ i = 3, \ldots, n \tag{3.17}$$

So the distance between the nth and $(n+1)$th grids is

$$x_n = [T_{tot} - (\frac{L_{ff}}{U_1^{(n)}} + \sum_{l=1}^{n-1} 2\frac{2x_l}{U_l^{(n)} + U_{l+1}^{(n)}})]\frac{U_n^{(n)}}{4} \tag{3.18}$$

In this way the voltage and the position of each reflectron grid is defined. As the energy increment dV is decreased and the number of grids and calculation steps is thereby increased, a solution for the voltage profile that will provide nearly perfect temporal focusing can be obtained. The calculated reflectron voltage profile could be used to focus isomass ions of all *m/z* values.

Paul Vlasak modified the above calculation procedure for the design of a reflectron for the TOF/TOF instrument. A constant increment for the distance between each reflectron grid position was used for each calculation step and the ion kinetic energy at each grid position was obtained. He also added a term in the equation to allow consideration of the angle of ion entry.

3.2.2 Temporal focusing of isomass ions with the zero initial kinetic energy, but different initial positions in the ion source.

For the segmented ring ion trap time-of-flight mass spectrometer, mass peak broadening due to the range of initial ion kinetic energies is minimized by applying a high voltage extraction pulse synchronized with the RF phase angle. Ions at different positions in the segmented ring ion source gain different kinetic energies during the ion extraction period. The reflectron can be regarded as a device that temporally focuses isomass ions with an initial spatial distribution in the ion source.

The essence of this temporal focusing is for all isomass ions to have the same flight time between the application of the extraction pulse and their arrival at the detector surface. The required profile for the reflectron voltage to achieve this can be obtained by the numerical calculation method as described below and illustrated in Figure 3-3. The ion extraction field normally consists of two linear fields. As discussed in a later section of this chapter, the reflectron

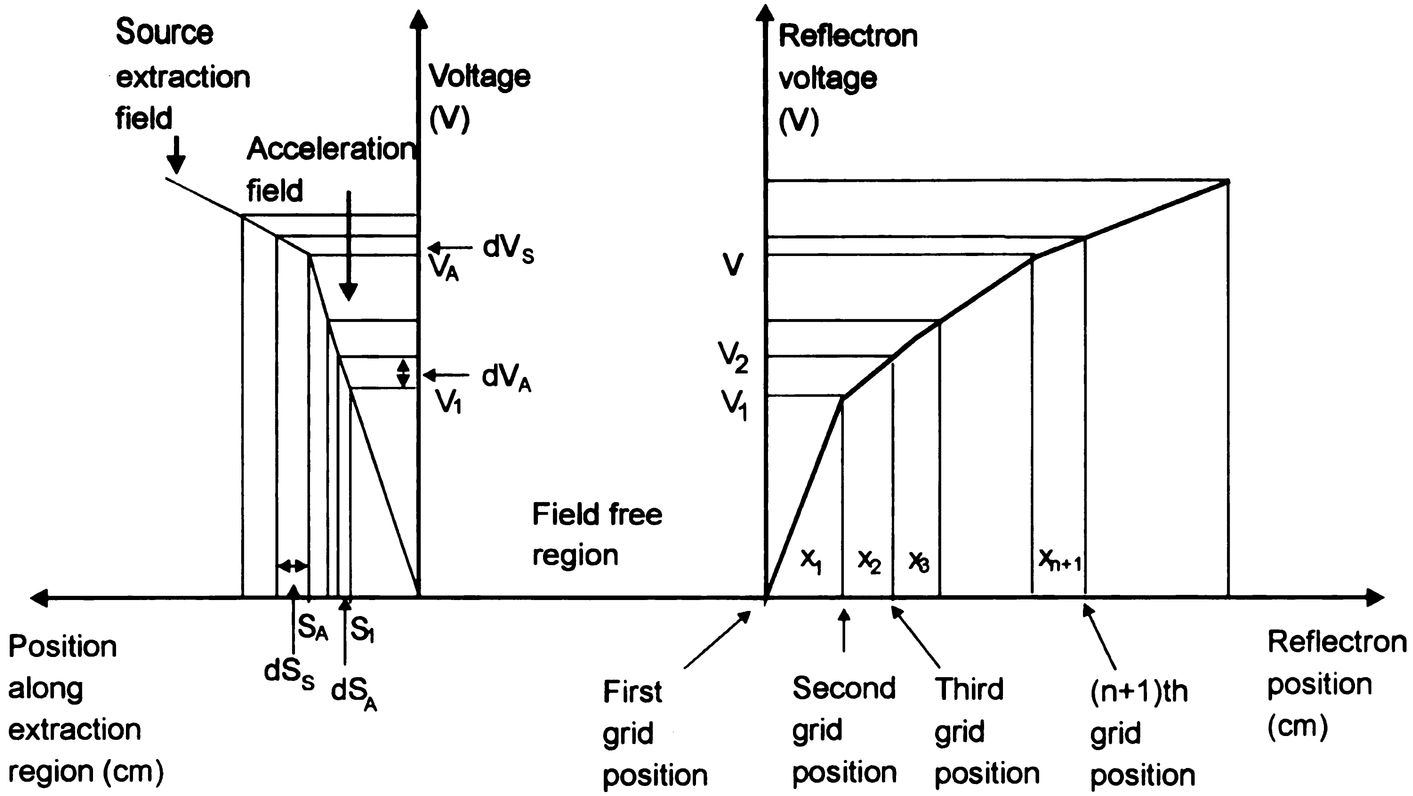

Figure 3-3. Representative diagram of the ion extraction and reflectron voltage profiles for the numerical construction of a reflectron voltage profile to focus isomass ions extracted from the ion extraction region. Isomass ions obtain different kinetic energies in the field free region due to their different initial positions in the ion extraction region.

desig
the a
regio
Ass
to V
posi
ion i
third
V_1+2
extra
the e
were

fligh

con
firs
in o
first

positi

designed should be able to focus isomass ions with kinetic energies lower than the actual minimum kinetic energy. So the ions initially in the acceleration field region as well as in the extraction field region need to be temporally focused. Assume that acceleration field has a distance of S_A and an extraction voltage up to V_A, The lowest energy ion needs to be temporal focused is extracted at the position S_1 with the extraction voltage of V_1 as shown in Figure 3-3. The second ion is initially at the position of S_1+dS_A with an extraction voltage of V_1+dV_A, the third ion is initially at the position of S_1+2dS_A with an extraction voltage of V_1+2dV_A, and the nth ion is initially at the position of $S=S_1+(n-1)dS_A$ with the extraction voltage of $V=V_1+(n-1)dV_A$. So the increments of the ion position and the extraction energy in the acceleration region for each consecutive calculation were $dS_A=S_A/(n-1)$ and $dV_A=V_A/(n-1)$.

The velocity of the first ion in the field-free flight region is $U_1^{(1)}=\sqrt{2\frac{V_1}{m}}$. The flight time upon entering the field free region is $t_s=\frac{2S_1}{U_1^{(1)}}$. The reflectron field construction process is same as that described in the previous section. Since first grid of the reflectron is 0 V, the next grid needs to be set at the voltage of V_1 in order to stop this first ion. This second grid is set at the distance x_1 away from first reflectron grid.

The velocity of the first ion in the field flight region and at the first grid position is $U_1^{(1)}=\sqrt{2\frac{V_1}{m}}$, so the average speed of the first ion at the region between grid one and grid two is $U_1^{(1)}/2$. The total flight time of ion reaching the detector is

$$T_{tot} = \frac{2S_1}{U_1^{(1)}} + \frac{L_{ff}}{U_1^{(1)}} + \frac{2x_1}{U_1^{(1)}}2, \tag{3.19}$$

the factor 2 is added in third term because the ion travels both forward and back backward through the reflectron.

The velocity of the second ion in the field free region is $U_1^{(2)} = \sqrt{2\frac{V_2}{m}}$, where $V_2 = V_1 + dV_A$ is the kinetic energy of the second ion obtained from the ion acceleration field. The flight time for the second ion to exit the acceleration region is $t_a = \frac{S_1 + dS_A}{U_1^{(2)}/2}$. The second ion with a kinetic energy $V_2=V_1+dV_A$ (eV) will pass the second grid, a third grid needs to be set at the voltage V_2 in order to stop the ion right at that grid position. In order to let the second isomass ion arrive at the detector at the same time as the first ion, the distance between the second grid and the third grid must be set at the distance x_2 that is obtained from following calculation.

The velocity of the second ion in the field free region and at the first grid position is $U_1^{(2)} = \sqrt{2\frac{V_2}{m}}$. The velocity of the second ion at the second grid position is $U_2^{(2)} = \sqrt{2\frac{dV_A}{m}}$, its the average velocity after the first grid is $(U_1^{(2)}+U_2^{(2)})/2$, and after the second grid is $U_2^{(2)}/2$.

The total flight time of the second ion is

$$T_{tot} = \frac{S_1 + dS_A}{U_1^{(2)}} 2 + \frac{L_{ff}}{U_1^{(2)}} + \frac{2x_1}{U_1^{(2)} + U_2^{(2)}} 2 + \frac{2x_2}{U_2^{(2)}} 2 \tag{3.20}$$

so

$$x_2 = [T_{tot} - (\frac{S_1 + dS_A}{U_1^{(2)}} 2 + \frac{L_{ff}}{U_1^{(2)}} 2 + \frac{2x_1}{U_1^{(2)} + U_2^{(2)}} 2)] \frac{U_2^{(2)}}{4} \tag{3.21}$$

For the *n*th ion, the ion velocity in the field-free flight region is

$$U_1^{(n)} = \sqrt{2\frac{V_n}{m}}; \; V_n = V = V_1 + (n-1)dV_A \tag{3.22}$$

and the flight time in the ion acceleration region is

$$t_s = \frac{S_A}{U_1^{(n)}/2} = \frac{S_1 + (n-1)dS_A}{U_1^{(n)}/2} \tag{3.23}$$

The velocity of the *n*th ion at the first reflectron grid position is

$$U_1^{(n)} = \sqrt{2\frac{V_n}{m}} \tag{3.23}$$

at the second grid position is

$$U_2^{(n)} = \sqrt{2(n-1)\frac{dV_A}{m}} \tag{3.24}$$

and at the 3rd to the *n*th grid positions is

$$U_i^{(n)} = \sqrt{2[(n-i)+1]\frac{dV_A}{m}}; \; i = 3, \ldots, n \tag{3.25}$$

The total flight time for the *n*th ion is

$$T_{tot} = \frac{S_1 + (n-1)dS_A}{U_1^{(n)}} 2 + \frac{L_{ff}}{U_1^{(n)}} + \sum_{i=1}^{n-1} (\frac{2x_i}{U_i^{(n)} + U_{i+1}^{(n)}}) + \frac{2x_n}{U_n^{(n)}} 2 \tag{3.27}$$

The distance between the *n*th and *(n+1)*th grids is

$$x_n = \{T_{tot} - [\frac{S_1 + (n-1)dS_A}{U_1^{(n)}} 2 + \frac{L_{ff}}{U_1^{(n)}} + \sum_{l=1}^{n-1} (\frac{2x_l}{U_l^{(n)} + U_{l+1}^{(n)}})]\} \frac{U_n^{(n)}}{4} \qquad (3.28)$$

After the ions extracted from the acceleration region are considered, the construction of the reflectron voltage profile should be extended to focus ions extracted from the source extraction region.

Assume the *(n+1)*th ion is initially located at the position of S_A+dS_S so the extraction voltage is $V_{n+1}=V_A+dV_S$, and the extraction field is dS_S/dV_S. The total flight time of the *(n+1)*th ion in the ion acceleration and extraction region is

$$t_s = \frac{S_A}{u_1^{(n+1)} + U_1^{(n+1)}} 2 + \frac{dS_S}{u_1^{(n+1)}} 2 \qquad (3.29)$$

where the velocity at the exit position of acceleration field region is

$$U_1^{(n+1)} = \sqrt{\frac{2V_{n+1}}{m}}; \; V_{n+1}=V_A+dV_S$$

and the velocity at the exit position of source extraction field region is

$$u_1^{(n+1)} = \sqrt{\frac{dV_S}{m} 2}$$

The velocity of the *(n+1)*th ion in the field free region and at the first grid position is

$$U_1^{(n+1)} = \sqrt{\frac{2V_{n+1}}{m}} \qquad (3.30)$$

at the second grid position is

$$U_2^{(n+1)} = \sqrt{(dV_S + (n-2)dV_A + V_1)\frac{2}{m}} \qquad (3.31)$$

and at the 3rd to the *n*th grid positions are

$$U_i^{(n+1)} = \sqrt{[dV_S + dV_A(n-i) + V_1]\frac{2}{m}};\ i = 3, \ldots, n \tag{3.32}$$

and at the *(n+1)*th grid position is

$$U_{n+1}^{(n+1)} = \sqrt{2\frac{dV_S}{m}} \tag{3.33}$$

So the total flight time for the *(n+1)*th ion is

$$\begin{aligned} T_{tot} = {} & \frac{dS_s}{u_1^{(n+1)}}2 + \frac{S_A}{u_1^{(n+1)} + U_1^{(n+1)}}2 + \frac{L_{ff}}{U_1^{(n+1)}} + \\ & \sum_{l=1}^{n}\left(\frac{2x_l}{U_l^{(n+1)} + U_{l+1}^{(n+1)}}\right) + \frac{2x_{n+1}}{U_{n+1}^{(n+1)}}2 \end{aligned} \tag{3.34}$$

and the distance of added grid after the *(n+1)*th grid is

$$\begin{aligned} x_{n+1} = {} & \{T_{tot} - [\frac{dS_s}{u_1^{n+1}}2 + \frac{S_A}{u_1^{n+1} + U_1^{(n+1)}}2 + \frac{L_{ff}}{U_1^{(n+1)}} + \\ & \sum_{l=1}^{n}(\frac{2x_l}{U_l^{(n+1)} + U_{l+1}^{(n+1)}})]]\}\frac{U_{n+1}^{(n+1)}}{4} \end{aligned} \tag{3.35}$$

For the *(n+k)*th ion, where *k* is the number to label the ions at the ion source position $S_A + k \cdot dS_S$. The total flight time in the source extraction region and acceleration region is

$$t_s = \frac{S}{u_k^{(n+k)} + U_k^{(n+k)}}2 + \frac{dS_s \cdot k}{u_k^{(n+k)}}2 \tag{3.36}$$

The ion velocity at the exit position of acceleration field region is

$$U_k^{(n+k)} = \sqrt{\frac{2V_{n+N}}{m}},\ V_{n+k} = V + k \cdot dv \tag{3.37}$$

The velocity at the exit position of source extraction field region is

$$u_k^{(n+k)} = \sqrt{2\frac{k \cdot dV_S}{m}} \tag{3.38}$$

The velocity of the *(n+k)*th ion at the first grid position is

$$U_1^{(n+k)} = \sqrt{2\frac{V_{n+k}}{m}} \tag{3.39}$$

and at the 2nd to the *n*th grid position is

$$U_i^{(n+k)} = \sqrt{(k \cdot dV_S + (n-i)dV_A + V_i)\frac{2}{m}};\ i = 2,\ldots,\ n \tag{3-40}$$

and at the *(n+1)*th to the *(n+k)*th grid position is

$$U_{n+j}^{(n+k)} = \sqrt{(k-j+1)\frac{dV_S}{m}2};\ j=1,\ldots k \tag{3-41}$$

The total flight time for the (*n+k*)th ion is

$$\begin{aligned} T_{tot} &= \frac{k \cdot dS_S}{u_k^{(n+k)}}2 + \\ &\frac{S_A}{u_k^{(n+k)} + U_1^{(n+k)}}2 + \frac{L_{ff}}{U_1^{(n+k)}} + \sum_{l=1}^{n+k-1}\left(\frac{2x_l}{U_l^{(n+k)} + U_{l+1}^{(n+k)}}\right) + \frac{2x_{n+k}}{U_{n+k}^{(n+k)}}2 \end{aligned} \tag{3-42}$$

So the distance between the *(n+k)*th and the *(n+k+1)*th grid is

$$\begin{aligned} x_{n+k} &= \{T_{tot} - [\frac{k \cdot dS_S}{u_k^{(n+k)}}2 + \frac{S_A}{u_k^{(n+k)} + U_1^{(n+k)}}2 \\ &+ \frac{L_{ff}}{U_1^{(n+k)}} + \sum_{l=1}^{n+k-1}(\frac{2x_l}{U_l^{(n+k)} + U_{l+1}^{(n+k)}})]\}\frac{U_{n+k}^{(n+k)}}{4}2 \end{aligned} \tag{3-43}$$

The above calculation strategy gives a voltage profile for a reflectron that is able to focus ions distributed initially at different positions in an ion source. The variables in the above calculation are the parameters related to the ion source (extraction field strengths, the dimensions of the two extraction field and the starting position at the first extraction field), and the variables related to the time-of-flight instrument construction such as the length of the first linear field region in the reflectron, the total length of the reflectron, and the length of the field-free region. The voltage profile of the reflectron obtained from the above calculation is applicable for isomass ions of all m/z values. A Mathcad program has been constructed to calculate the voltage profile according to practical instrumental parameters. Computer simulation (SIMION) has been used to assist in the reflectron design and examine isomass ion temporal distributions at the temporal focus position.

3.3. Computer simulation and practical design consideration

The voltage profile obtained from the Mathcad calculation is a voltage profile along the reflectron axial direction. Isomass ions with different kinetic energies entering the reflectron will be near perfectly focused to the detector position with a small temporal distribution. For a practical design, a stack of stainless steel ring electrodes is used to achieve this reflectron voltage profile. A calculated voltage profile that could be easily obtained in the real reflectron design is the most desirable one.

The SIMION program for computer modeling of ion trajectories was used to model the temporal focusing of several possible practical designs. The computer simulation of the ion trajectories of a set of ions (*m/z* 100) initially distributed in the ion source at various initial positions is shown in Figure 3-4. An 1800 V acceleration voltage is applied to the ion acceleration electrode. An additional 800 V is applied across the ion source region. The total length of the

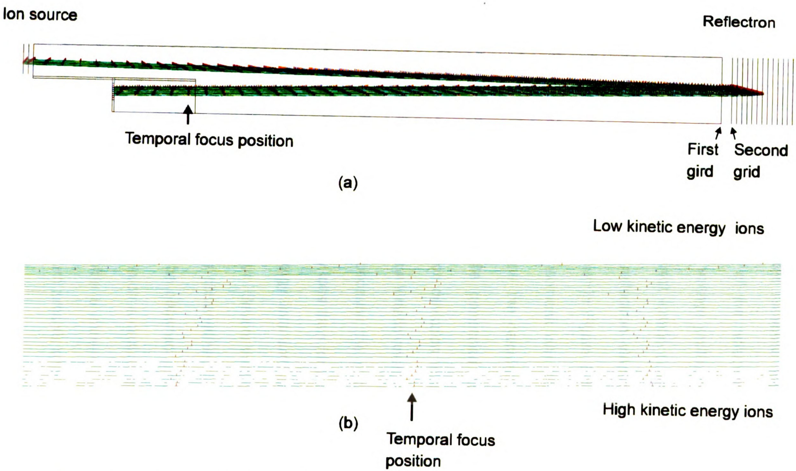

Figure 3-4. Computer simulation of the ion trajectories (green lines) of m/z 100 ions initially at different positions in the ion source.
The groups of red dots show the ion positions at 0.5 μs intervals along the flight path.
The voltage profile applied to the reflectron is shown in Figure 3-5.

field-free region before and after the front of the reflectron is 118 cm. The first grid and the second grid of the reflectron are 2 cm apart. Twelve grids were added after the second grid of the reflectron. The space between adjacent reflectron grids is 1 cm. The voltage profile along ion axis of the reflectron is shown in Figure 3-5. The lowest kinetic energy ion (1800 eV kinetic energy) turns around at the second reflectron electrode. The ion distribution at the temporal focus position is shown in Figure 3-4(b). From this figure we can see that a temporal distribution of isomass ions (250 ns) still exists at the temporal focus position. This is because the calculated voltage profile is not exactly followed by the voltage profile generated between two adjacent reflectron electrodes. Also the ion position deviation from the temporal focus position is much larger for the ions with low kinetic energy than that for the ions with high kinetic energy. This is partly because the relative energy distribution ratio is larger for the low kinetic energy ions than for the high kinetic energy ions. More significantly the low kinetic energy ions turn around at the reflectron position closest to the second grid position. Severe field curvature exists in this region as shown in Figure 3-5. From this observation, it is reasonable to expect that a better temporal focusing could be obtained by using only the back part of the reflectron. A voltage profile for such a design is shown in Figure 3-6; The ion trajectory simulation for this profile is shown in Figure 3-7. In this design, the lowest energy ions (1800 eV) turn around after the fourth reflectron electrode.

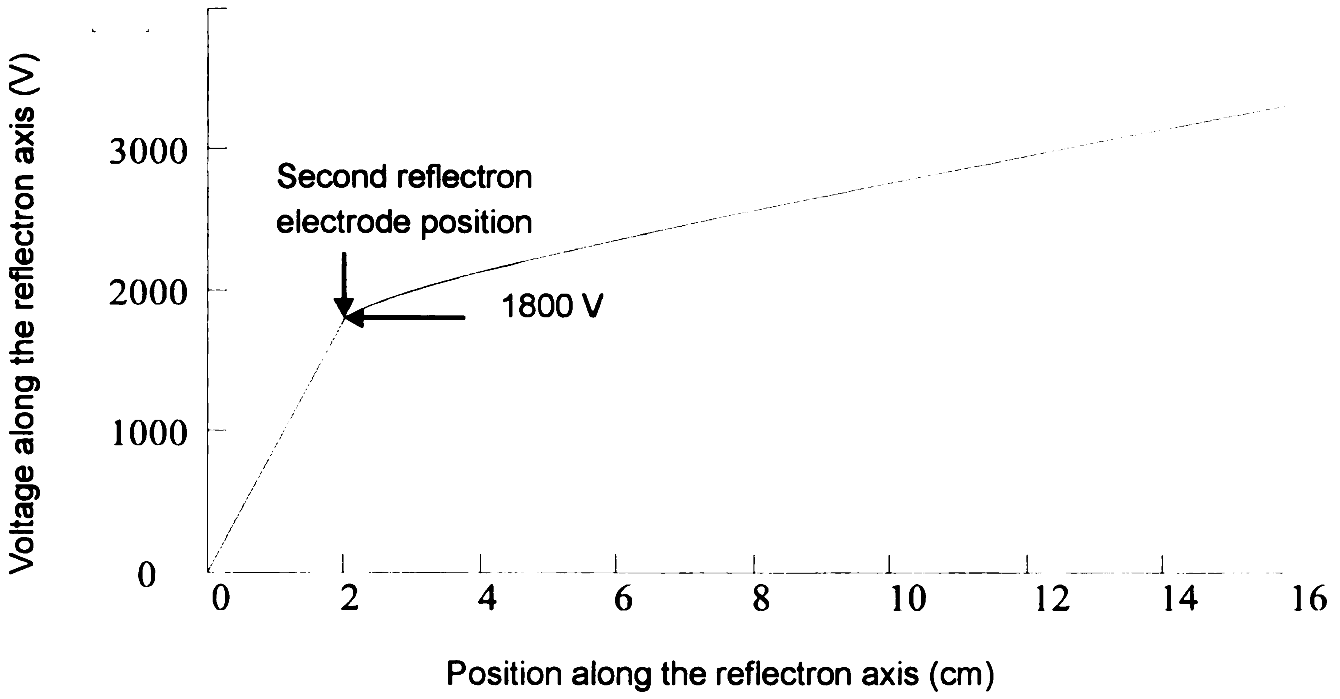

Figure 3-5. The voltage profile applied to the reflectron shown in Figure 3-4. The lowest energy ions turn around at the second reflectron grid position.

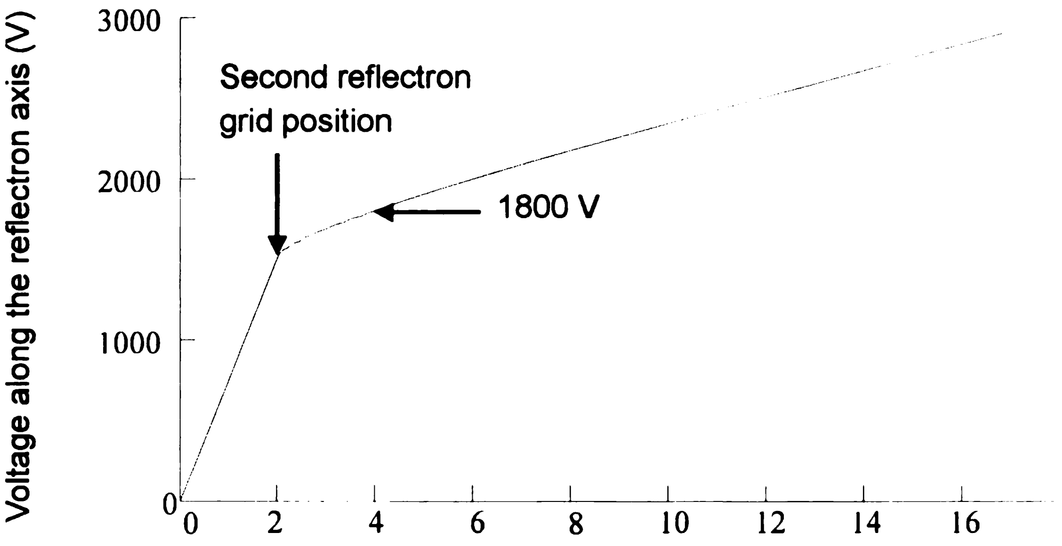

Positon along the reflectron axis (cm)

Figure 3-6 .The voltage profile applied to the reflectron shown in Figure 3-7. The lowest energy ions turn around after the fourth reflectron electrode.

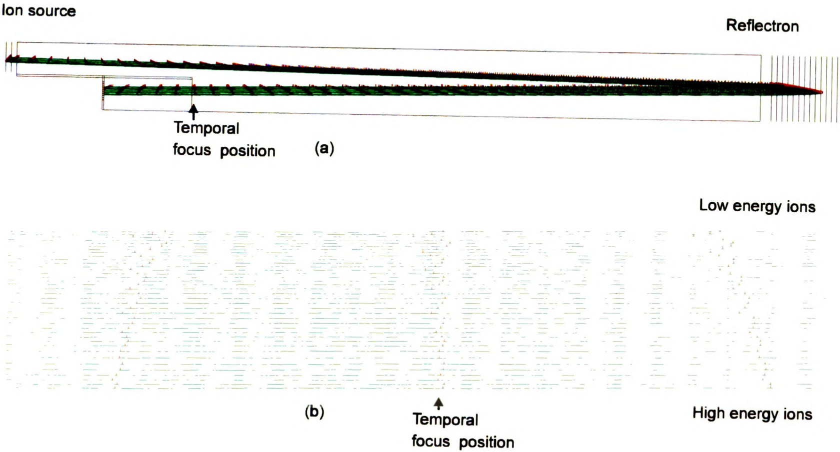

Figure 3-7. Computer simulation of the ion trajectories of m/z 100 ions initially at different positions in the ion source. The groups of red dots show the ion positions at 0.5 μs flight time intervals along the flight path.

An arrival time distribution (64 ns) still exists at the temporal focus position for isomass ions but the magnitude of the deviation is decreased.

Using reflectron electrodes that are covered with mesh screens will give a reflectron voltage profile along the reflectron axial direction that is close to the calculated value. In a practical design, the more reflectron grids there are in the ion flight path, the more ions will be lost due to the transmission efficiency of these mesh screens. Much higher ion transmission would be obtained if fewer mesh screens were used along the flight path. After the mesh screens from the third reflectron electrode to the 11th reflectron electrode are removed, the ion trajectory simulation changes from that shown in Figure 3-7 to that shown in Figure 3-8. The temporal focusing position moves 19 cm closer to the front of the reflectron. A large temporal distribution (178 ns) and a increased radial dispersion at the temporal focus position results. The equipotential contour of the reflectron shown in Figure 3-8 is shown in Figure 3-9. The black lines represent the reflectron electrodes. The red lines are equipotential contours with the same voltages as applied to the corresponding electrodes. Since the reflectron field along the axial reflectron direction after the second reflectron electrode is not linear, the voltage profile distortions become more severe after the removal of the mesh screens. The deviation from the derived voltage profile changes the temporal focus position and the quality of the temporal focusing at the temporal focus position for isomass ions with a broad distribution of kinetic

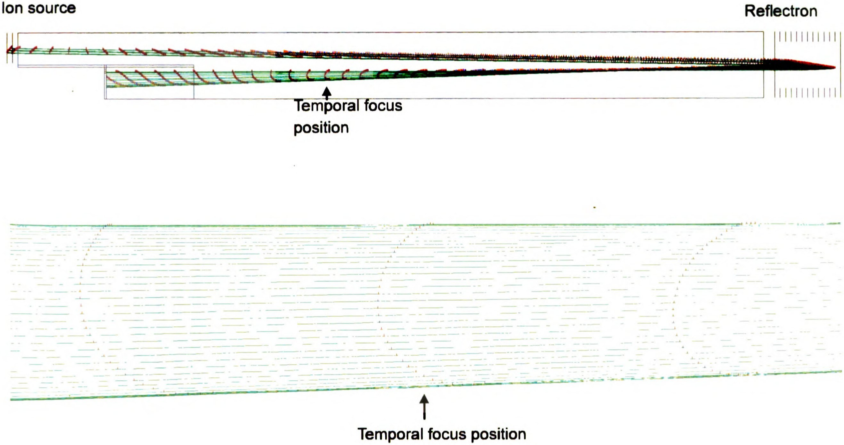

Figure 3-8. Computer simulation of the ion trajectories (green lines) of m/z 100 ions initially at different positions in the ion source. The groups of red dots show the ion positions at 0.5 μs along flight path.

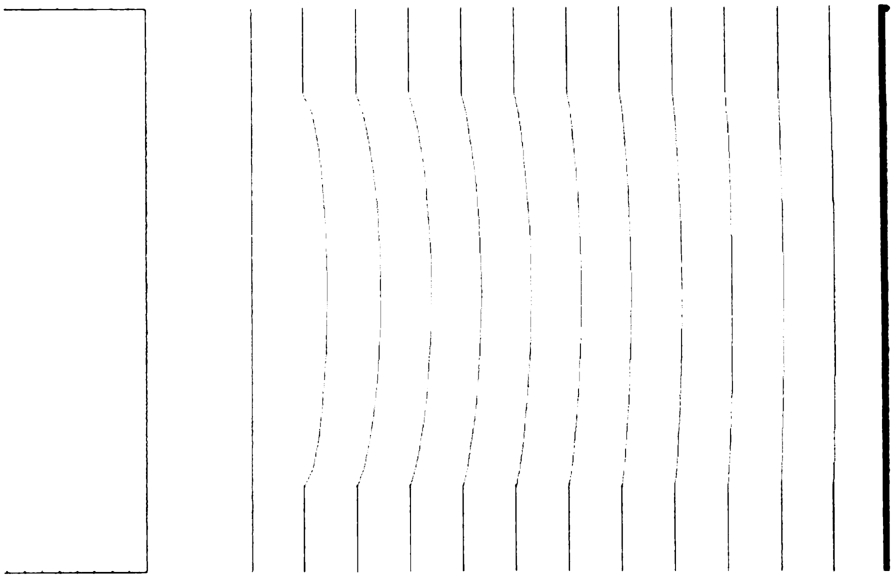

Figure 3-9. Equipotential contours of the reflectron in Figure 3-8. The deviation of the voltage profile in the center of the reflectron from the voltage profile applied to the reflectron electrodes creates a distortion of the desired field and introduces an ion lensing effect.

energies. The lens effect caused by the curvature of the field lines spreads out isomass ions in the radial direction.

These problems could be minimized by using the following two approaches. First, we can readjust the reflectron electrode voltages manually following the computer simulation to bring the voltage profile along the ion flight path closer to the calculated values. In a practical situation, a reflectron quite similar to the simulated reflectron (in three-dimensional scale) needs to be constructed and then the electrode voltage values obtained from the simulation adjustment could be applied to the real reflectron electrodes. For the reflectron voltage profile shown in Figure 3-6, the reflectron field dramatically changes before and after second reflectron grid. A dramatic voltage change will result in severe field distortion in the vicinity of the mesh grid. A reflectron voltage profile having a small field change in the vicinity of the second grid area is preferred.

The second approach is to adjust the reflectron design parameters to obtain voltage profile such that a real voltage profile close to the calculated one along the axial direction of the reflectron could be easily achieved by simply applying the calculated voltages to the reflectron electrodes.

At this particular energy focusing situation (800 eV kinetic energy distribution and 1800 V acceleration voltage, a voltage profile close to a linear field as shown in Figure 3-10, was obtained through the Mathcad program calculation by setting the total reflectron length to 50 cm, the total field-free region distance (before and after the front the reflectron position) to 164 cm and

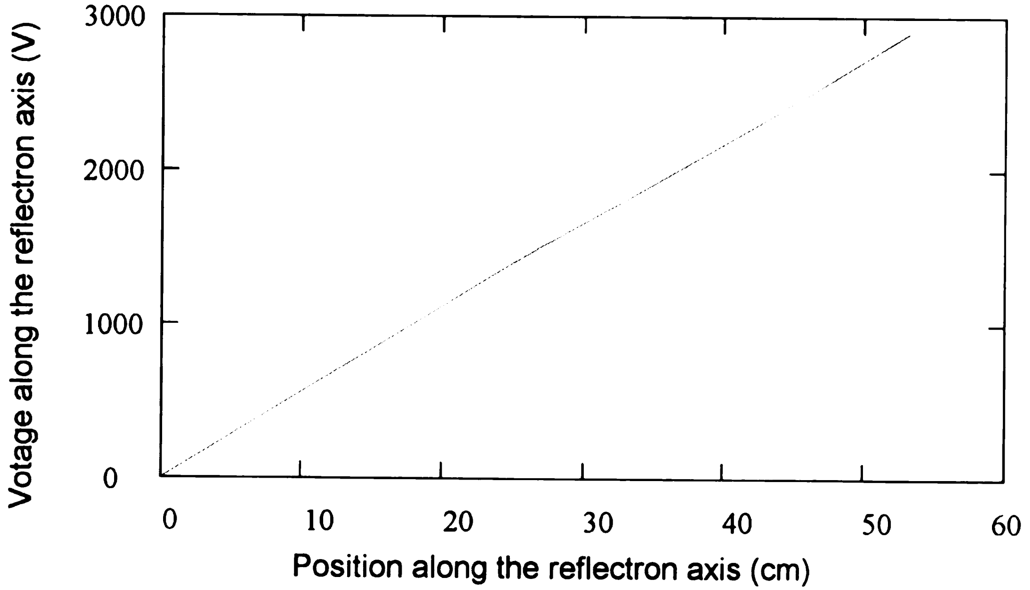

Figure 3-10. Voltage profile applied to the reflectrons shown in Figures 3-11, 3-12, 3-13.

the first linear field distance between the first reflectron electrode and second reflectron electrode to 25 cm. An ion trajectory simulation of the time-of-flight instrument with this reflectron configuration, and the applied voltage profile shown in Figure 3-10 is shown in Figure 3-11. All the reflectron electrodes are covered with mesh screens. The field between the first and the second reflectron electrode is linear (In a practical construction situation, a series of reflectron electrodes with voltage dividers will be needed to generate the linear field in this region). An additional 25 electrodes, separated by 1 cm, are employed. The total field-free region flight path before and after the reflectron is 176 cm. A small isomass ion temporal distribution (11 ns) at the temporal focusing position and a collimated ion beam are achieved using this reflectron configuration and this voltage profile. After the mesh screens from the third reflectron electrode to the 26th reflectron electrode are removed, the ion trajectory simulation is shown in Figure 3-12. A collimated ion beam and a small temporal isomass distribution (24 ns) are maintained. This remains true even when only the first and last electrodes are covered with mesh screen as shown in Figure 3-13. The collimated ion trajectory beam and the small temporal distribution of isomass ions (24 ns) at the temporal focusing position still exists. Considering that the total flight time for an m/z 100 ion to reach the temporal focusing position is 51 μs, a resolution of 2000 (FWHM) will result if only the initial spatial distribution broadening is considered. After some of the reflectron grids are removed as shown in Figure 3-12 and Figure 3-13, the temporal focus positions only move

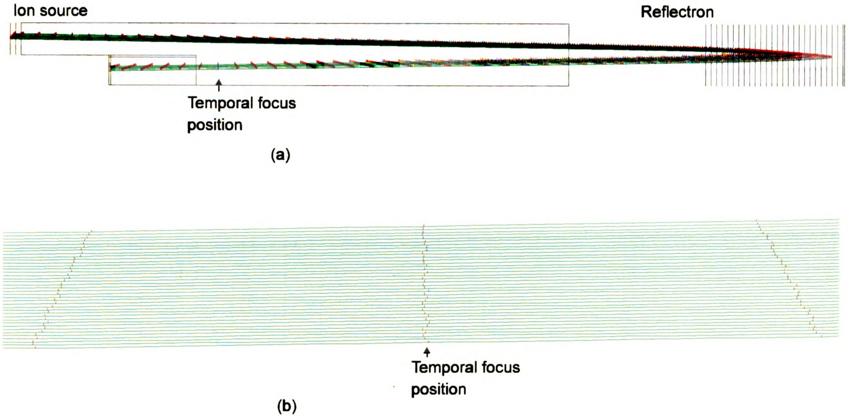

Figure 3-11. Computer simulation of ion trajectories (green Lines) of m/z 100 ions initially at different positions in the ion source. The groups of red dots show the ion positions at 0.5 μs intervals along the flight path.

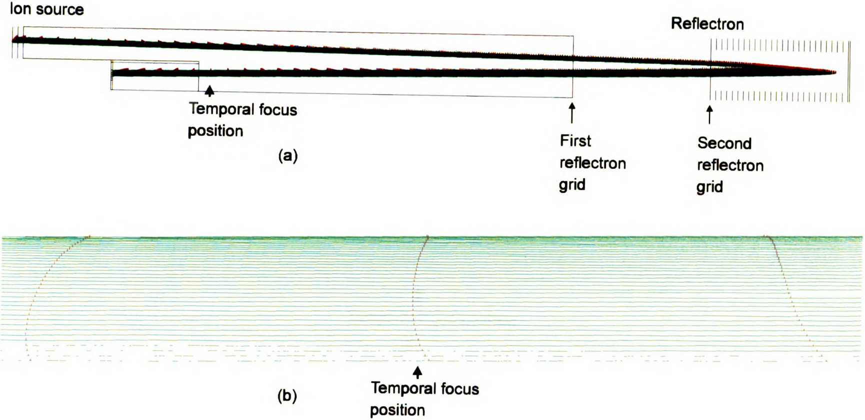

Figure 3-12. Computer simulation of the ion trajectories (green lines) of m/z 100 ions initially at different positions in the ion source.
The groups of red dots show the ion positions at 0.5 μs intervals along the flight path.

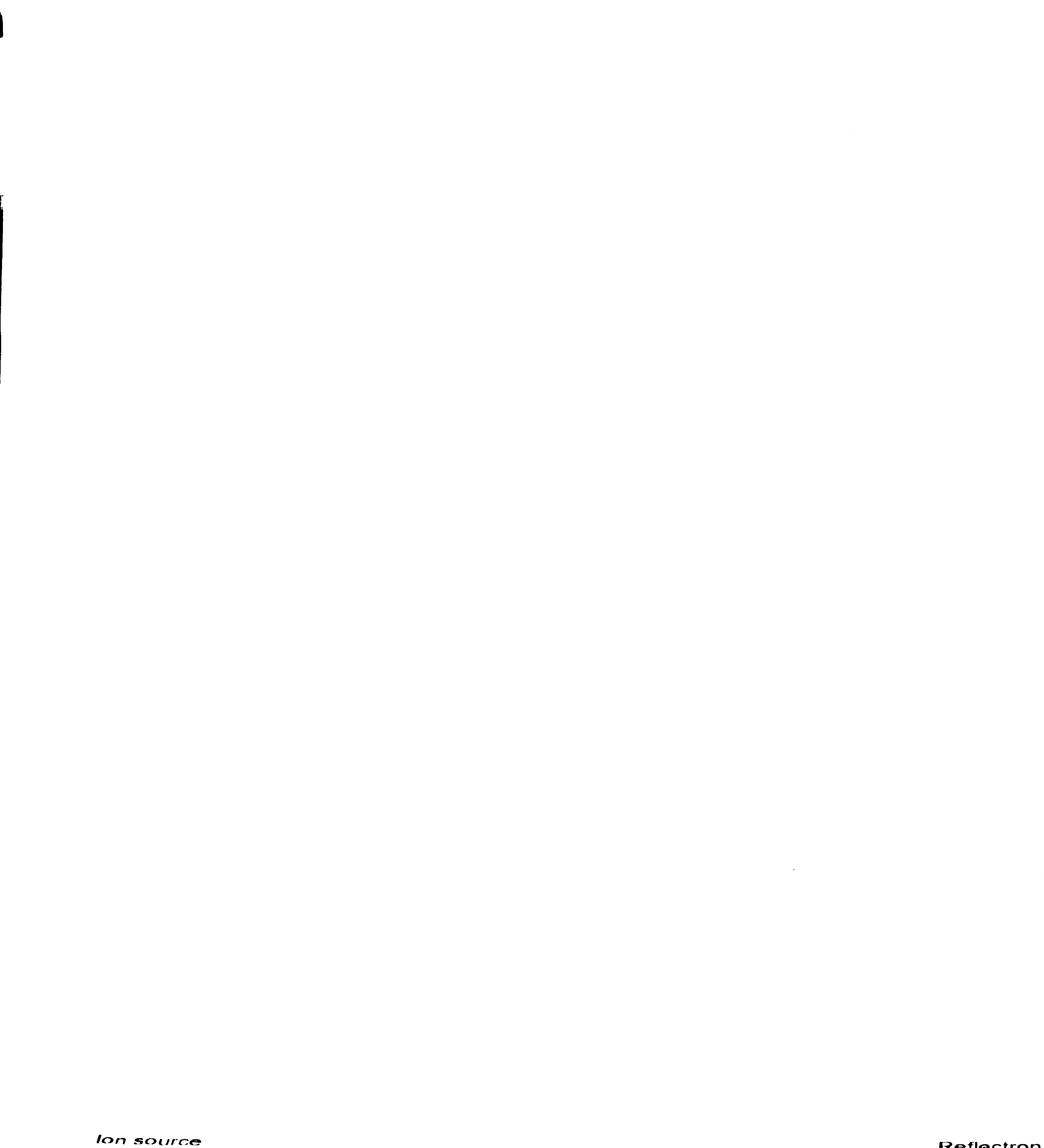

Ion source
Reflectron

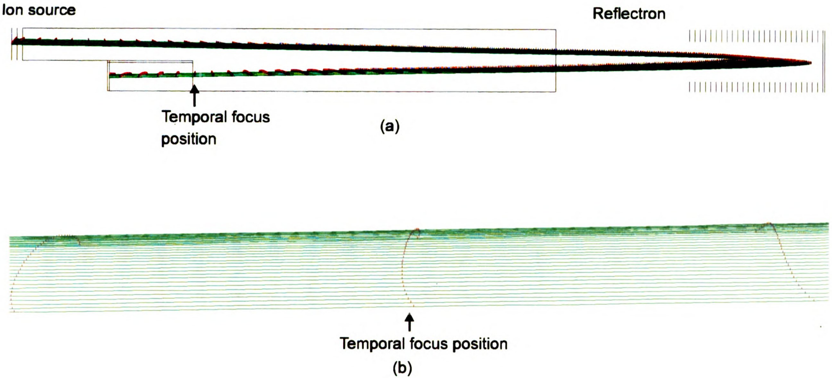

Figure 3-13. Computer simulation of the ion trajectories (green lines) of m/z 100 ions initially at different positions in the ion source.

The groups of red dots show the ion positions at 0.5 μs flight time intervals along the flight path.

1.7

equ

13

con

volt

Be

are

ion

ten

as

calc

sim

volt

dist

focu

Sm

dist

the

calc

som

1.7 cm and 3.3 cm further away from the front of the reflectron respectively. The equipotential contours for the reflectron configurations shown in Figures 3-12, 3-13 are shown in Figure 3-14. The electrodes are in black and the equipotential contours are red lines. The voltage of each contour line is the same as the voltage calculated and applied to the corresponding reflectron electrode. Because the voltage profile is close to linear, these equipotential contour lines are almost parallel and straight. These uniform contours provide the collimated ion trajectory beams and the small isomass ion temporal distributions at the temporal focusing position as they appear in Figures 3-12, 3-13.

A linear field voltage profile is applied to the same reflectron configuration as shown in 3-15. The red line is the voltage profile obtained from the Mathcad calculation. The black line is the linear voltage profile. The ion trajectory simulation of the time-of-flight instrument with the reflectron that uses this linear voltage profile is shown in Figure 3-16. A much larger isomass temporal distribution at the temporal focus position (170 ns) results. The temporal focusing obtained with the reflectron is quite sensitive to the voltage applied. Small deviations from the calculated voltage profile results in a large temporal distribution at the temporal focus position as shown in Figure 3-16. Increasing the density of the reflectron electrodes generates voltage profiles close to the calculated values along the axial reflectron direction.

The mesh screen that remains on the front reflectron electrode will cause some field distortion near the grid aperture of the screen. However, since the

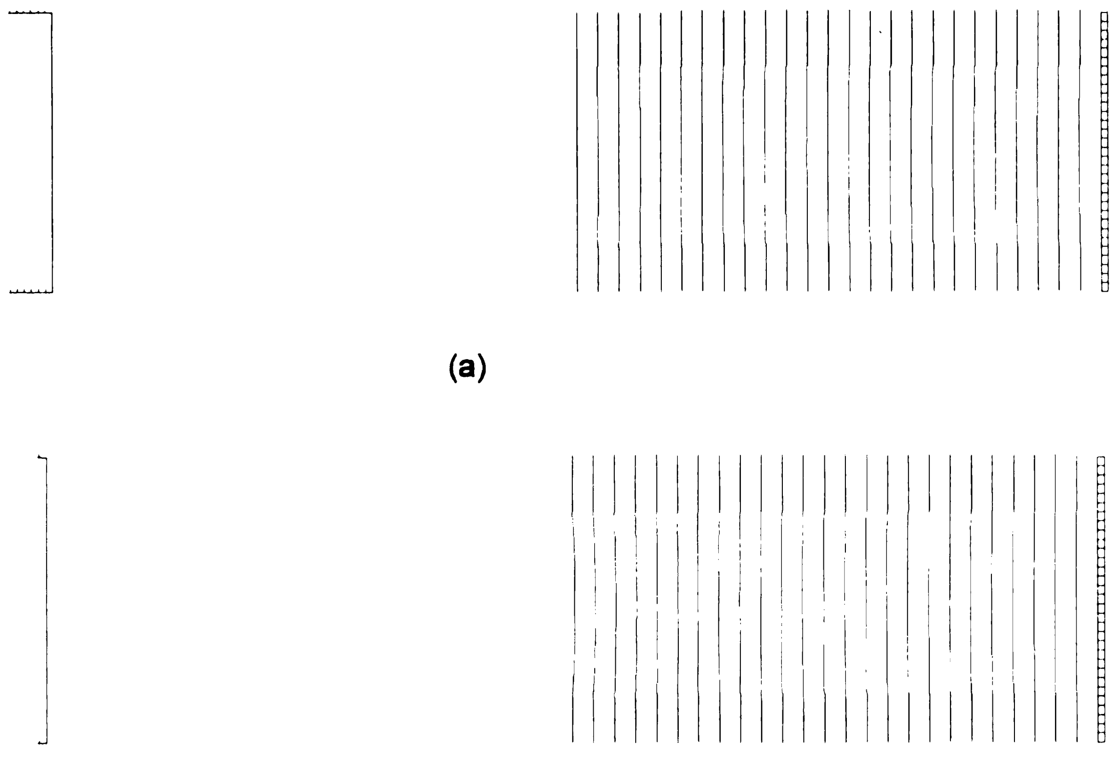

(a)

(b)

Figure 3-14. Equipotential contours (red lines) of the reflectron in which the second reflectron electrode is covered with a grid (a) or not covered with a grid (b) as shown in Figure 3-12 and Figure 3-13 respectively. Electrodes are in black and equipotential lines are red.

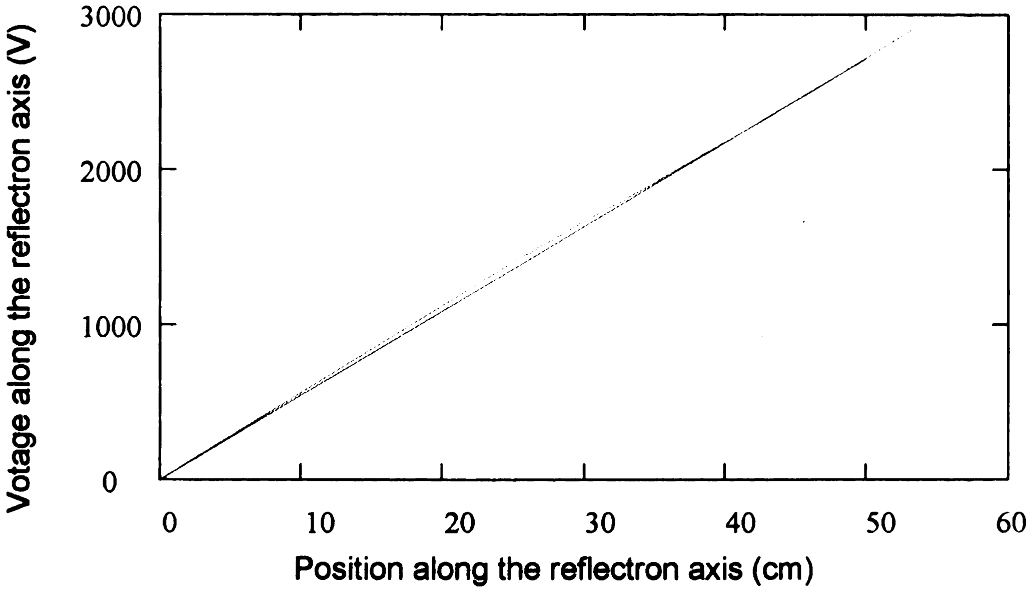

Figure 3-15. The voltage profiles applied to the reflectrons shown in Figures 3-13, 3-16. The red line is obtained from calculation for perfect temporal energy focusing. The black line represents the linear voltage profile applied to the reflectron shown in Figure 3-16.

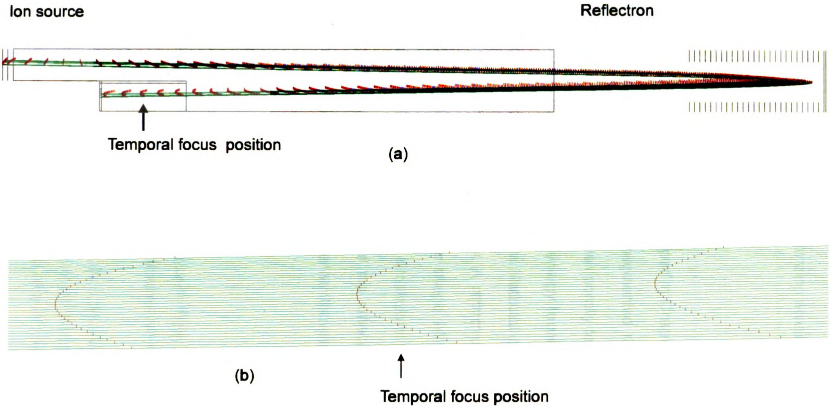

Figure 3-16. Computer simulation of the ion trajectories (green lines) of m/z 100 ions initially at different positions in the ion source.
The groups of red dots show the ion position at 0.5 μs flight time intervals.
The voltage profile applied to the reflectron is linear.

ior

ha

in

3.

Th

de

ext

in

vol

the

and

the

use

stor

Ref

---

of th

June

Broad

Spect

ions enter the reflectron at their maximum speed, this field distortion effect will has less effect than that of a grid separating areas of different field strength later in the reflectron.

3.4. Conclusion

The theoretical considerations developed in Chapter Two formed a basis for the design considerations of an actual segmented ring ion source. Isomass ions extracted from the ion source can be temporally focused at the detector position in a narrow ion bunch with a broad energy focusing reflectron. The reflectron voltage profile can be obtained from a Mathcad program calculation based on the strategy explained in this chapter. A reflectron with an appropriate length and a reflectron field with near linear shape will be the most desirable. The theoretical calculations and computer simulations of the reflectron design were used to guide the practical design of the reflectron for the segmented ring, storage time-of-flight mass spectrometer as discussed in the next chapter.

***References*:**

---

1 Rockwood A. L.: An Improved Time-of-Flight Mass Spectrometer. Proceedings of the 34th ASMS conference on mass spectrometry and allied topics, Cincinnati, Ohio, June 8-13, 173-174 (1986)

2 a. Ji, Q., Vlasak, P. R., Beussman, D. J., and Enke, C. G.: A Reflectron for Broad Energy Focusing of Ions. Proceedings of the 42nd ASMS Conference on Mass Spectrometry and Allied Topics, Chicago, IL, May 29 - June 3, 1039 (1994)

Me
Soc

Ion
117

Refl
Sov.

JETP

Trans
Proce

Time
Anal

Acce
37-43

89-11

Longi
Proces

Spectro
411-414

---

b. Vlasak, Paul R., Beussman, Douglas J., Ji, Qinchung, and Enke, C. G.: A Method for the Design of Broad Energy Range Focusing Reflectrons. Accepted, J. Am. Soc. Mass. Spectrom. (1995).

3 a. Karataev, V. I., Mamyrin, M. A. and Shmikk, D. V.: New Method Focusing Ion Bunches in Time-of-Flight Mass Spectrometers. Sov. Phys. Tech. Phys., 16, 1177-1179 (1972)

b. Mamyrin, B. A., Karataev, V. I., Shmikk, D. V., and Zagulin V. A.: The Mass Reflectron, a New Nonmagnetic Time-of-Flight Mass Spectrometer with High Resolution. Sov. Phys. JETP, 37, 1, 45-48 (1973)

c. Mamyrin, B. A., and Shmikk, D. V.: The linear Mass Reflectron. Sov. phys. JETP 49, 5, (1979)

4 Ioanoviciu, D., Yefchak, G. E. and Enke, C. G.: Second Order Space-Time Transfer Matrix of the Two-Stage Electrostatic Mirror. Int. J. Mass Spectrom. Ion Processes, 94, 281-291 (1989)

5 Boesl U., Grotemeyer J., Walter, K. and Schlag, E. W.: A High-Resolution Time-of-Flight Mass Spectrometer with Laser Desorption and a Laser Ionization Source. Analytical Instrumentation, 16, 1, 151-171 (1987)

6 Chen. C. C., and Su, C. S.: A Time-of-Flight Mass Spectrometer with an Accelerating Field in the Reflecting System. Int. J. Mass Spectrom. Ion Processes, 124, 37-43 (1993)

7 Wollnik, H.: Time-of-Flight Mass Analyzer. Mass Spectrometer Reviews, 12, 89-114 (1993)

8 Kutscher, R., Grix, R., Li, G. and Wollik, H.: A Transversally and Longitudinally Focusing Time-of-Flight Mass Spectrometer. Int. J. Mass Spectrom. Ion Processes, 103, 117-128 (1993)

[9] Gohl, W., Kutcher, R. Laue, H. J. and Wollnik, H.: A Time-of-Flight Mass Spectrometer for Ions of Large Energy Spread. Int. J. Mass Spectrom. Ion Processes, 48, 411-414 (1983)

---

[10] Grix, R., Kutscher, R., Li, G., Gruner, U., and Wollnik, H.: Rapid Comm. Mass Spectrom., 2, 5, 83-85 (1988)

[11] Cornish T. J. and Cotter R. J.: A Curved-Field Reflectron for Improved Energy Focusing of Products in Time-of-Flight Mass Spectrometry. Rapid Commun. Mass Spectrom., 7, 1037-1040 (1993)

[12] Makarov, A. A., Raptakis, E. N., and Derrick P. J.: Pitfall on the Road to the Ideal Time-of-Flight Mirror: Ideal Time Focusing in the Second Stage of Tandem Mass Spectrometers. Int. J. Mass Spectrom. Ion Processes, 146/147, 165-182 (1995)

Ch

sto

4.1

Th

wi

199

fee

det

Mic

refi

ma

the

the

199

vol

the

He

inst

He

con

Chapter 4 Design and construction of a segmented ring, ion trap storage source/reflectron/time-of-flight mass spectrometer

4.1 Background

The design and construction of the reflectron time-of-flight mass spectrometer with a segmented ring, ion trap storage source started late in the summer of 1993. The vacuum system with electronic feedthroughs and mechanical motion feedthroughs, the mechanical parts of the reflectron, and the parts of the detector and the source were mainly fabricated in the machine shops at Michigan State University before the summer of 1994. The modifications of the reflectron, the source and detector elements were completed with the help of the machine shops at the University of New Mexico. The static voltage supplies to the reflectron electrodes, the detector, and the ion source were constructed at the University of New Mexico during the fall semester, 1994. Beginning in spring, 1995, Michael Davenport helped with the design and construction of the dynamic voltage supplies for the segmented ring ion storage source which is critical to the success of this project. In a later experimental stage of this project, Eric Hemenway helped convert the Labwindows CVI program of the TOF/TOF instrument for data acquisition using a LeCroy oscilloscope. Dr. Yefchak and Hewlett Packard Inc. provided the data acquisition board with software for the continuous spectrum acquisition. Dr. Overney wrote a data processing program, wh

ca

4.2

4.2

The

sto

for

to

gen

stor

rea

des

and

sync

trans

cons

dete

differ

contr

interf

oscill

which uses a peak finding technique for noise reduction, and which provides the capability to obtain reconstructed ion chromatograms.

4.2 Design and construction of the time-of-flight mass spectrometer

4.2.1. Instrument overview

The reflectron time-of-flight mass spectrometer with a segmented ring, ion trap storage source is shown in Figure 4-1. An HP 5890 gas chromatograph is used for sample introduction. During the ion storage period, an RF voltage is applied to the segmented ring electrode and both end caps are grounded. Ions generated by electron impact ionization are stored in the segmented ring ion storage source. During the ion extraction period, high voltages are applied to the rear end cap and ring electrode elements. An electronic circuit was specially designed for this instrument for fast switching between the extraction voltage and the RF voltage. The timing circuit designed for this instrument is able to synchronize the extraction pulse with the RF phase as well as the trigger for the transient recording of the spectra. A broad kinetic energy focusing reflectron was constructed to give a small temporal distribution of isomass packets at the detector position. Ten-turn pots are used for the adjustment of the voltages for different instrument parts and the control of the timing system. Computer-controlled data acquisition is achieved by using a Gateway P5-90 computer interfaced to a Precision Instrument Transient Recorder board or a LeCroy oscilloscope with GPIB board, The instrument is intended to demonstrate the

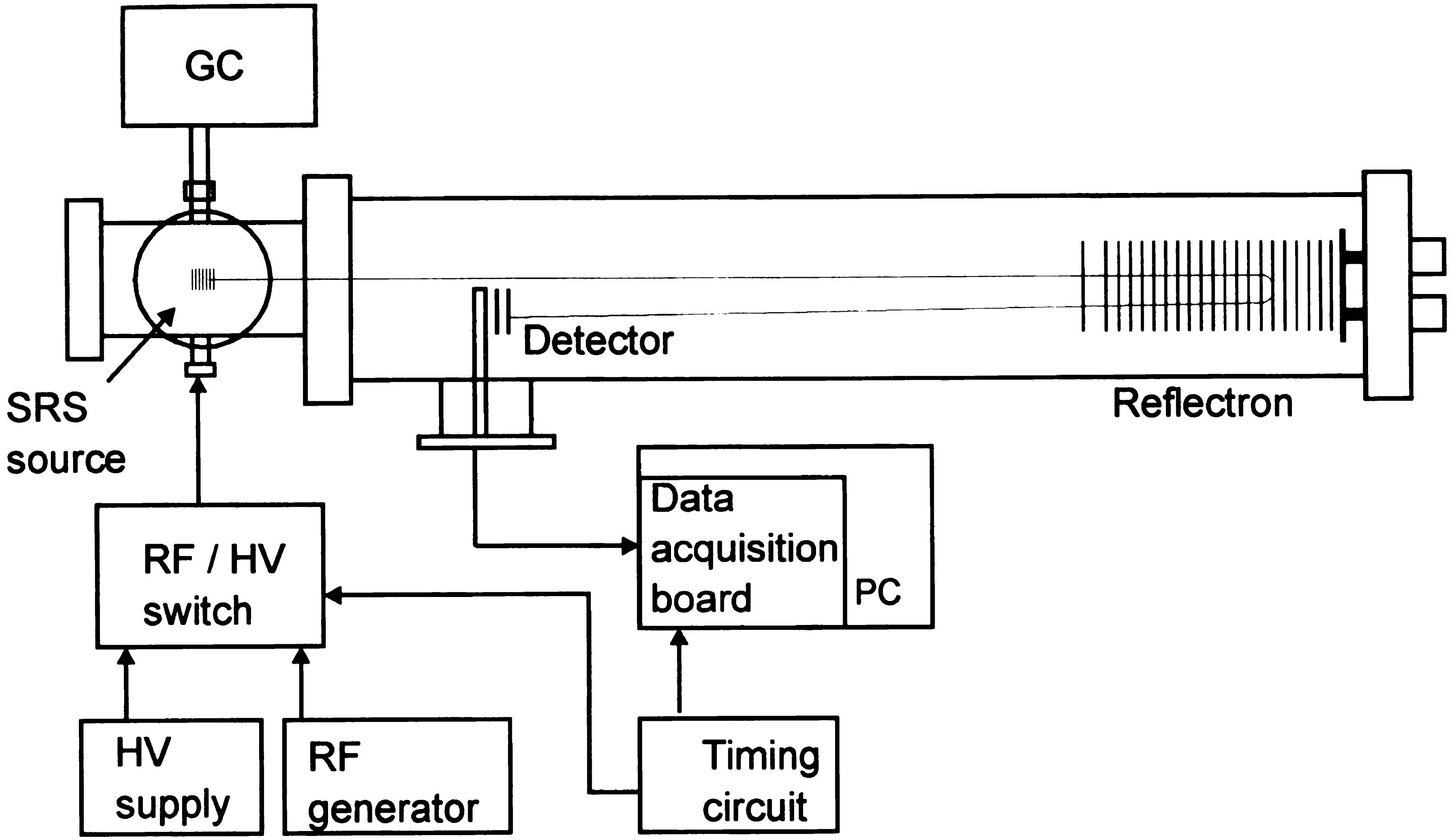

Figure 4-1. A block diagram of the reflectron time-of-flight instrument with segmented-ring ion trap source.

adv

spe

seg

rate

dyn

4.2

The

sho

inn

are

for

mo

flan

flan

atta

tub

dia

fron

A 6

inch

pum

othe

advantages of using the segmented ring ion trap source for time-of-flight mass spectrometry or the time-of-flight mass analysis of ions generated in the segmented ring ion storage trap. These advantages are fast spectral generation rate, good mass resolution, very high sample utilization efficiency, and wide dynamic range.

4.2.2 Vacuum system

The details of the vacuum system for the time-of-flight mass spectrometer are shown in Figure 4-2. The source chamber is a fourway cross made of a 6 inch inner diameter stainless steel tube. Six half nipples with 1 inch inner diameter are located on both sides of the cross. They are designed to be used as ports for sample introduction, vacuum gauge mounting, and RF electronic feedthrough mounting. A glass viewport is mounted on the top flange of the cross. One side flange is for the source and electronic feedthrough mounting and another side flange was modified for the attachment of the flight chamber. The bottom port is attached to one turbo molecular pump through a ISO/ CF converter. The flight tube is a 58 inch long stainless steel tube with a 10 inch diameter. A 5 inch inner diameter half nipple is welded to the one side of the flight tube (7 inches away from the source side flange) for the attachment of the detector mounting flange. A 6 inch inner diameter half nipple is welded to the bottom of the flight tube (20 inches away from the source side flange) for the attachment of the other turbo pump. One end of the flight tube is attached to the source chamber and the other end is for the attachment of the reflectron mounting flange. A baffle is

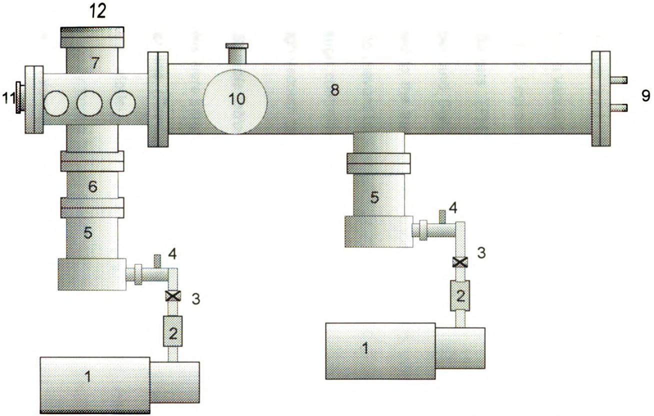

Figure 4-2. A detailed diagram of the vacuum system for the time-of-flight mass spectrometer.

1. Rough pumps; 2. Filters; 3. Butterfly valves; 4. Thermocouple gauges; 5. Turbo Pumps; 6. ISO/CF adapter; 7. Fourway cross source chamber; 8. Flight tube; 9. Flange for reflectron mounting; 10. Flange for detector mounting; 11. Flange for source mounting; 12. View port

pla

An

baf

tube

Two

mou

Two

cha

attac

pum

ion g

and

4.2.3

Samp

transf

Packa

contin

by inje

introdu

of diffe

placed between the fourway cross source chamber and the flight tube chamber. An 8 inch long stainless steel tube of 1 inch inner diameter passes through the baffle. This allows ion transmission between the source chamber and the flight tube while limiting the vacuum conductance to allow the differential pumping. Two 1 inch inner diameter half nipples are attached to this flight tube for mounting a vacuum gauge and an electronic feedthrough.

Two Leybold Trivac D8A rotary vane pumps are used as rough pumps. Two Balzers TPH 520 turbomolecular pumps are attached to the source chamber and flight tube respectively. An oil filter and a butterfly valve are attached to the transfer line between the rough pump and the turbomolecular pump to prevent back streaming of the pump oil. Two Granville-Phillips GP 270 ion gauge controllers are used to monitor the pressures in the rough vacuum and high vacuum region.

4.2.3 Sample introduction

Samples were introduced through a glass capillary column contained in a heated transfer line (Finnigan MAT, San Jose, CA) and emanating from a Hewlett-Packard Model 5890 chromatograph. Samples were either introduced continuously from a helium-swept vial contained in the chromatograph oven, or by injection through the chromatograph's injection port. For steady-state sample introduction, the sample introduction rate is controlled by using a guard column of different inner diameters or by adjusting the GC oven temperatures.

4.2

A

lon

cha

to

Th

ion

volt

elec

occu

intro

incre

4.2.5

The

base

draw

A re

capa

distan

cover

2.5 m

with C

4.2.4 Field free flight region voltage

A 7 inch inner diameter cylinder made of stainless steel mesh that is 50 inch long is placed in the flight tube. It is electrically isolated from the vacuum chamber by attaching ceramic spacers to it. A voltage of -1800 V (maximum up to - 2500 V) is applied to this mesh to provided a field free flight region voltage. This configuration allows the DC and RF voltages applied to the segmented ring ion trap source to be referenced to the ground potential. The relatively low voltages required in the source region, because of the floating flight path, avoids electric discharge when the ion source is operated at the higher pressures that occur with chromatographic introduction of the sample. Unfortunately, introduction of the stainless steel mesh introduces a large surface area which increases the time required to reach a low pressure in the vacuum chamber.

4.2.5 Segmented ring ion storage source with electron impact ionization

The design and construction of the segmented ring, ion trap storage source is based on the computer simulation results described in Chapter Two. A detailed drawing of the electrodes used in the source assembly is shown in Figure 4-3(a). A representative diagram of the ion source with electron impact ionization capability and ion acceleration electrodes is shown in Figure 4-3 (b). The distance between the exit and rear end cap is 9.4 mm. These two elements are covered with 86% transmission mesh screens. The ring electrode elements are 2.5 mm apart. An additional three electrodes are placed after the exit end cap with 0.15 inch ceramic spacers between them, three electrodes and the exit end

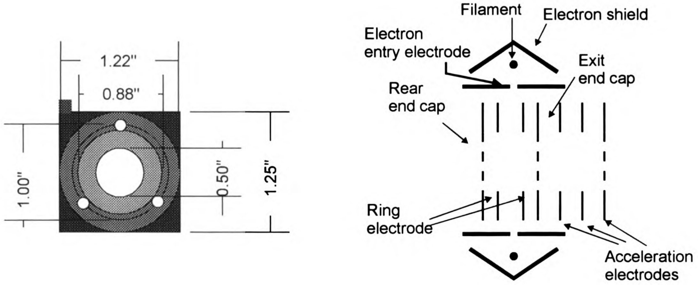

(a)

(b)

Figure 4-3. Detailed drawing of the source ring element (a) and a cross section view of the segmented-ring ion trap storage source with acceleration electrodes and filament for electron impact ionization (b) The thickness of the electrode element in Figure 4-2(a) changes from 0.01,0.02 to 0.03 inches as the color of the part changes from light to dark.

cap

res

acc

ele

two

are

ele

ion

des

inc

com

Fig

and

els

app

ele

fron

des

by

Dur

ele

cap are electrically connected to a voltage divider made up of three 2MΩ resistors, this divider provides a linear ion acceleration field. The last acceleration electrode is also covered with a mesh screen. Two electron entry electrodes located above and below the segmented ring ion trap source provide two 1x10 mm^2 slits to guide the electron beam into the ion source. Two filaments are located above and below the two entry slits. The two electron shielding electrodes are designed to help guide electrons into the ion source and reduce ion generation outside of the ion source.

In order to obtain a uniform extraction field, the source elements were designed (as shown in Figure 4-3(a)) to have 0.01 inch, 0.02 inch and 0.03 inch increasing thickness from the inner diameter to the outer diameter. The computer simulated extraction field of this unique ion source design is shown in Figure 4-4. The voltages across the acceleration electrodes are -600 V, -1200 V, and -1800 V. The voltages applied to the exit end cap, the two ring electrode elements, and the rear end cap are 0 V, 200 V, 500 V, and 700 V. The voltages applied to the electron entry electrode, the filament and the electron shield electrodes are 0 V,-25 V, and -50 V. The red lines are equipotential contours from 50 to 650 V in 100 V increments. The important advantage of this source design is that the uniform, linear extraction field remains essentially undistorted by the filament electrode elements of the electron impact ionization source. During the ion storage period, an RF voltage is applied to the ring electrode elements. The computer simulated electron trajectories at ring electrode

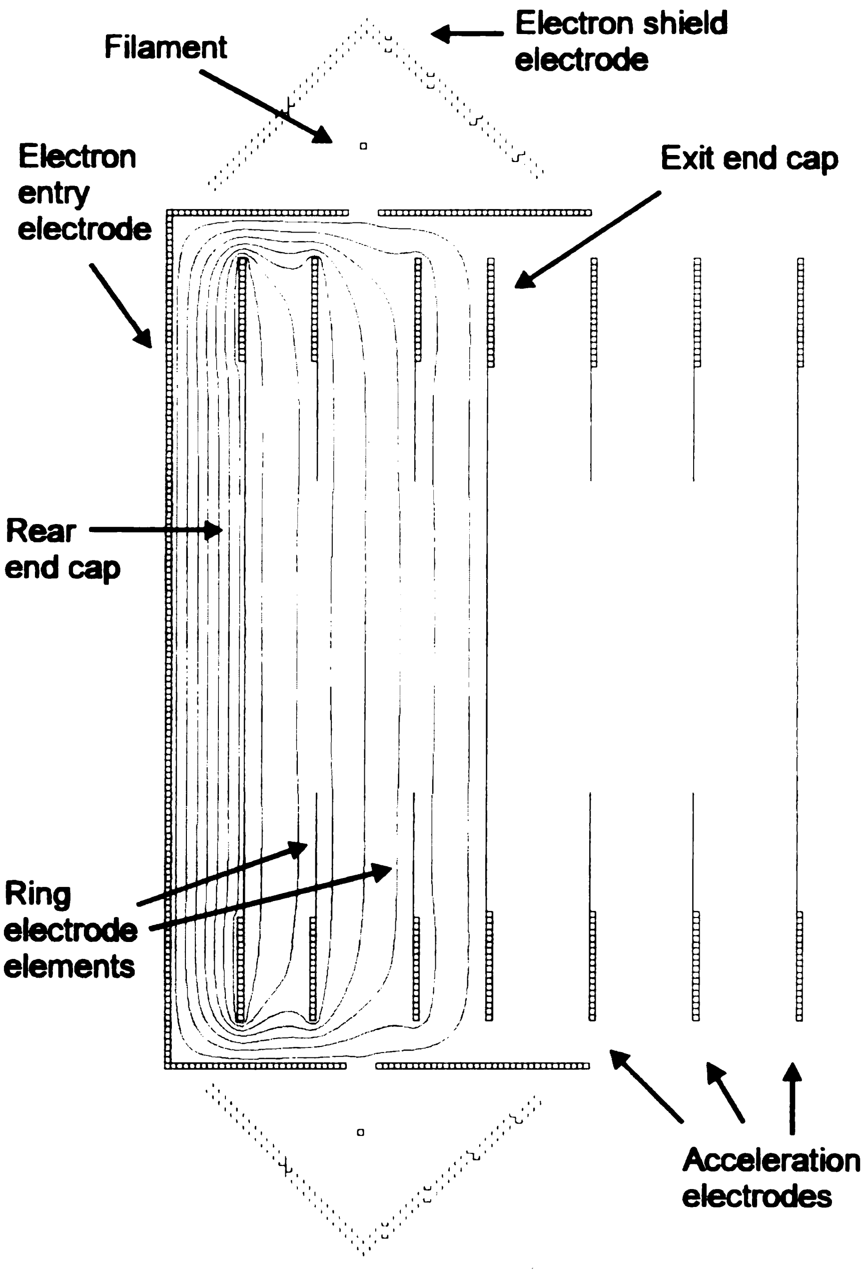

Figure 4-4. Equipotential contours of the ion source during the ion extraction period. The voltages across the acceleration electrodes are -600 V, -1200 V, -1800 V. The voltages applied to the exit end cap, two ring electrode elements, and the rear end cap are 0 V, 200 V, 500 V, 700 V. The voltages applied to the electron entry electrode, the filaments and the electron shield electrodes are 0 V, -25 V, -50 V. The red lines are contours from 50 to 650 V in 100 V increments.

vc
tra
are
rin
ove
ele
RF
inte
the

the
ma
pos
qui
not
ion
affe
dur
mo
cyc
mo

voltages of 0 V, -300 V, and 300 V are shown in Figure 4-5. The green lines are trajectories. The electrodes are shown in black and the voltages applied to them are the same as described in Figure 4-4, except for the voltage applied to the ring electrode. When the RF is at 0 V, electrons enter the ion source and spread over almost the entire source region. When the RF voltage is at -300 V, the electrons don't have enough kinetic energy to get into the ion source. When the RF voltage is at 300 V, electrons are pulled through the ion source by the internal field. The electron trajectories are quite sensitive to the configuration of these related electrodes and the voltages applied to them.

The components such as the electron entry electrode, the filament and the electron shield were made and assembled by myself and are not accurately machined. Each time they are taken apart and assembled again, the relative position of these electrodes shifts slightly. The overall behavior of the source is quite reproducible although the optimized bias voltage applied to the filament is not exactly the same each time. Another concern is that electrons get into the ion source only during the positive half of the RF cycle. However, this need not affect the ionization efficiency significantly because the sample introduced during the negative half of the RF cycle, considering the diffusion velocity of molecules, will be still in the ion source when the RF changes to the positive half cycle. Although ionization does not occur throughout the whole RF cycle, molecules introduced over the whole RF cycle can be ionized.

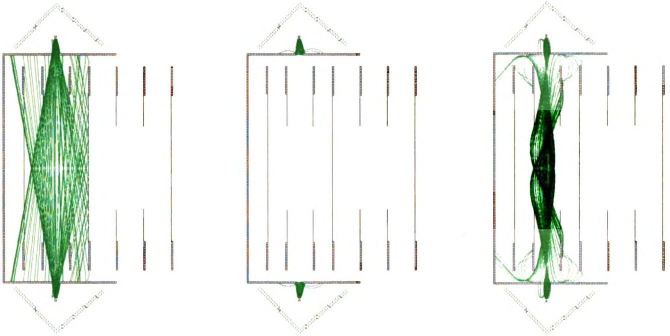

(a) (b) (c)

Figure 4-5. Computer simulation of electron trajectories (green lines)
The voltage of two end caps is 0 V. The electron entry electrodes, the electron shield electrode and the filaments are 0V, -50 V and -25 V. The voltage of the ring electrode is 0V (a),-300 V(b), 300 V (c).

4.2.6 Einzel lens and deflection plate

A detailed drawing of the Einzel lens is shown in Figure 4-6. Three cylindrical stainless steel lens elements are separated by two 0.05 inch ceramic spacers. The inside diameter of these lens elements is 0.62 inches. The length of the lens elements on both sides are 1 inch and that of the center lens element is 0.5 inches. Computer simulation of the ion beam focusing is shown in Figure 4-7. A diverging beam with 1800 eV kinetic energy is collimated by this lens. The lens voltages applied are 0 V, -1800 V, and 0 V respectively. The focal length of the Einzel lens depends on the lens voltages applied and the kinetic energy of the ion beam passing through it. The simulation shown in Figure 4-7 is an ideal case. In a practical situation, the distribution of ion kinetic energies and the radial distribution away from the lens axis will result in both a chromatic aberration (due to different kinetic energies) and a coma effect (due to initial positional deviation from the axis). On the other hand, the degree of ion dispersion depends on the geometry of the ion source. With the unique design of the segmented ring ion trap, a uniform extraction field is generated. So the dispersion velocity perpendicular to the flight axis is mainly due to the random thermal motion and the RF trapping field. Compared with the high velocity in the direction along the ion flight path axis, the resultant degree of dispersion is very small.

An ion deflection electrode assembly that consists of two stainless steel plates is located after the Einzel lens electrodes. One of the stainless steel

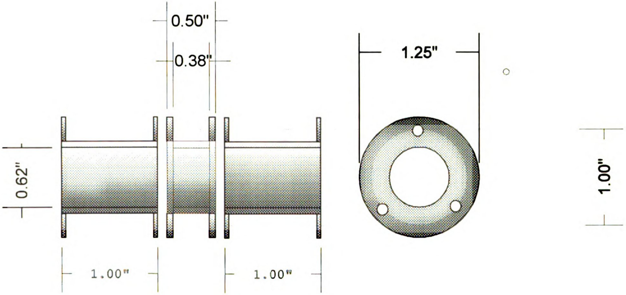

Figure 4-6. A detailed drawing of the Einzel lens.

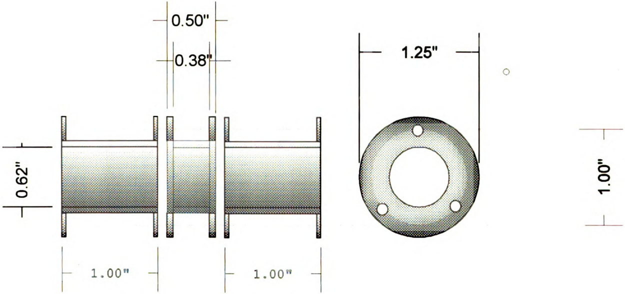

Figure 4-6. A detailed drawing of the Einzel lens.

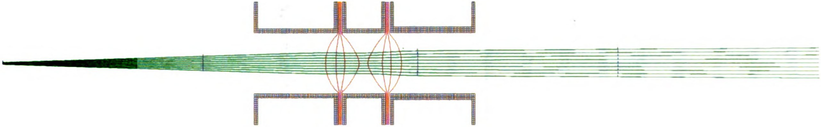

Figure 4-7. A computer simulation the ion trajectories(green lines) through a Einzel lens assembly(black).The voltage applied to the lens electrodes are 0 V. -1500 V, 0 V. The ions have a kinetic energy of 1800 eV The red lines are equipotential contours from -300 V to 1200 V in 300 V increments. The group of blue dots represent the ion positions at 0.1 μs along the flight path.

plates is a 3 inch long and a 3/4 inch wide. It is connected with a voltage near the field free flight voltage to steer ions in a correct direction in the flight path. The other is 3 inches long and 1/2 inch wide. It is connected with a voltage (400 V to 800V) higher than the field free region voltage during the ionization period (to block ions into the field free flight chamber) and at the field free region voltage during the ion extraction period (to allow ions into the field free flight chamber). A computer simulation of the ion trajectories of these two situations is shown in Figure 4-8. During the ionization period (Figure 4-8 (a)), one plate has a more positive voltage than the field free voltage as shown in the figure. The red lines represent the equipotential contours from -1200 V to -1800 V at 50 V increments. The green lines are ion trajectories of ions with 1800 eV kinetic energy. They are deflected as they pass the deflection plates. During the ion extraction period (Figure 4-8 (b)), all of the electrodes have the field free voltage and the ions pass without deflection.

4.2.7 Broad energy range focusing reflectron

Based on the developmental method discussed in Chapter Three for a broad energy range focusing reflectron design, a reflectron as long as 50 cm needs to be constructed and a nearly linear reflectron voltage profile should be applied to the reflectron electrodes to give a good temporal focusing of isomass ions with broad kinetic energy distribution. Our present system prevents the implementation of this design concept; the two motion feedthroughs attached to one 10 inch CF flange are not strong enough to support the weight of so many

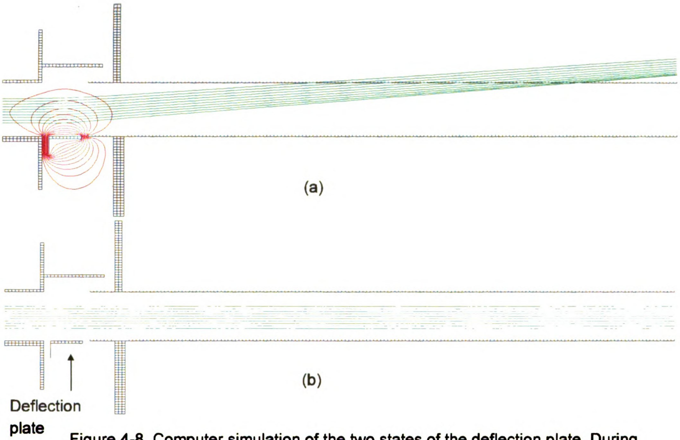

Figure 4-8. Computer simulation of the two states of the deflection plate. During the ionization period (a) the deflection plate was a more positive voltage than the field free voltage as shown.

The red lines represent the equipotential contours from -1200 V to -1800 V at 50 V increments. The green lines are ion trajectories of ions with 1800 eV kinetic energy. They are bent as they pass the deflection plate.

During the ion extraction period (b), all of the electrodes have the field free voltage. Ions pass without bending.

reflectron electrodes. The actual reflectron design is shown in Figure 4-9. Each reflectron electrode is a stainless steel ring that has a 4.5 inch outer diameter, a 3 inch inner diameter and a thickness of 0.03 inches. The first and the second reflectron grids are reflectron electrodes covered with 86% transmission mesh screens. A linear field is formed by applying the voltages to these two reflectron grids and connecting the electrodes between them with 3 MΩ resistors in series. The rest of the electrodes are provided with adjustable voltages from another 20 electrical feedthroughs. A detailed description of the electronic voltage adjustment for this reflectron is described in a later section. All the reflectron electrodes and grids are separated with ceramic spacers with a thickness varying from 0.382 to 0.385 inches purchased from Newark Electronics. Two motion feedthroughs mounted on one end flange and a stainless steel rod (0.25 inch diameter) mounted to that flange provide mechanical support and directional adjustment of the reflectron to steer the ion beam to the detector surface. The electron voltages applied to the reflectron electrodes are first calculated from the Mathcad program described in Chapter Three. Because the length of the spacers is not an integer unit, an accurate computer simulation and an iterative adjustment from the computer simulation are not possible. A manual tuning of the 21 pots which control the reflectron electrode voltages was used to obtain the best resolution. The Mathcad program calculation and computer simulation , however, provided a good "first approximation" for this adjustment.

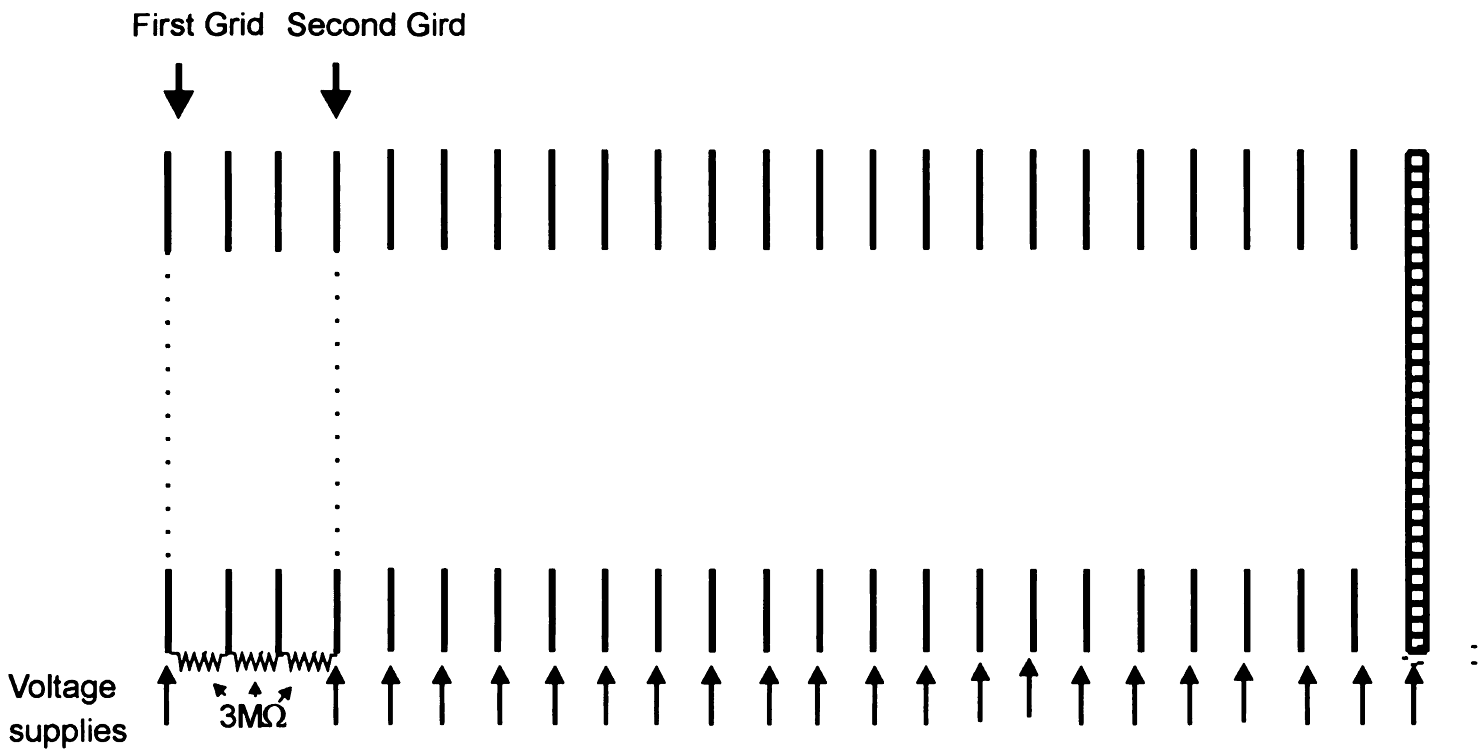

Figure 4-9. A diagram of the cross section of the reflectron assembly. The reflectron ring electrodes are stainless steel rings with a 4.5 inch outer diameter, a 3 inch inside diameter, and a 0.03 inch thickness. The linear field between the first and second grid is generated by connecting the reflectron ring electrode with 3 M Ω resistors. Twenty-two electric feedthroughs are used to provide individual tunable voltages to the reflectron electrodes.

4.2.8 Detector

A "Chevron assembly" detector using two 40 mm diameter MCP plates is shown in Figure 4-10 (a). The anode is a 0.03 inch thickness, 2.75 inch outer diameter gold plated stainless steel plate. The ion entry electrode was covered with a 86% transmission mesh screen so the electric field in the field free region will not be distorted by the voltages applied to the detector electrodes. A detailed drawing of the detector ring electrodes are shown in Figure 4-10(b). They are stainless steel rings of 0.03 inch thickness, 1.75 inch inside diameter and 2.75 outer diameter. These rings were made as flat as possible to keep good contact between the ring electrodes and MCP plates.

4.2.9 Electronic control system for the time-of-flight mass spectrometer

4.2.9.1 Static voltage supply

The schematic of the static voltage supplies for the field free region voltage, detector voltage, and lens voltages is shown in Figure 4-11. A Bertan -2 kV adjustable power supply is used to provide the field free flight path voltage, Two Acopian power supplies (200 V and -200 V) are referenced to this voltage. Four ten-turn pots of 100 kΩ in parallel are connected to the positive and negative output of these two power supplies to give the 400 V variation over the shielding potential for the lens electrodes and ion deflection electrodes. Another four adjustable high voltage power supplies of -300 V, -1.5 kV, -2.5 kV and -5 kV are

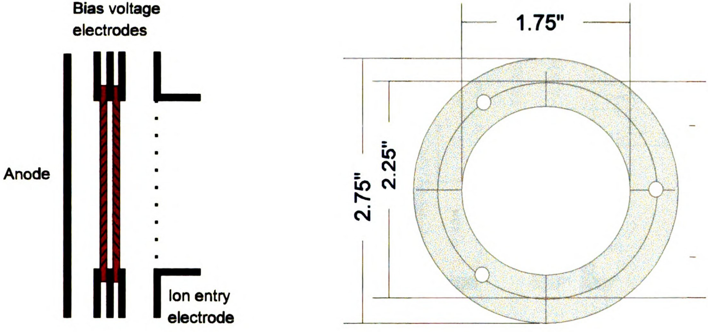

(a)

(b)

Figure 4-10. A diagram of the "Chevron assembly" detector design (a) and the detail drawing of the ring electrode (b). Microchannel plates are in red color. The anode is floating and the ion entry electrode is set at the same voltages as field free region. The voltage across the three bias voltage electrodes is around 1700-2000 V according to the gain required.

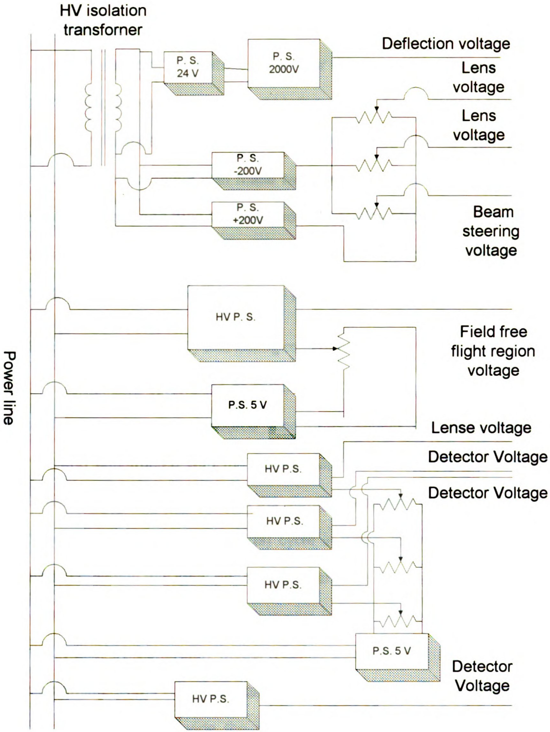

Figure 4-11. Schematic of DC voltage supplies for the ion source, Einzel lens, and the detector

used to provide the voltages for the three ring electrodes and the middle Einzel lens electrode.

The schematic of the voltage control for reflectron electrodes is shown in Figure 4-12. A positive 1.5 kV and a negative 1.5 kV power supply provide the high and low reference voltages for the reflectron. Twenty-one 10 turn pots (50 kΩ) are connected in series with these two power supplies. These twenty one pots are used to set and tune the reflectron electrodes starting from the second reflectron grid as shown in Figure 4-9. These reflectron voltages are manually monitored by using a KEITHLEY 195 high precision digital multimeter.

4.2.9.2 Dynamic voltage supply and timing control system

The electronic system for generating the RF voltage and the extraction voltage for segmented ring source electrodes shown in Figure 4-13 was designed and constructed with the help of Michael Davenport. To obtain the highest resolution and intensity from the storage/extraction cycle, it is important to find the best phase of RF (storage) cycle in which to initiate the extraction cycle and to maintain this ideal phase relationship for all experiments. This ideal timing for the SRS-TOF mass spectrometer begins with a common timebase (Wavetek Function Generator, model 171) to drive the RF amplifier and the extraction timing. The TTL signal from the function generator is routed through an adjustable delay to provide the optimum phase for all subsequent timing functions. This delayed clock is connected to a programmable modulus counter to generate an extraction clock signal with a frequency 1/128 to 1/16384 that of

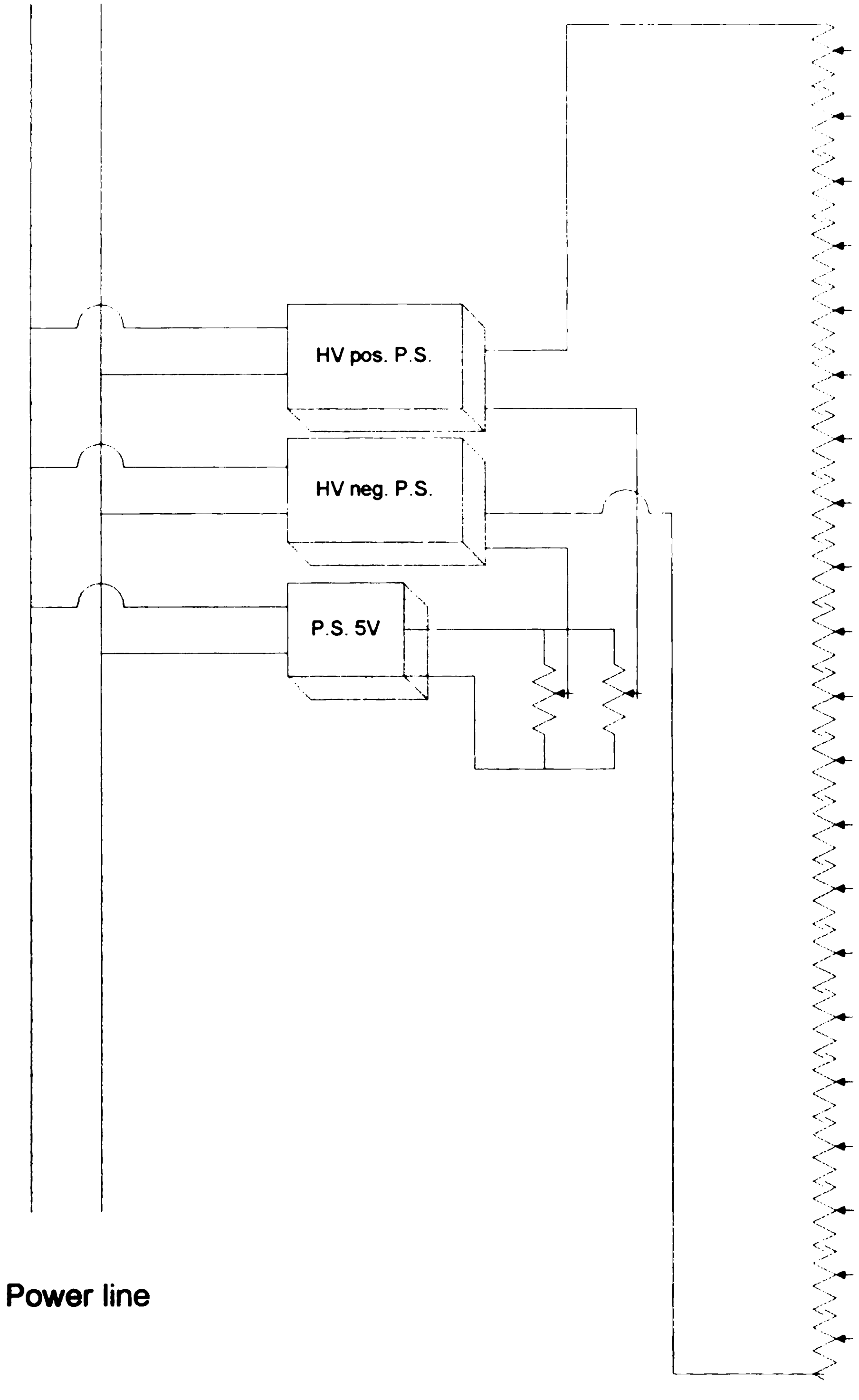

Figure 4-12. Schematic of the voltage supply for the reflectron electrodes

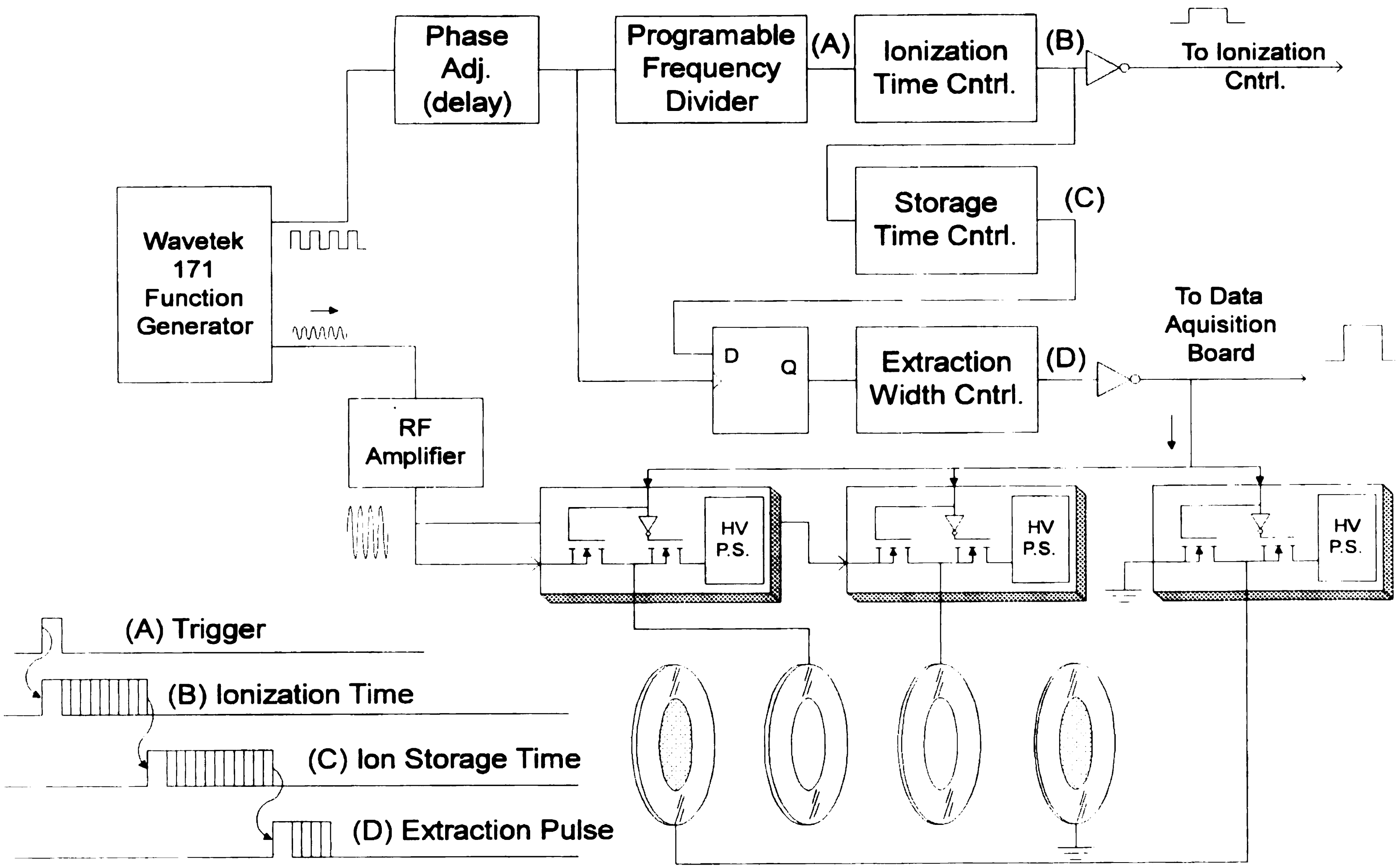

Figure 4-13. Schematic of the timing control and dynamic voltage supply to the source electrodes

the RF frequency. The extraction clock signal triggers an ionization timer, enabling electrons to enter the trap for an adjustable time from 6 µsec to 600 µsec. The end of the ionization time triggers the extraction delay timer with a range from 8 µsec to 1000 µsec. The end of this ion storage time triggers the ion extraction pulse generator. To preserve the desired RF phase/extraction timing relationship, the extraction trigger is synchronized with the delayed TTL clock signal by a HC74 D latch. The typical extraction trigger pulse width is 2µ sec. The synchronized extraction trigger is buffered and routed to the data acquisition system, detector display, and high speed HV switches attached to the electrode elements of the segmented ring. Prior to the extraction trigger, a 1.2 MHz, RF signal adjustable from 200 Vpp to 900 Vpp is applied to the segmented ring of the ion trap through a high speed, high voltage N-channel MOSFET assembly. At the command of the extraction trigger pulse, the RF side is turned off and the extraction voltage FETs are turned on for the duration of the extraction pulse. At the falling edge of the extraction trigger, the extraction voltage MOSFET switches are turned off and the RF side is turned back on. All switch operation is break-before-make. Extraction voltages for the ring discs are supplied by individual 10-1200 V Spellman MP power supplies. The RF is generated with a high speed, high power APEX PA09 op amp and the Hi-Q RF head from an early model Extrel quadrupole power supply.

4.2.10 Data acquisition of the time-of-flight mass spectrometer

After each high extraction voltage pulse is applied to the ion source, the arrival times of the isomass ion packets to the detector and the voltage response of the anode current over a 50 Ω terminator are recorded as a single mass spectrum transient. Since the time-of-flight instrument can give several thousand extractions per second, the spectral generation rate is limited by the speed of data acquisition. The speed of the data acquisition is mainly depended on the transient recorder characteristics such as the acquisition time of the each data point, the time for each transient summation, and the data transfer time of every set of summed mass spectra to the data storage device. The summing rate is inversely proportional to the number of the data points to be acquired in each transient. In order to get a good quality spectrum, a certain amount of data points is required. Another important characteristic of the transient recorder is the resolution of the signal intensity. This directly affects the signal to noise ratio obtained when the signal intensity is extremely low.

4.2.10.1 Data acquisition with the LeCroy oscilloscope and GPIB board

The LeCroy 9450 digital oscilloscope interfaced to a P5-90 computer by a GPIB board is used for data acquisition during the initial period of the experimentation. A Labwindows/CVI program written in C language is used to obtain the spectrum data from the oscilloscope.

The LeCroy 9450 digital oscilloscope provides the true summed average, 450 megasamples per second for each transient and 10 bit analog to digital conversion resolution for the signal intensity. This data acquisition setup is mostly used to record spectra when steady state sample introduction is used. The mass spectral peak area is calculated from the ASCII file obtained by using a commercial application program called ORIGIN.

4.2.10.2 Data acquisition with the Precision Instruments Transient Recorder board

A Precision Instruments model 9825 transient recorder located in a Gateway 2000 P5-90 computer was provided by Hewlett Packard. Software written by Dr. George Yefchak is used to obtain the spectrum transient data when using this transient recorder. The Precision Instruments model 9825 transient recorder provides 200 megasample data points per second for each transient and 8 bit analog to digital conversion resolution for the signal intensity. The data storage time for each summed transient spectrum is 16 ms if each spectrum has 16 k data points. The maximum signal input voltage for the Precision Instruments could be up to 1V. This data acquisition setup is used to evaluate the detection limit and dynamic range of this instrument. The data file obtained is in DPI format. Dr. Gregor Overney wrote a C program to convert a set of consecutive mass spectra, which is acquired in one sample injection, into a reconstructed ion chromatogram (RIC) for that injection. A peak finding technique is used in this RIC program to reduce background electrical noise. Two parameters (peak width and threshold) are input for maximum accuracy in peak detection.

The performance and its advantages as a detector for gas chromatograph of this segmented ring, ion trap storage/reflectron/time-of-flight mass spectrometer were evaluated. The experiments performed and the results obtained are discussed in the following chapter.

Chapter 5 Characterization of the segmented ring ion trap source/reflectron/time-of-flight mass spectrometer

5.1 Introduction

The performance of the SRS/TOF mass spectrometer was evaluated with regard to mass resolution, mass range, linear response and detection limit for GC introduced analytes. Ion storage capability was demonstrated using several compounds. Time-of-flight mass analysis was used to determine the m/z values and the abundances of the ions present in the trap at the time of extraction. The controlled parameters were the ionization conditions (filament offset relative to the rear cap electrodes and filament current, the ionization time, the RF voltage, and the delay time between the cessation of ionization and ion extraction.

5.2 Mass resolving power of the SRS/TOF mass spectrometer

One measure of the merit of time-of-flight mass analysis is the resolution obtainable over the mass range being measured. For time-array detection, adequate resolution must be obtained over the entire mass range populating each extraction. In this study, the resolution is determined by the uniformity of the extraction field, the magnitude of the extraction and accelerating fields, the phase relationship between the extraction field and the RF field, and the energy focusing ability of the ion reflectron and the total flight path. The mass spectrum of PFTBA obtained with this system is shown in Figure 5-1. The RF voltage

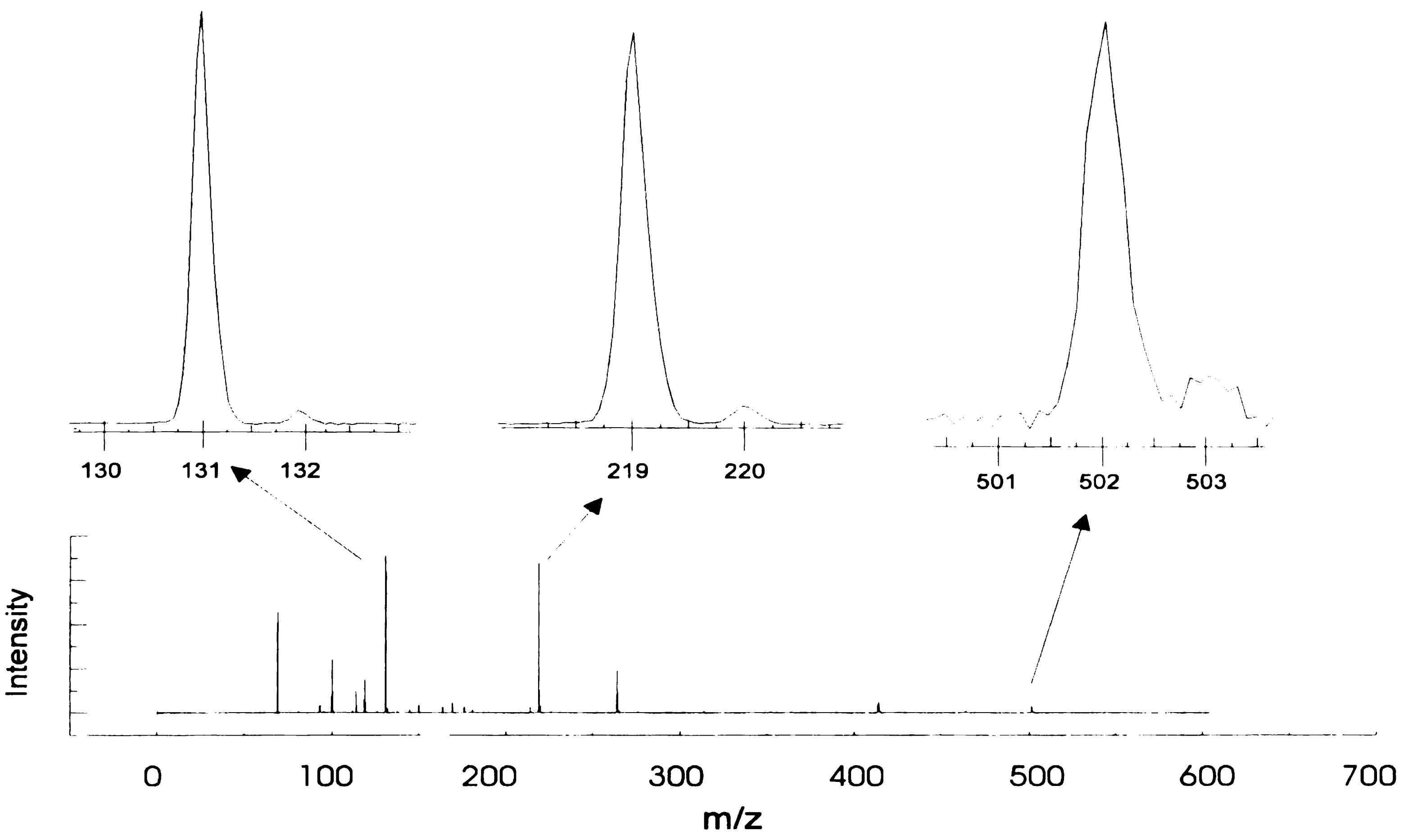

Figure 5-1. The mass spectrum of PFTBA obtained at V_{rf} =800 volts (peak to peak). f_{rf}= 1.2 MHz. The insets illustrate the resolution at three points along the mass axis at m/z 131, 219, and 502.

applied is 800 V. Three regions of the mass spectrum are expanded to show the mass resolution obtained in each area. In every instance, the resolution achieves or exceeds that necessary for unit resolution.

Further improvement of the mass resolving power could be obtained by constructing a reflectron that has a reflectron voltage profile close to the theoretical profile as discussed in chapter three. As proposed in the competitive grant renewal proposal submitted on November, 1995 for this project, a reflectron with a calculated voltage without steep field change will give much higher resolution. A more accurate and closer spacing between electrodes as well as accurate voltage settings for each reflectron electrode will also improve mass resolution.

5.2.1 The effect of RF phase at the time of ion extraction on mass resolution

At the time of ion extraction, the RF voltage is turned off and the extraction pulse is applied. The effect of the phase of the RF field at the time of extraction on the sensitivity and resolution of the TOF analyzer was studied. Ideally, the extraction pulse should be applied to the ion source when the ions are at their minimum kinetic energy. As discussed in chapter 4, electrons pass through the ion source with a maximum density and kinetic energy at an RF phase angle of 90^0 (sinusoidal wave). It is expected that most ions are generated in this RF phase region. As discussed in Chapter 2, ions generated at the 90^0 RF phase angle will have a minimum kinetic energy at RF phases 90^0 and 270^0. Ion extraction applied at these two RF phases should give the best resolution. The relationship of the extraction pulse with the phase angle of the RF voltage applied to the two ring electrode elements and the rear end cap of the ion source is shown in Figure 5-2. The effects of the phase angle of the extraction on the mass spectra of PFTBA are shown in Table 5-1. The data in this table clearly document the importance of the moment of extraction relative to the phase of the RF field. Considering only the effect of field-induced acceleration on the ions during a single RF cycle, at the phase angle of 270°(a), ions are at their lowest kinetic energy and the direction of the RF voltage change is same as the direction of the extraction voltage change. This gives the best mass resolution and greatest peak intensity as shown in Table 1.

At the 0° moment (b), the ions are at their maximum acceleration away from the center of the ion source at the time of extraction voltages are applied. Because the direction of the extraction voltage change is the same as the direction of change of the RF voltage, this gives the second best resolution and intensity. At the 90° phase, the ions are also assumed to be at a minimum kinetic energy. The direction of change of the extraction field at this RF phase angle is opposite to the direction of RF field change. As a result, significant delay period exists between the 90^0 phase angle and the rise time of the pulse as shown in Figure 5-2(c). It is quite possible that Ions are initially scattered by the opposite directions of the extraction and RF fields. Both the sensitivity and resolution are diminished at this phase angle. At the 180° position(d), the ions are at their

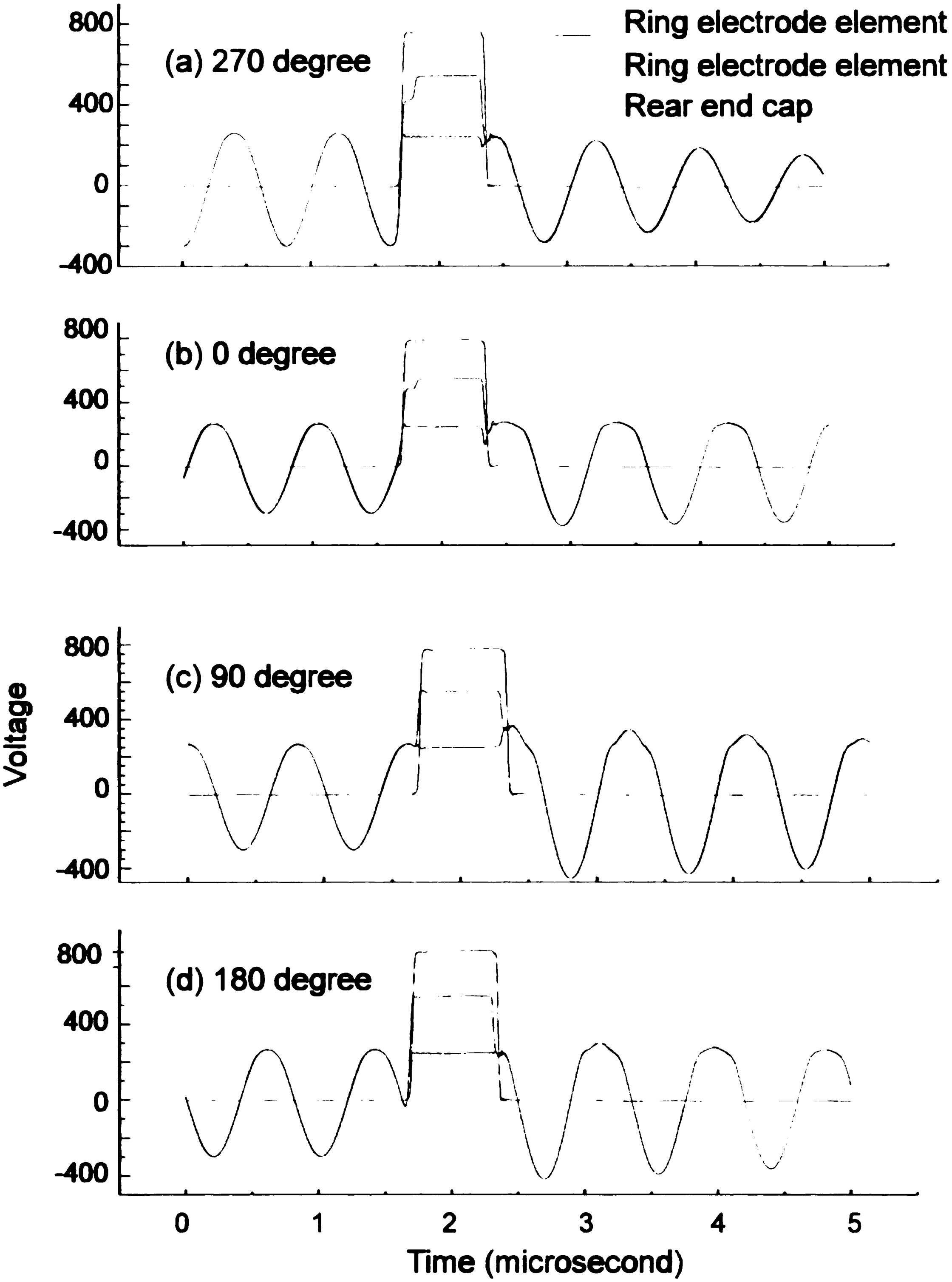

Figure 5-2. Synchronization of the extraction pulse with RF phase at RF phases of (a)270°, (b)0°, (c)90° and (d)180°.

TABLE 5-1

Effects of the timing of the extraction pulse in relation to the RF phase

	m/z 69	m/z 131	m/z 219
RF Phase	height/ resolution	height / resolution	height/ resolution
270^0	40,489 / 756	16,702 / 857	11,353 / 1019
0^0	41,510 / 663	16,760 / 772	11,415 / 986
90^0	15,370 / 541	4,815 / 562	2,936 / 767
180^0	5,394 / 359	1,995 / 412	1,378 / 645

highest energy position moving away from ion trap center and along the extraction axis, but the direction of extraction voltage is opposite to the direction of RF voltage change. Again the resolution and sensitivity are both greatly reduced. The significant loss in peak height and resolution at these latter two phase angles means many of the trapped ions are not effectively extracted.

For all of the phase angles studied, the direction of ion motion in the trapping field appears to have little effect on the quality of the resulting TOF analyses. It also appears not to be the kinetic energy of the ions when the extraction pulse is applied but rather the direction of the field changes upon application of the extraction that most affects the quality of the mass spectrum. Regarding the advantageous cases, the similarity of the results at 270°and 0° suggests that optimum performance may be achieved with a considerable leeway along the phase axis from 270 to 0°.

5.2.2 The effect of the electron bias voltage on mass resolution

For the conventional quadrupole ion trap with electron impact ionization, the trajectories of the electrons are effected greatly by the RF voltage[1]. For the segmented ring ion trap source, the electron trajectories are quite responsive to the electronic configuration of the source assembly and RF voltage. Because some parts of the ion source assembly such as the filament assembly and the electron shield electrodes were not accurately machined, the relative positions of the electrodes are not exactly the same after cleaning and reassembly and the optimum bias voltage will change. However, the overall performance of the instrument is essentially unchanged. The effect of the bias voltage on the observed trapped ions was investigated using chlorobenzene as the analyte. The peak heights of the major ions in the spectrum as a function of the voltage difference between the filament and the electron entry electrode are shown in Figure 5-3(a). The RF voltage applied is 600 V_{p-p}. In the ion trap, the filament bias voltage is not a direct measure of the ionizing electron energy because of the large effect of the RF field on the electron trajectories. However, the filament bias voltage is a measure of the energy the electrons possess when first encountering the RF field and it is reasonable to assume that the more energy the electrons have at this point, the more energy, on the average, the electrons will possess throughout their trap excursions. The initial slope of this response is similar to that observed for other types of mass spectrometers where sufficient energy for effective ionization must be present. The maximum is reached at lower applied energies than with other sources, undoubtedly due to the accelerative effects of the RF fields. The negative slope at the higher energies is interesting since the trap should not lose these ions. When the peak areas are plotted, as in Figure 5-3(b), the apparent decrease in abundance at the higher filament bias voltages largely disappears. This is an indication that, at higher bias voltages, it is the temporal focus at the detector that is suffering, not the ion abundance.

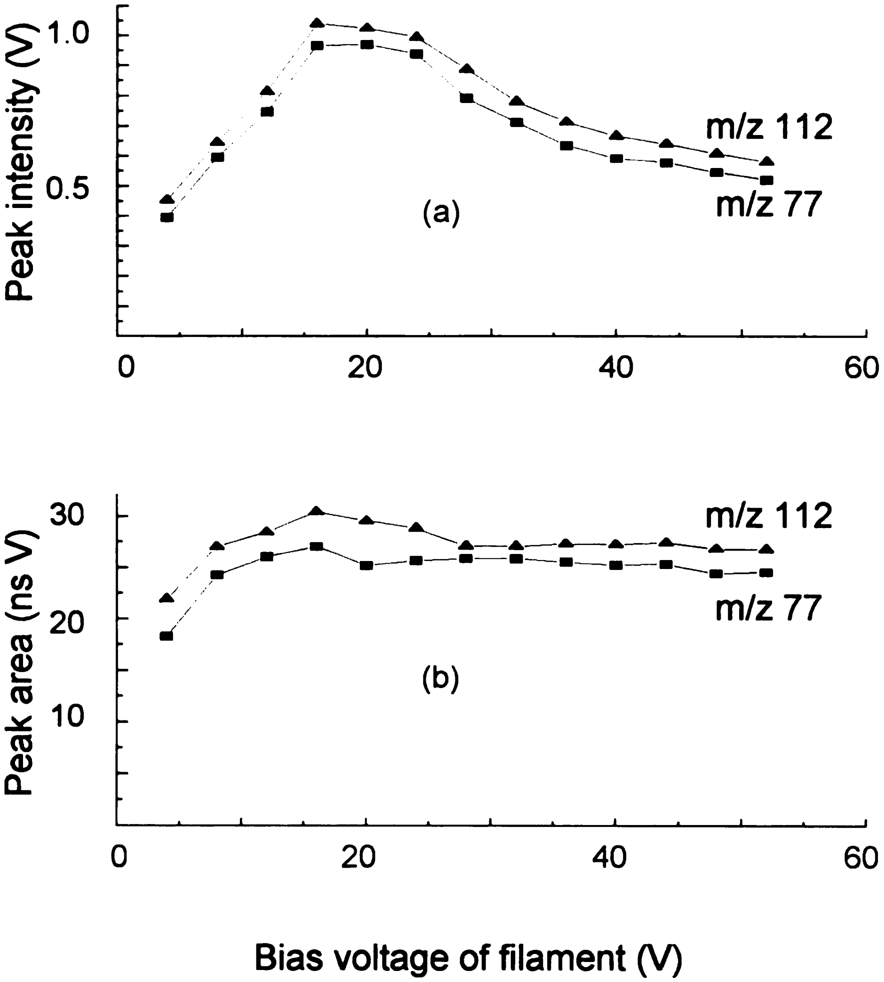

Figure 5-3. The effect of filament bias voltage on the peak height (a) and the peak area (b) of the major ions of chlorobenzene

5.3 Characterization of ion storage of the segmented ring ion trap

5.3.1 Ion loss for the normal electron impact ion source for the time-of-flight mass spectrometer

For the normal ion source for the time-of-flight mass spectrometer, the potential well generated by electron beam may store a small portion of ions generated. Most of ions will leave the ion source due to ion charge repulsion and thermal ion motion. Without an RF voltage applied, acetone was introduced into the ion source chamber. The pressure in the source chamber was $9x10^{-7}$ torr. The peak area of the m/z 43 ions was obtained for different delay times between the cessation of ionization and the start of ion extraction as shown in Figure 5-4. More than 80% of the ions leave the ion source after 4.7 μs. This demonstrates the importance of ion storage between extractions for making a significant improvement in the ion utilization efficiency of TOF mass spectrometry.

5.3.2 Storage mass range with the RF voltage

The m/z range over which ions will be efficiently trapped is dependent on the frequency and amplitude of the RF voltage as well as the dimensions of the ion trap[2]. The expected relationship is shown in equation(1) which is derived from the Mathieu equations of motion in the trap. Since no DC voltage is applied, only the function for q_z need be considered.

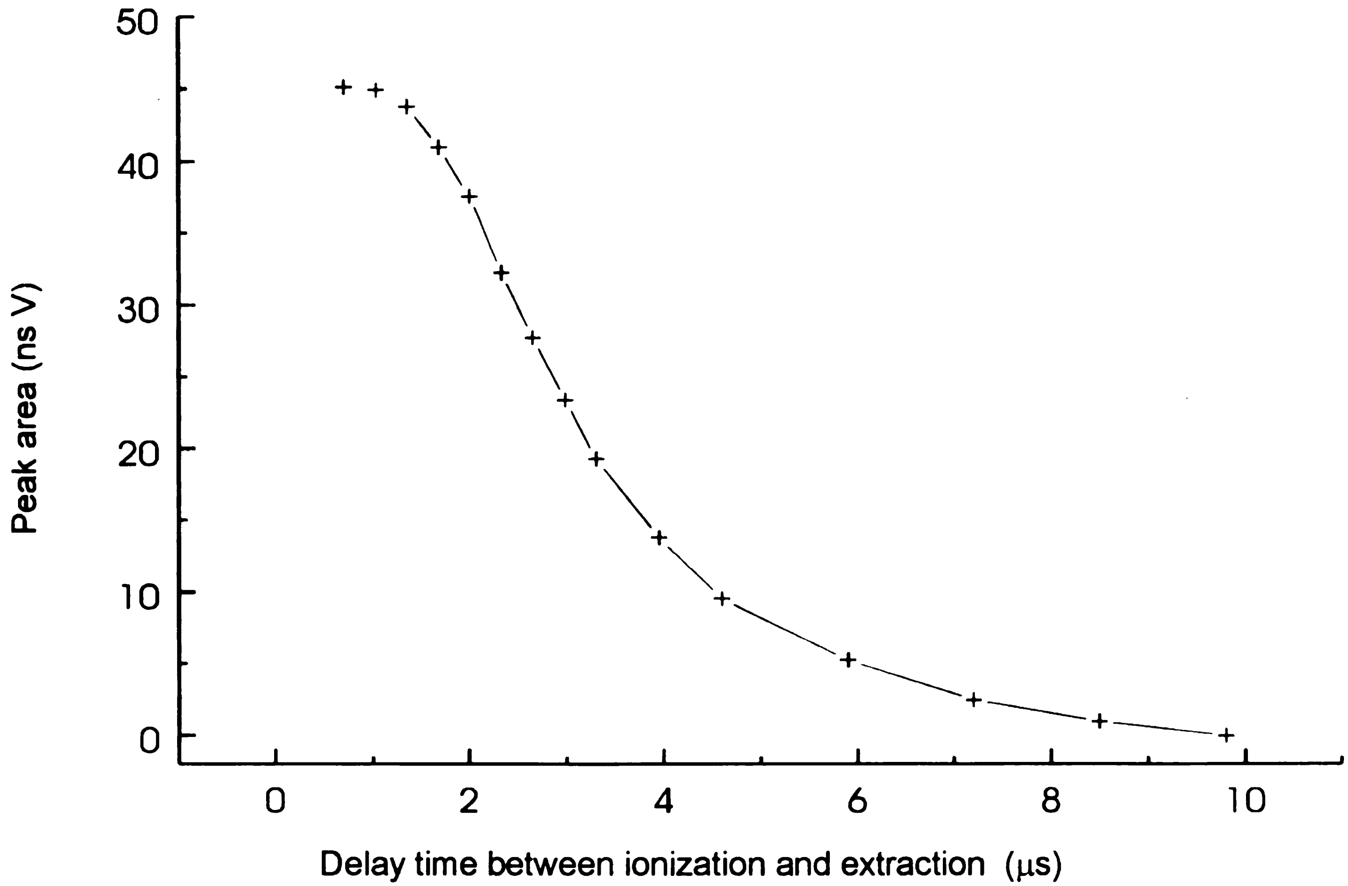

Figure 5-4. The peak area of m/z 43 ion of acetone vs. the delay time between cessation of ionization and ion extraction.

$$m/z = \left(1/q_z\right)\left(2eV/r^2\omega^2\right) \qquad \text{(equation 1)}$$

The terms in equation 1 are: *m/z* = mass to charge ratio, *V* = RF voltage (peak to peak), ω = RF frequency, *r* = the ring electrode radius and *e* is the electron charge.

This relationship was studied in our system by observing changes in the spectrum of PFTBA as a function of the RF voltage as shown in Figure 5-5(a-f). In these experiments, the dimensions of the source and the RF frequency were invariant. An estimate of the value of q_z at the low mass cutoff was obtained by observing the beginning of attenuation of m/z 69 at V = 800V. From equation 1, a boundary value of q_z for the low mass cutoff was calculated to be about -0.84. The high mass cut-off for zero DC voltage is not predicted by the theoretical stability diagram; rather it is caused by decreasing depth of the potential well as q_z decreases below ~-0.7 as m/z increases. In the current segmented ring ion trap storage source, the practical high-mass limit is between 7 and 8 times the low-mass cutoff. The use of ion cooling in normal ion trap mass spectrometers results in a larger mass range for these devices. However, the mass entrapment range of the segmented ring trap is sufficient without cooling for most gas chromatographic applications.

An attempt to increase the storage mass range was made by adding a small DC offset to the end cap electrodes of the ion storage source. Although the stability diagram obtained by computer simulation of the segmented ring ion trap

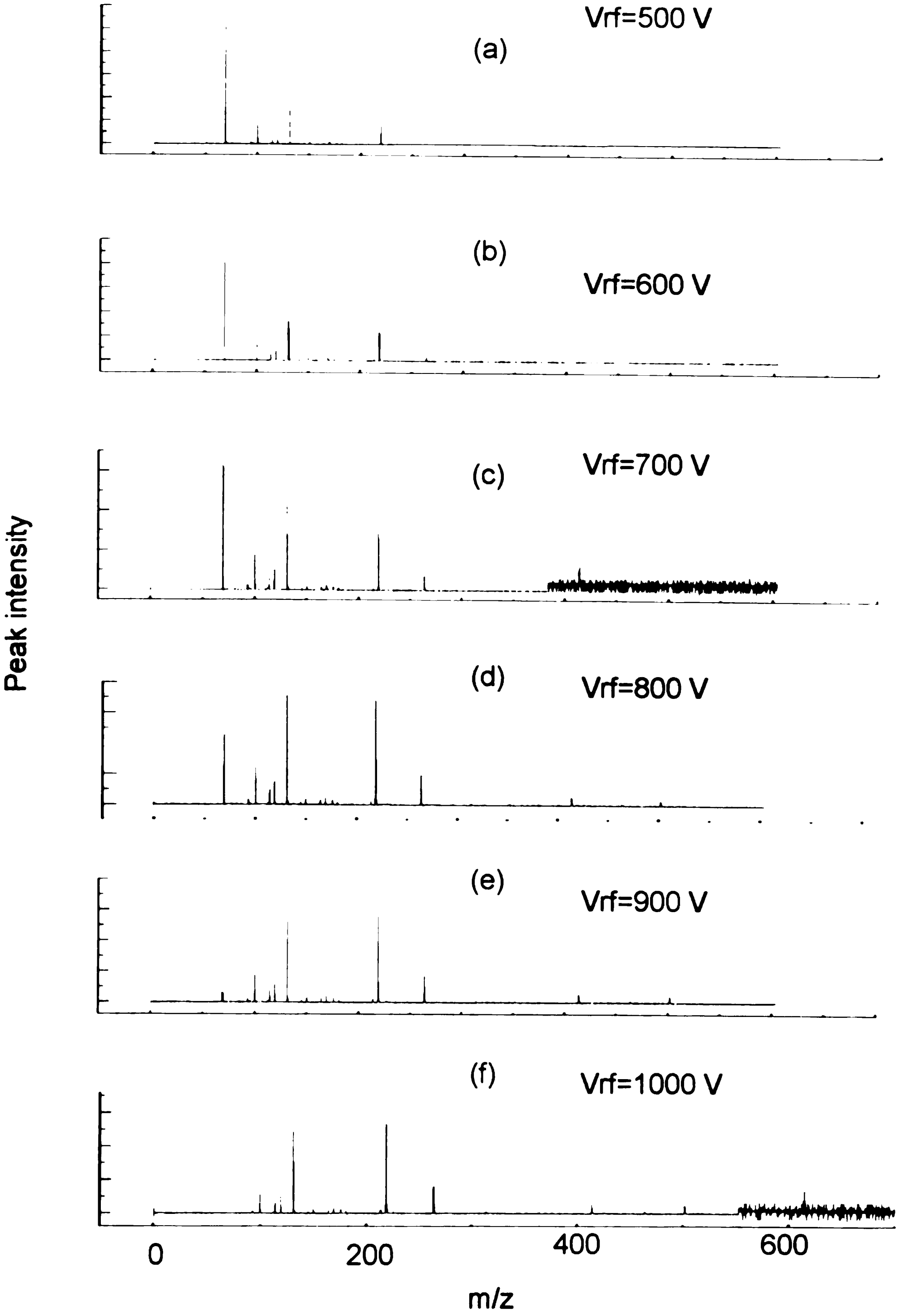

Figure 5-5. Mass spectra of PFTBA taken with various RF voltages on the ion trap. As the RF voltage is increased, increases in both low mass and high mass cutoff occur.

as discussed in Chapter 2 indicates that the maximum mass range would be achieved at zero DC offset, in the quadrupole ion trap, the actual maximum storage mass range is often obtained when a small degree of DC offset is applied. The ion storage mass range is examined with a DC offset voltage applied from -3 V to +3 V. The representative mass spectra of PFTBA are shown in Figure 5-6. There is almost no effect when a DC +3V offset voltage is applied. When -3V is applied, *m/z* 502 peak, which existed in the zero offset or +3 V offset conditions disappears. This indicates that there is no significant space charge or RF demodulation contribution to the field sensed by ions.

Although no significant improvement was achieved by applying a DC offset, we believe a still wider mass range can be obtained by optimization of the physical dimensions and electrical parameters, or, if necessary, by switching between values of V_{rf} to obtain low and high mass ends of the spectrum alternately. Additionally, further improvements in the ion storage capacity and mass range may be achieved by changes in the SRS geometry and electronic control. Experiments of different radial to axial dimension ratios, RF frequency and voltage could make significant improvements as demonstrated in the history of the development of the quadrupole ion trap. As proposed in the competitive grant renewal of this project, more segmented ring elements could be used to form a field closer to the optimum ion storage field.

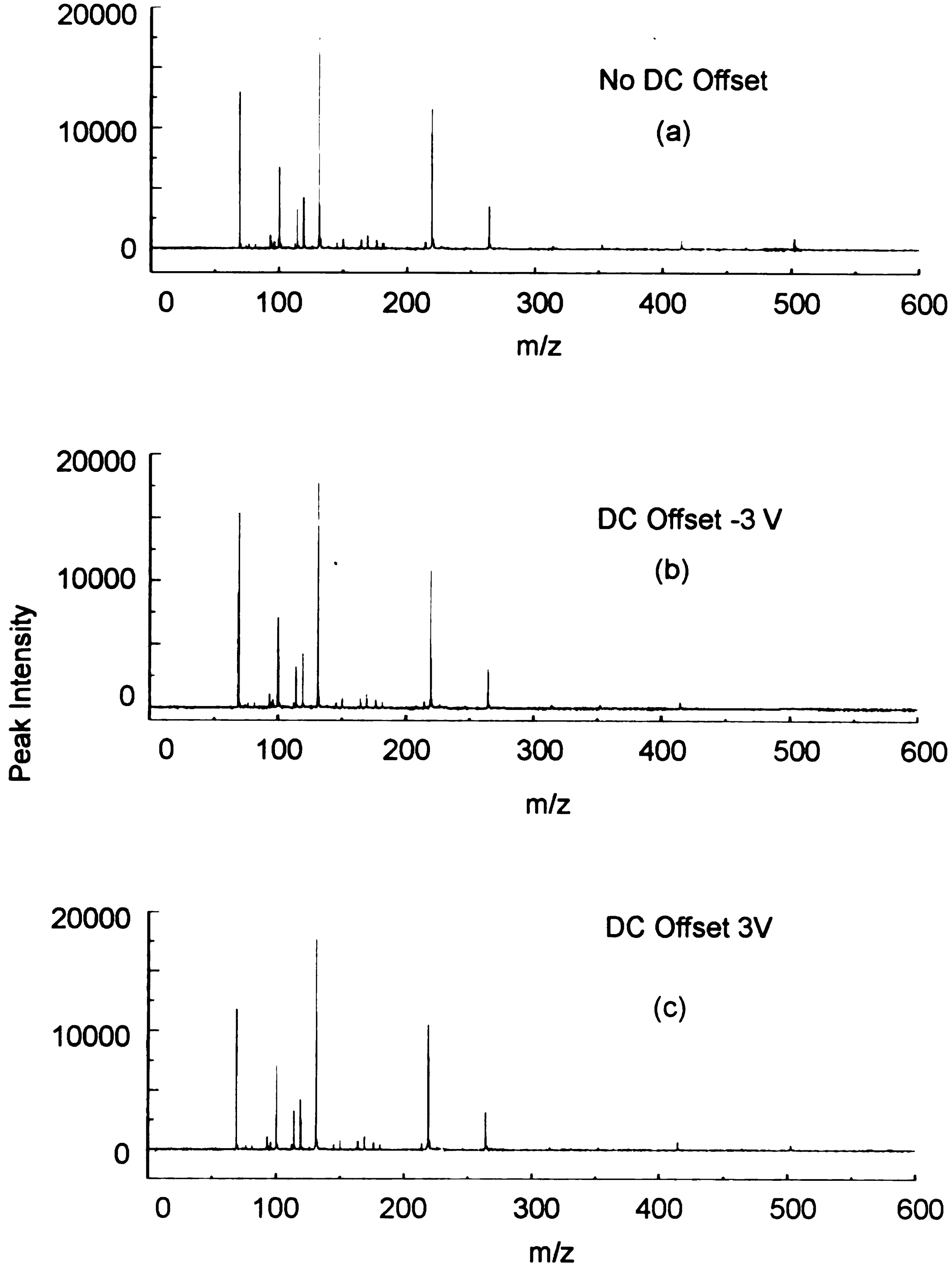

Figure 5-6. The effect of DC offset on the ion storage mass range.

5.3.3 Ion buildup and ion storage of the segmented ring ion source

The trapping characteristics of the segmented ring ion source were documented in a series of experiments designed to reveal the nature of the ion accumulation during the ionization part of the cycle. A sample vial of chlorobenzene was placed in the GC oven with constant temperature (25 ^{0}C). Helium gas was introduced to this sample vial to carry the vapor of chlorobenzene into the ion source through an capillary guard column. This arrangement maintained a steady-state pressure of chlorobenzene in the source. The filament current was set to 6.5 A. Ions were formed for various lengths of time after which the ions were immediately extracted and the abundances of the major ions (m/z 112 and 77) were determined. The results of this experiment are shown in Figure 5-7(a). The ion abundance follow a consistent growth with increasing ionization time as discussed below.

To separately determine the trapping efficiency and the nature of the ion loss, a series of experiments were performed in which an adjustable delay time was introduced between ion formation and ion extraction. In Figure 5-7(b), the measured abundance of the chlorobenzene ions are shown as a function of the delay time after an ionization time of 142 μs. In this experiment, essentially no ion loss is observed. Repeating this same experiment after an ionization time of 342 μs (Figure 5-7(c)) again shows no loss for periods up to 475 μs. From this experiment, it seems clear that the loss mechanism observed during ion

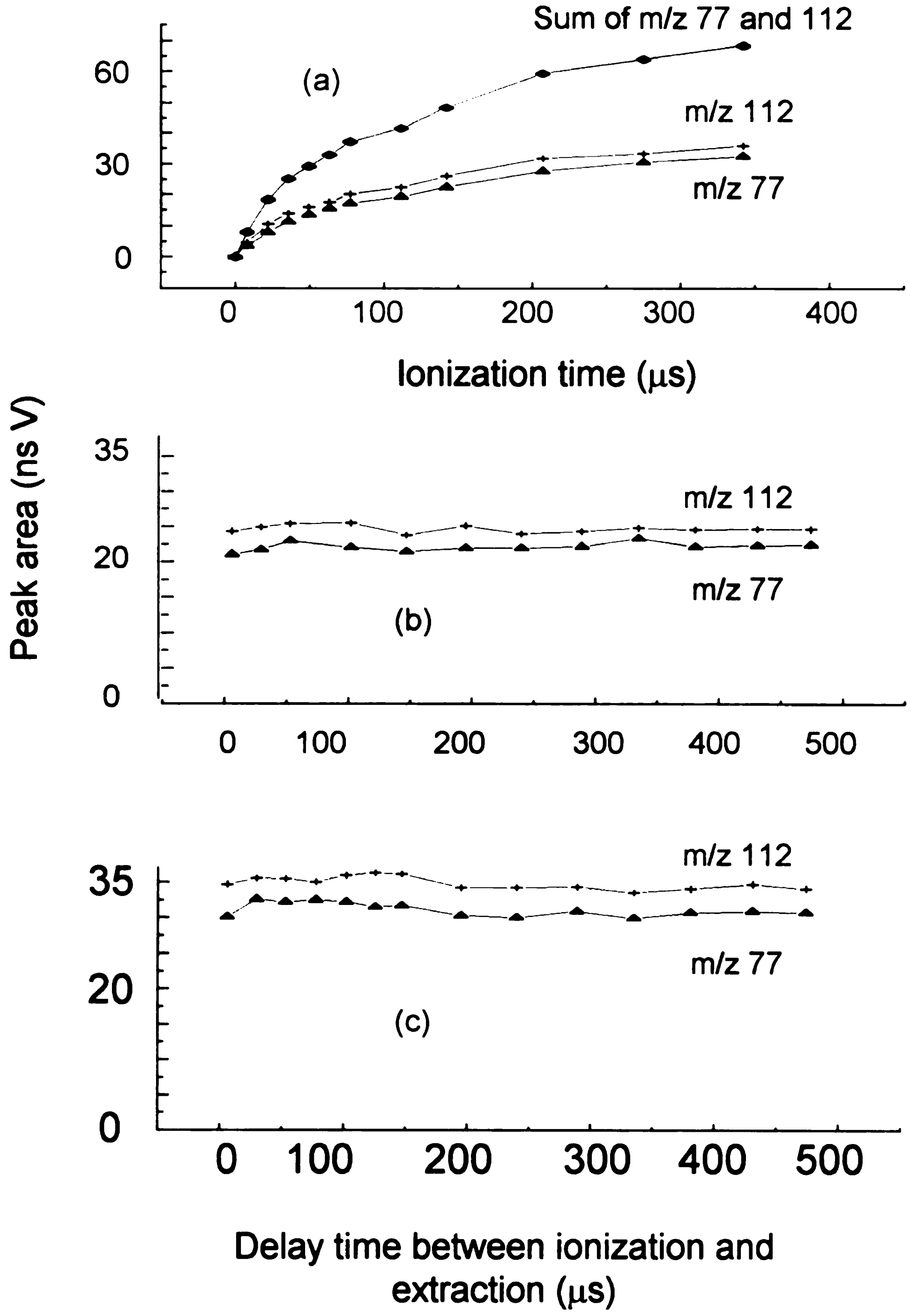

Figure 5-7. The abundance of the major ions of chlorobenzene as a function of (a) continuous ionization time and (b) extraction delays after an ionization time of 142 μs and (c) 342 μs. The RF applied is 600 volts (peak to peak) and 1.2 MHz.

formation is related to processes occurring during the ionization, not to processes occurring during ion storage.

A further study in the dynamics of the increases in ion population in the trap as a function of ionization time was undertaken. In this case PFTBA was chosen for the analyte so that a wide range of m/z values would be represented. Oven temperature was varied to change the concentrations of PFTBA introduced into the ion source. The abundance of the major ions of PFTBA as a function of ionization time for three GC oven temperatures is shown in Figure 5-8. The curves represented by different symbols are actually data points for ions with different m/z values. The population growth curves follow a first order loss against a constant rate of generation according to the equation:

$$dN/dt = k_f p - k_l N \qquad \text{(equation 2)}$$

where N is the ion abundance, k_f and k_l are the formation and loss rate constants and p is the sample pressure. The experimental data points in the first 380 μs ionization time(except the data in Figure 5-8(c)) in Figure 8 are fit to the integrated form of equation 3 shown below.

$$N = \frac{k_f}{k_l} p\left(1 - e^{-k_l t}\right) \qquad \text{(equation 3)}$$

The goodness of this fit confirms that a constant rate of ion formation is countered by a loss mechanism whose rate is proportional to the total number of ions in the trap. The time constant $1/k_l$ for the resulting best-fit exponential growth curves of the different m/z values is from 200 to 300 μs. As shown in

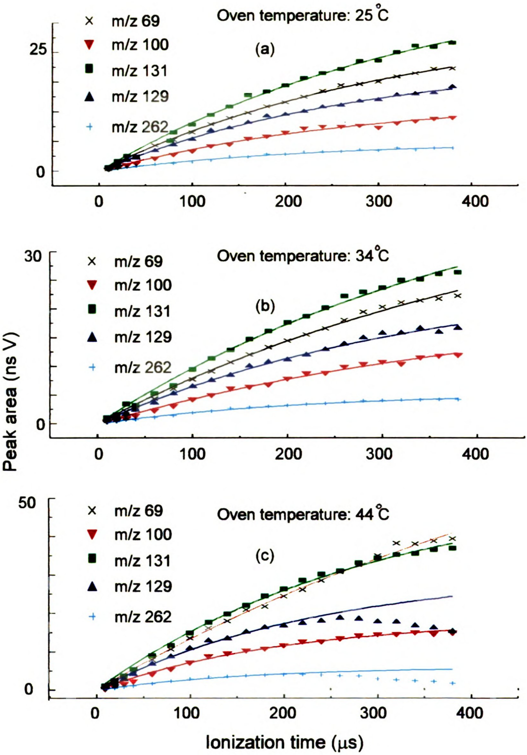

Figure 5-8. Ion build-up curves of major ions of PFTBA at oven temperatures of (a) 25 °C, (b) 34° C, and (c) 44° C.

Figure 5-8, most of the ions are continuously accumulated in the ion source. Ion formation rate is increased by increasing oven temperature from 25 ^{0}C to 34 ^{0}C, but the relative intensity of these ion peaks is almost the same. When the oven temperature is increased to 44 ^{0}C as shown in Figure 5-8 (c), the abundance of the m/z 264 and 219 ions diminishes after 200 µs. This indicates that some kind of ion-molecule reaction becomes significant in the ion source when the sample pressure is increased. Although a clean picture of the ion loss mechanism can not be drawn, it is important to note that if extraction is accomplished within the first 200 µs of ionization, the relative ion abundance remains a reproducible parameter, characteristic of the sample molecule and amenable for quantitation. The advantage of this fact for GC chromatographic detection is further discussed in a later section.

5.4 Interface between gas chromatograph and the SRS/TOF mass spectrometer

5.4.1 Dynamic working curve and Detection limit

Overall instrument performance for sensitivity and dynamic range was tested by obtaining a working curve as shown in Figure 5-9. The analyte for this study was chlorobenzene. A volume of 1 µl of chlorobenzene in hexane solvent was injected into the gas chromatograph operating in the split injection mode. Analyte concentrations varied from 20 ng/µl to 10µg/µl. The column was a HP-5 capillary column of 10 m length , 0.1 mm inner diameter and 0.17 µm film thickness. The total flow rate of helium was set at 50 ml/min. The volumetric flow rate of 0.091 ml/min is calculated by following equation[3]

Volumetric Flow Rate (ml/min)= $0.785x(D^2L/t_r)$

Where : D(mm) is column diameter

L(m) is the column length

t_r(min) is the retention time of an unretained components measured.

A linear range was confirmed from 36 pg to 18 ng as shown in Figure 5-9. The detection limit was first evaluated by injecting 1ul of chlorobenzene at a concentration of 20 ng/ul. The split ratio of 1:550 was used. The reconstructed ion chromatogram from m/z=112 of the 36 pg sample injection is shown in Figure 5-10. A peak-finding technique was used to differentiate the signal peak and background noise in the individual mass spectrum. In Figure 5-11 the major peak of the mass spectrum of chlorobenzene taken at spectrum number 19 is shown. Each mass spectrum was the sum of 256 transients. The signal to noise ratio of greater than 3 was obtained for this 36 pg sample at a spectral generation rate of 4 spectra per second.

These data were collected with an ionization time of 100 μs and an extraction rate of 1000 Hz. They verify the earlier assumption that at 100 μs ionization time, the trapped ion population is a valid measure of the amount of sample being introduced into the source. Better results could be obtained with an extraction rate of 6 kHz which is the reciprocal of the maximum ion flight time.

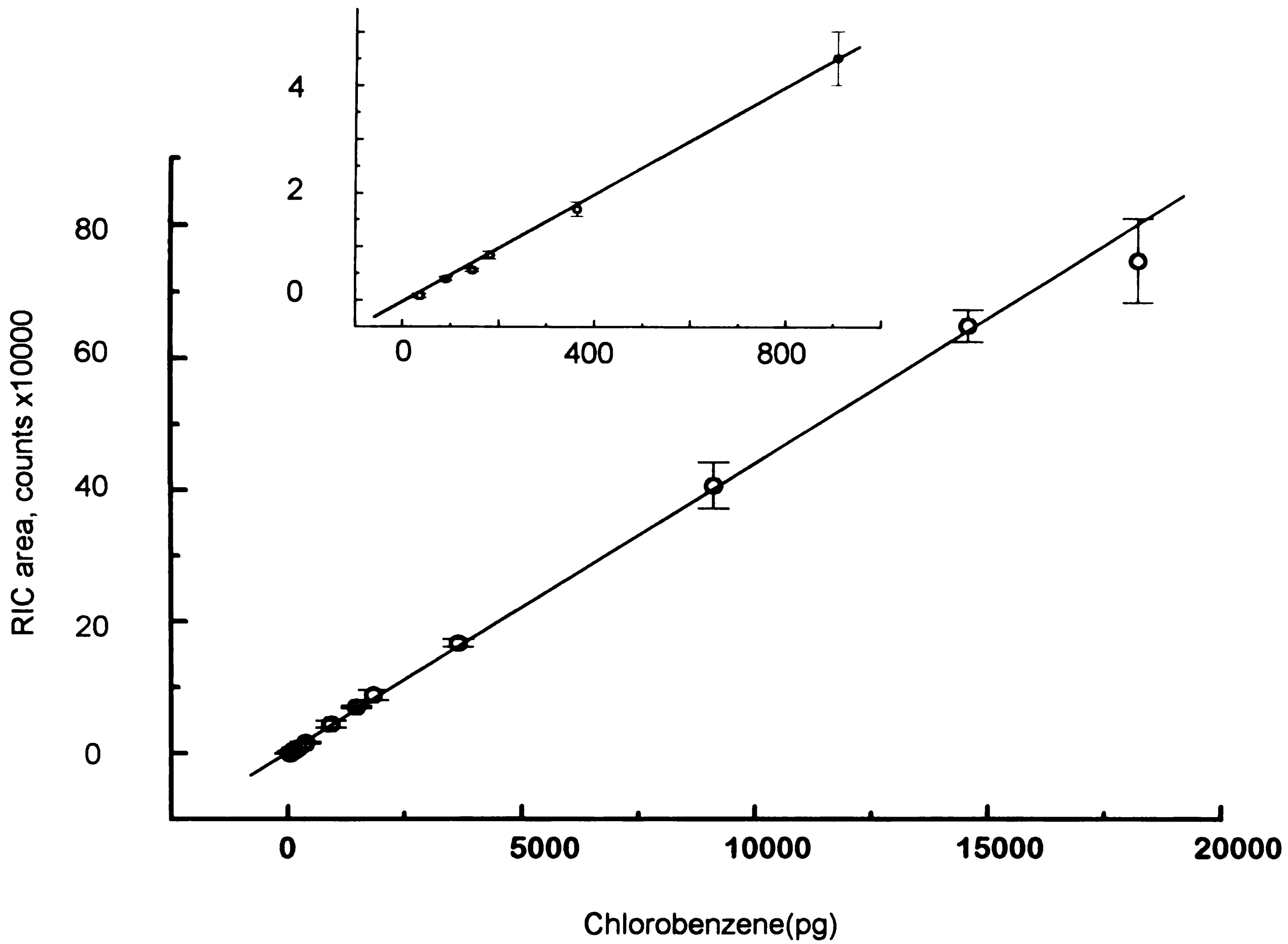

Figure 5-9. A working curve for chlorobenzene illustrating a linearity of response over nearly three orders of magnitude.

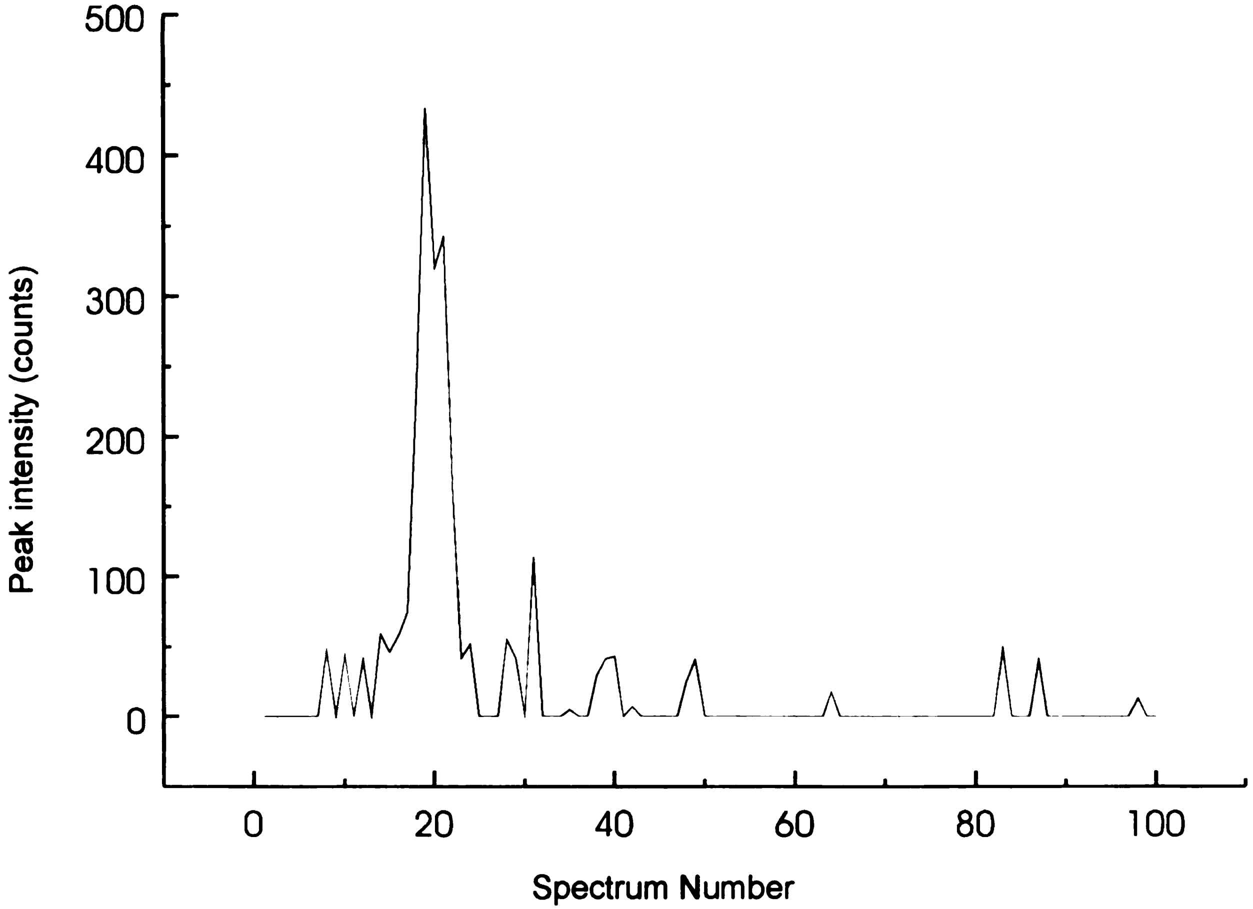

Figure 5-10. A reconstructed ion chromatogram (RIC) for m/z = 112 for 36 pg of chlorobenzene on column. Due to the noise near the detection limit, a peak finding technique (threshold = 20) was used.

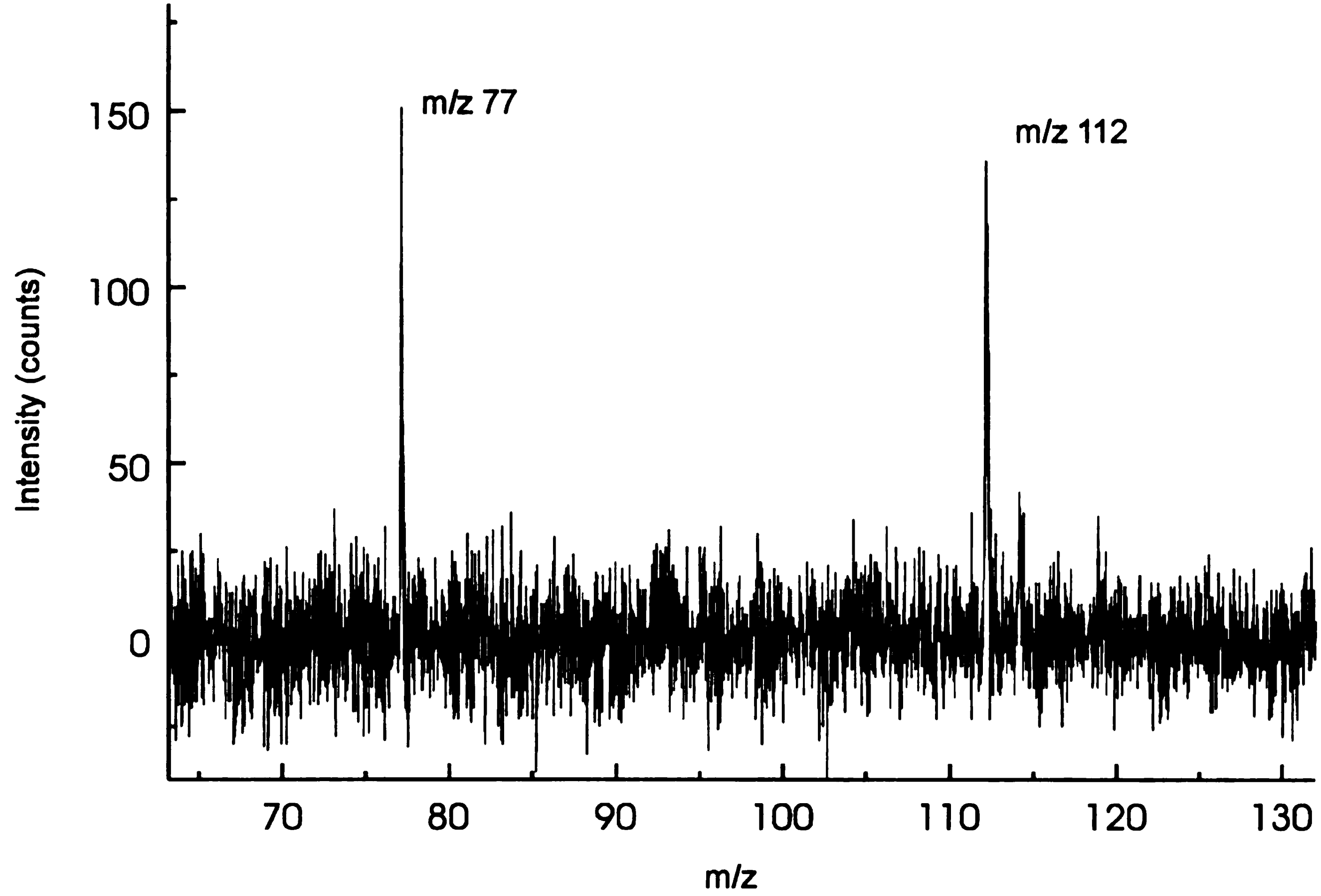

Figure 5-11. Mass spectrum of scan no. 19 from the RIC of Figure 10 with background subtraction. This spectrum is obtained by summing 256 transients.

In our current system, the maximum extraction frequency is limited by the nature of the RF generator and the transient recorder used and not by the ion storage, extraction, and focusing optics. Achievement of the maximum extraction rate of 6 kHz would provide the same signal to noise ratio obtained for the 36 pg of chlorobenzene in Figure 11, but at 24 spectra per second. Conversely, the better sensitivity obtained with the 6 kHz extraction at a lower number of spectra per second will improve ion statistics at the limit of detection increasing the linear range of measurement.

The RF voltage applied to the ring electrode elements in the above experiments was 600 V_{p-p}. The source vacuum chamber pressure was approximately 2 x10^{-6} torr. Each MCP plate had a voltage of 800 V across it and the detector gain was limited by the background (especially the helium) ions. These low mass ions continuously leave the source and a significant portion of them reaches the detector. The resulting background current has a high level of shot noise and limits the usable detector gain.

An ion deflector which consists of two parallel stainless steel plates described in Chapter 4 was added along the ion flight path. A pulsed voltage (up to 850 V higher than the field free region voltage), synchronized with the ionization period, can be applied to one deflection plate while the other deflection plate remains at the field free region potential. This has the dual effect of lowering the background current and allowing a much higher gain in the electron multiplier detector. The anode current of the detector was decreased to less than 1×10^{-6}A, even when each MCP plate of the detector had 980 V across it. The improvement afforded is shown by the test below.

Thirty-six picograms of chlorobenzene were introduced into the mass spectrometer by injecting 1 µl of a solution of analyte concentrations of 20 ng/µl through a gas chromatograph with a split ratio of 1:550. The Reconstructed Ion Chromatograph (RIC) of m/z 112 is shown in Figure 5-12 and the mass spectrum of the chlorobenzene at spectrum no. 34 (background subtracted) is shown in Figure 5-13. The peaks shown are due to the chlorobenzene and background chemical noise. The instrumental noise relative to the m/z 112 peak of chlorobenzene is about 2%. This suggests a detection limit with a S/N of 50 at about 36 pg.

5.4.2 Advantage of less interference from ion/molecule reactions

As several researchers have addressed[4, 5, 6, 7, 8, 9], the problem of the occurrence of ion molecule reactions during GC/MS analysis with a conventional quadrupole mass spectrometer complicates the unambiguous identification of the compounds as well as affecting the accuracy of quantitative analysis. The occurrence of such reactions (commonly termed as self chemical ionization), results in excessive $[M+1]^+/M^+$ ratios and other adduct peaks for many classes of compounds that are analyzed typically by GC/MS. McLuckey and Glish et al. showed that the extent of the ion/molecule reaction in the ion trap can be minimized by either reducing the amount of sample introduced or reducing the trap time between ionization and ion analysis[7]. Yost et al.[8] demonstrated that

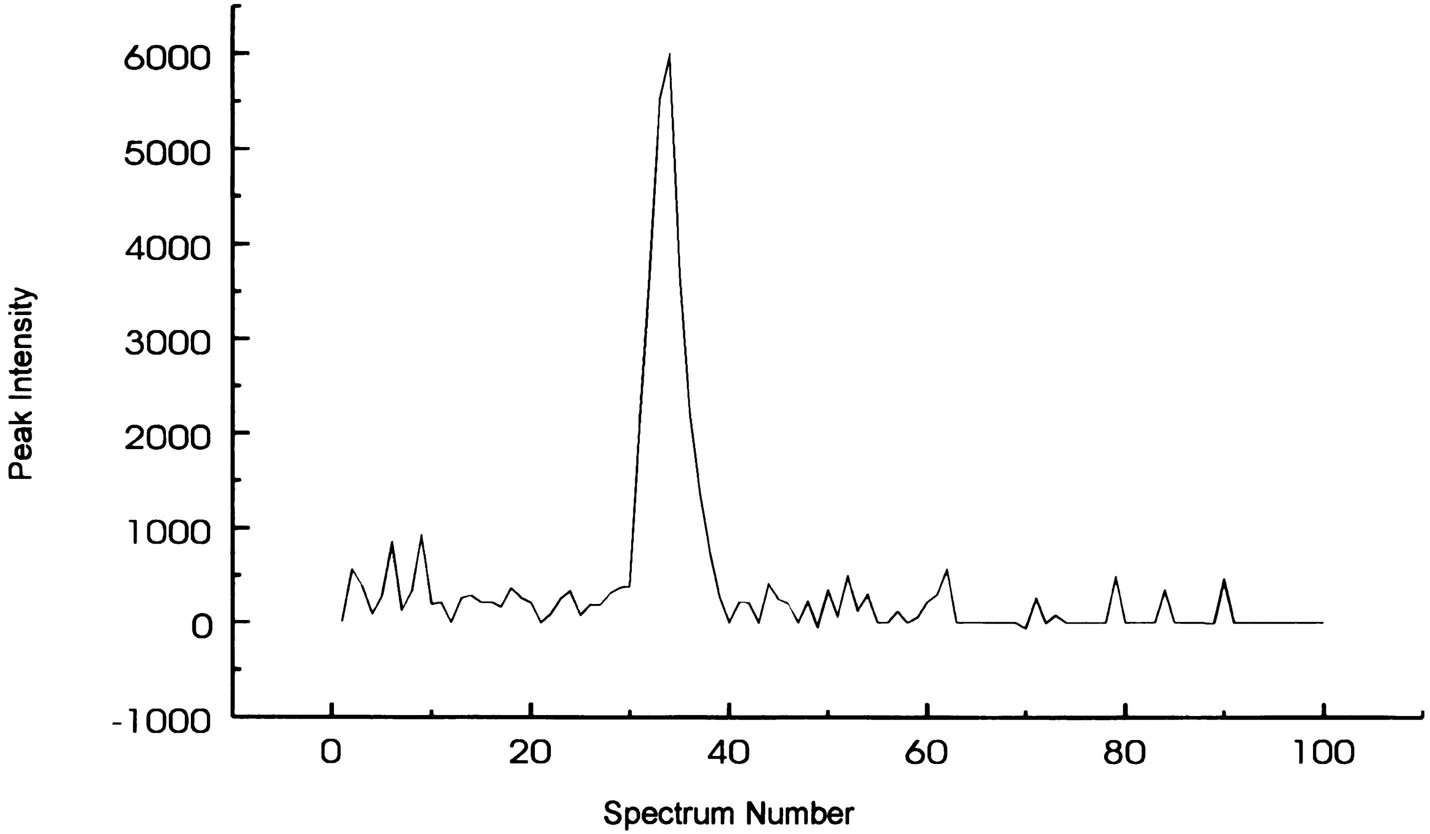

Figure 5-12. A reconstructed ion chromatogram (RIC) for m/z = 112 for 36 pg of chlorobenzene on column. A ion deflection electrode was used to deflect background ions during the ionization period.

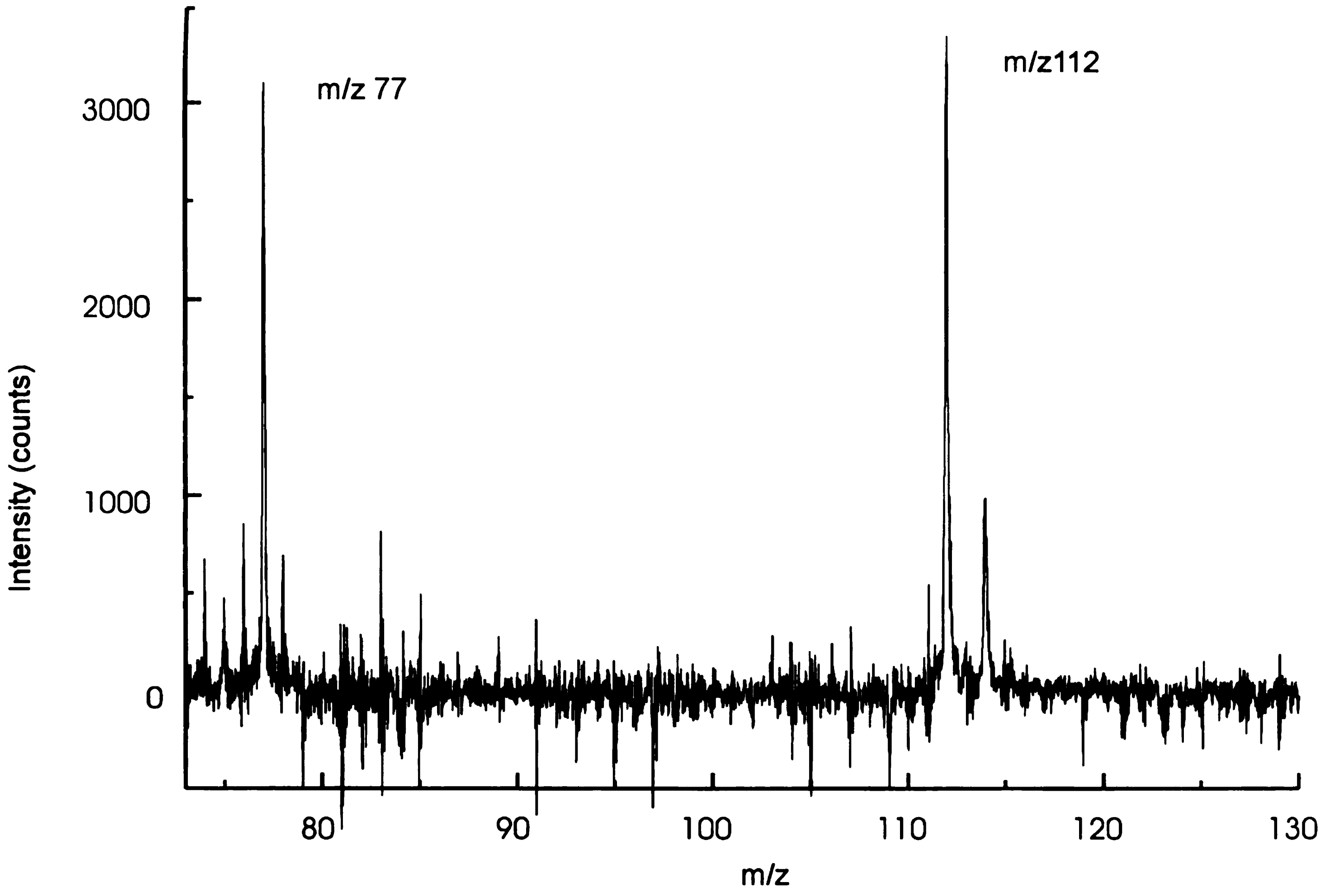

Figure 5-13. Mass spectrum of scan no. 34 from the RIC of Figure 12 with background subtraction. This spectrum is obtained by summing 256 transients. Each MCP plate of detector has 980 V across and most background ions are deflected during the ionization period.

the ion/molecule reaction could be eliminated by using external electron ionization for benzophenone at least up to 500 ng.

For the SRS-TOF mass spectrometer operated at an extraction frequency of 5 kHz, ions would be stored in the ion source for only 200 μs. Benzophenone, a compound very prone to self-CI in normal ion trap spectra, was used to evaluate the self-chemical ionization interference in the SRS ion source. Analyte concentrations varied from 0.55 mg/ml to 55 mg/ml. With a split ratio of 1:550, 1 ng to 100 ng benzophenone was introduced into the mass spectrometer for each 1μl injection. Because the Precision Instrument transient recorder board can only be used for a signal intensity up to 1 V, the detector gain was set low by applying 720 V across each MCP plate. The linear relationship between the peak areas of the m/z 77, 105, 182, 183 at the maximum chromatographic elution concentration position and the amount of sample injected is shown in Figure 5-14(a). The peak area ratios of $[M+1]^+/M^+$ versus the amount of sample introduced into the mass spectrometer are shown in Figure 5-14 (b). The peak area ratio closely follows the isotopic ratio of 14.5% of the molecular ions of benzophenone up to at least a 100 ng sample introduction. As the sample introduced increases from 5 ng to 100 ng, no adduct ions are observed.

Yost et al.[9] showed that the peak ratio of the $[M+1]^+/[M]^+$ increased linearly with the amount of benzophenone injected and it reaches a ratio more than 0.6:1 when 50 ng of analyte was injected into a normal ion trap . The self-chemical ionization did not happen in his external electron ionization ITMS. Both

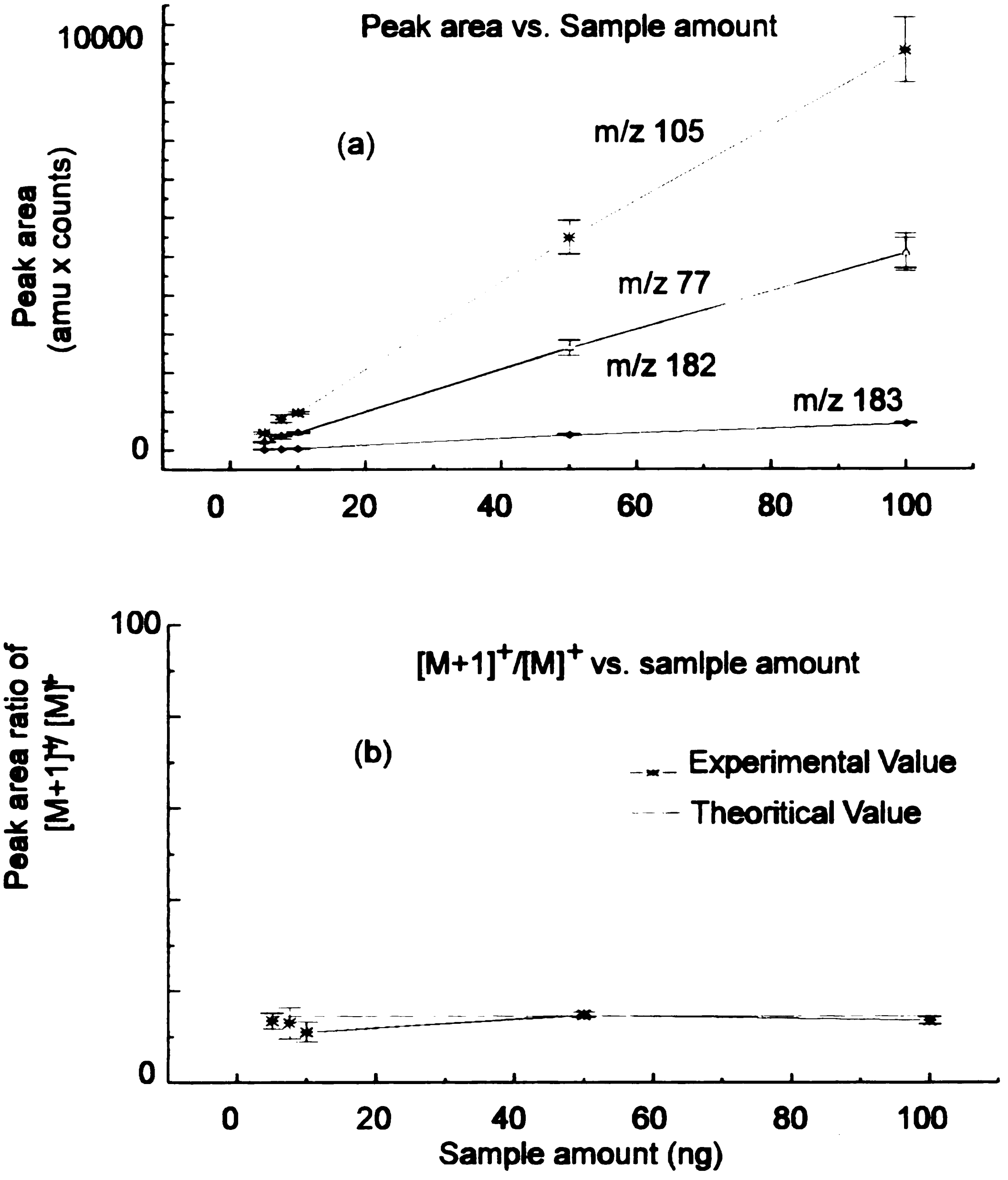

Figure 5-14. The intensity of major ions of benzophenone vs. amount of sample introduced (a) and the peak area ratio of $[M+1]^+/[M]^+$ of bezophenone vs. amount of sample introduced (b).

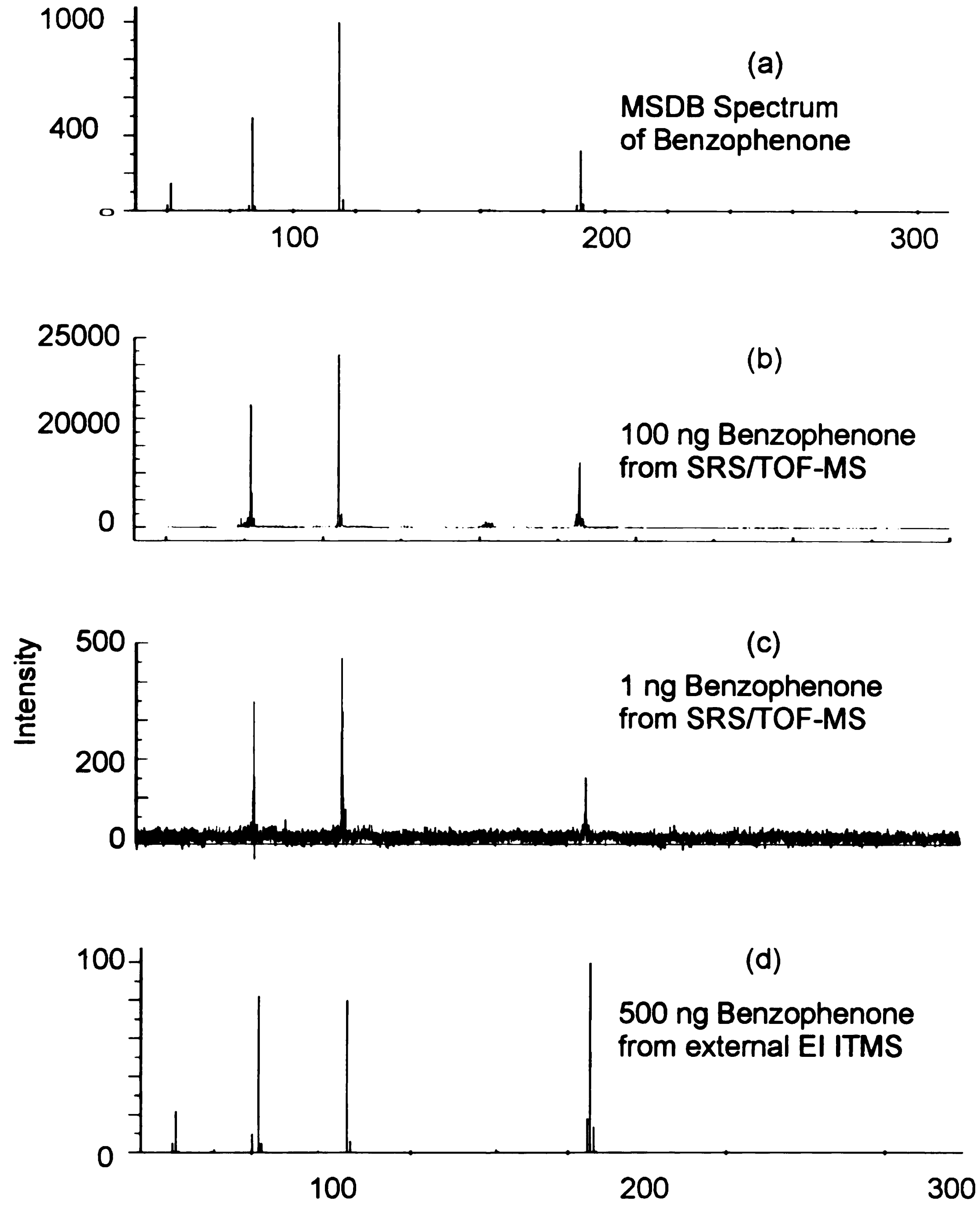

Figure 5-15. Spectra of Benzophenone obtained from different instruments. (a) MSDB data base. (b) and (c) SRS/TOF mass spectrometer. (d) ITMS with external electron impact ionization.

the external electron impact ionization ITMS and our SRS-TOF/MS can generate mass spectra without self-chemical ionization interference for higher analyte concentrations. The mass spectrum of benzophenone obtained from Mass Spectral Data Base (MSDB)[10], our instrument and an External Ionization ITMS[6] are shown in Figure 5-15. The mass spectrum obtained from the SRS-TOF mass spectrometer has a relative abundance similar to the MSDB spectrum for existing ion peaks. The experimental results documented above demonstrate that the SRS/TOF-MS provides a characteristic mass spectrum even at high sample concentrations and without adjustment of ionization time.

References:

---

[1] Hart, K. J.; McLuckey, S. A.; Glish, G. L.: Proc. 39th ASMS Conf. Mass Spectrometry and Allied Topics, Nashville, 1991 p.1495.

[2] Mather, R. E., Waldren, R. M., Todd, J. F. J., and March, R. E.: Some Operational Characteristics of a Quadrupole Ion Storage Mass Spectrometer Having Cylindrical Geometry. Int. J. Mass Spectrom. Ion Phys. 33, 201-230 (1980).

[3] Operating Manual for HP 5890 Series II Gas Chromatograph. Hewlett Packard, chapter 4, p11, October (1991)

[4] Pannell, L. K., Pu, Q. L., Fales, H. M., Mason, R. T., and Stephenson, Jr.; Anal. Chem., 61, 2500-2503 (1989)

[5] Ratnayake, W. M. N.; Timmins, A.; Ohshima, T,; Ackman, R. G.; Lipids. 21, 518-524 (1986)

[6] Olson, E. S.; Diehl, J. W.; Anal Chem., 59, 443-448 (1987)

[7] Mcluckey, S. A., Glish, G. L., Asano, K. G.; Van Berkel, G. J.; Anal. Chem., 60, 2312-2314 (1988)

---

[8] Booth, M. M. , Stephenson, J. L. J., and Yost, R. A.; Proc. 41st ASMS Conf. Mass Spectrometry and Allied Topics. San Francisco p.716a (1993)

[9] Yates, N. A., Booth, M. M., Stephenson Jr., J. L. and Yost R. A.: Practical Aspects of Ion Trap Mass Spectrometry, Vol. 3, 121-186, CRC Press (1995)

[10] MSDB, NIST Standard Reference Database Series 1a, the NIST/EPA/MSDC Mass Spectral Database Version 3.02, June (1990)

Chapter 6 Significance and potential advantages for SRS/TOF mass spectrometer as a detector for chromatography

The segmented ring trap with its cylindrical geometry exhibits the ability to trap ions and hold them for several hundred microseconds or more. The mass range of entrapment closely follows the expected stability diagram for the cylindrical ion trap which, for the parameters used, closely follows the classical quadrupole equations as well. The fields are surely not perfectly quadrupolar, but perfectly quadrupolar fields are not required for broad mass range ion storage, only for selective m/z value rejection.

The uniform extraction fields possible with this geometry enable good mass resolution to be achieved without the need for ion cooling prior to mass analysis. The high voltage extraction is designed to minimize the effect of the *turn around time* on the mass resolution. For electron impact ionization, It was discovered that the best RF phase angle for application of the DC extraction pulse is 270^0. At this RF phase angle, ions will be at their lowest field-induced kinetic energy state. Also at this RF phase angle, the direction of the DC extraction voltage is same as the direction of the RF voltage change. A general method which guides the construction of a reflectron that is able to focus isomass ions with a broad energy distribution, due to RF trapping field and high extraction voltage, was developed. Unit mass resolution for m/z 502 has been obtained with this non-optimized prototype instrument.

Without component optimization, the present unit readily generates information for up to 1000 spectra per second. As shown in Figures 5-7 and 5-8, population growth is still in the nearly linear phase at a 100 μs ionization and storage time. Analytically reliable linear growth to this point is confirmed by the data in Figure 5-9 where a series of varying analyte concentrations show a linear response of ion population to concentration with this ionization timing.

With a 100 μs ionization time and a 1 kHz extraction rate, the sample utilization duty cycle is very nearly 10%. With improved electronics and adjustments to the source design, one can realistically envision a continuous sample duty cycle approaching 100% for chromatographic applications. A high ion compaction value is achieved; all the ions of each m/z value generated during 100 μs arrive at the detector within approximately 80 ns. This gives rise to an instantaneous peak detector current that is 1200 times greater than that produced by the average ion generation rate. A signal to noise ratio more than 10:1 for 7 pg of chlorobenzene will be readily achievable with a clean vacuum system (reduction of chemical noise) as shown in Figure 5-13. With optimization of ion optics and improvements in electronic design, the SRS-TOF mass spectrometer will provide gas chromatographic detection with a speed and sensitivity better than existing ion trap and quadrupole filter mass spectrometers while still producing full mass range spectra.

Experimental results have also revealed that the SRS-TOF mass spectrometer can give characteristic mass spectra for gas chromatographic eluents. The obtained mass spectra exhibit no self-chemical ionization interferences, which are a bane to normal ion trap operation, and peak relative abundances are similar to library spectra obtained by electron impact ionization and a scanning sector mass spectrometer.

The significance of the performance of the SRS/TOF mass spectrometer is that it has the potential to be a nearly ideal detector for chromatographic separation. Consider, for example, the following categories.

a. A compact SRS/TOF mass analysis detector for fast GC/MS analysis of trace amounts of small molecules for environmental, industrial and biomedical applications.

The mass range of ion storage and resolution currently achieved is more than sufficient for small molecules. With optical, mechanical and electronic improvements, this performance could be maintained while the actual size of the instrument could be much smaller. The ion storage capability gives good detection limits and the absence of ion molecular reaction distortion will give a linear response for varieties of organic compounds. The physical simplicity of time-of-flight mass analysis and the segmented ring ion storage source will provide economical advantages in the commercialization of this instrument.

b. A high profile SRS/TOF mass spectrometer for fast gas chromatographic detection of complex mixture analysis with the possibly a GC/MS/MS capability.

The speed, sensitivity and characteristic mass analysis of the SRS/TOF-MS will provide rich information for the chromatographically eluted components. Even for unresolved peaks, the frequent and complete mass spectral information will enable the direct application of effective mathematical routines for the differentiation of coeluting compounds. If more segmented ring electrode elements are used, the improved storage field could possibly allow ion selective storage during the ionization period by adding a modulated RF signal to the ion source end caps. This selective ion storage will provide a possible basis for the MS/MS capability of this instrument. In an alternative mode, an interface between this segmented ring ion trap storage source and a tandem time-of-flight mass spectrometer will provide GC/MS/MS capability with good detection limits on the chromatographic time scale.

c. A high profile SRS/TOF mass spectrometer for chromatographic separations interfaced with external ionization techniques such electrospray ionization and continuous flow matrix laser desorption.

It is quite possible that the open structure of the segmented ring ion trap storage source will be accessible for ion introduction of externally generated ions. The interface of condensed phase chromatography (such as liquid chromatography and capillary electrophoresis) to the ionization techniques (such as electrospray ionization, matrix laser desorption ionization) has increased the demand for fast mass spectrometric detection. With improved mass range and exploration of ion injection and continuous ion trap accumulation, a segmented ring ion trap storage device should give fast, mass spectrometric detection for these chromatographic separation techniques.